NSF Grants ATM-9500108 and ATM-9726464

National Science Foundation

# MULTIPARAMETER INVESTIGATION OF SIGNIFICANT LIGHTNING PRODUCING STORMS IN NORTHEASTERN COLORADO

by Michael L. Gauthier and Steven A. Rutledge

Colorado State University

DEPARTMENT OF ATMOSPHERIC SCIENCE

PAPER NO. 682

# MULTIPARAMETER INVESTIGATION OF SIGNIFICANT LIGHTNING PRODUCING STORMS IN NORTHEASTERN COLORADO

by

**Michael L. Gauthier**

**and**

**Steven A. Rutledge**

Department of Atmospheric Science

Colorado State University

Fort Collins, CO 80523

**Research Supported by**

**National Science Foundation**

under Grants ATM-9500108 and ATM-9726464

Summer 1999

Atmospheric Science Paper No. 682

ABSTRACT

**MULTIPARAMETER INVESTIGATION OF SIGNIFICANT LIGHTNING PRODUCING STORMS IN NORTHEASTERN COLORADO**

We present a regional, summer season, climatology of cloud-to-ground (CG) lightning immediately east of the central Rocky mountains from 1996-98 using data from the National Lightning Detection Network (NLDN). We document the spatial and temporal variations of summer season CG lightning activity within the region. Our examination focused on describing how CG lightning characteristics (multiplicity and peak current) for each polarity (positive and negative) changed as the percentage of positive CG lightning changed. Specifically, we found that as the positive CG fraction within a storm increased, the average positive (negative) peak current increased (decreased). Similarly, our findings revealed that increases in positive CG fraction were also associated with small increase in positive CG multiplicity and more significant decreases in negative CG multiplicity values.

Additionally, we examined the co-evolving microphysical and electrical characteristics of four "significant" lightning producing storms in northeastern Colorado using the CSU-CHILL multiparameter radar and cloud-to-ground (CG) lightning data. Using the multiparameter variables of $Z_h$, $Z_{dr}$, $\rho_{hv}(0)$, LDR and $K_{dp}$, emphasis was placed on determining the three-dimensional distribution of various hydrometeor types in these storms (especially during periods of electrical transition from one CG polarity to another),

as well as estimates of rain and hail rates. Our goal in examining these cases was to try and determine the mechanism by which positive ground flashes in mature thunderstorms dominate over negative ground flashes. Specifically, we investigated the following hypothesis: (1) the tilted dipole hypothesis, (2) the enhanced lower positive charge hypothesis, and (3) the precipitation "unshielding" hypothesis.

We argue that the majority of our findings tend to support the third hypothesis, precipitation "unshielding", where intense precipitation leads to a large precipitation currents which removes charge from the negative charge center, thereby "unshielding" the upper level positive charge center. Once this "unshielding" occurs, conditions are favorable for positive CG lightning. Typically, peaks in positive CG flash rates were observed within 25 minutes of observed peaks in surface mass fluxes, resulting from the descending ice mass aloft.

## ACKNOWLEDGEMENTS

I would like to thank my advisor Dr. Steven Rutledge for his guidance and encouragement during my program of study. I thank Dr. Graeme Stephens and Dr. Steve Robinson for serving on my graduate committee. I wish to thank the entire CSU-CHILL radar staff for their assistance and for providing the multiparameter data used in this thesis. I would also like to express my gratitude to Paul Hein for his expert radar software and systems support. I thank my fellow members of the "Radar Meteorology Group" for their advice and encouragement.

The U. S. Air Force supported this research under its Air Force Institute of Technology (AFIT) graduate meteorology program and paid all salary and tuition costs. This research was also supported under National Science Foundation Grants ATM-9500108 and ATM-9726464.

## TABLE OF CONTENTS

## LIST OF TABLES

## LIST OF FIGURES

# CHAPTER 1

# INTRODUCTION

## 1.1 Project Motivation

Positive cloud-to-ground (CG) lightning has been observed in a variety of weather systems. In particular, positive CG lightning has been studied in highly sheared, shallow winter thunderstorms in Japan (e.g., Takeuti et al., 1978; Brook et al., 1982), the trailing stratiform regions of mesoscale convective systems (MCS's) (e.g., Rutledge and MacGorman 1988; Rutledge et al. 1990; Engholm et al. 1990; Stolzenburg 1990) and the anvil regions of severe storms (e.g., Pierce 1955; Fuquay 1982; Rust et al. 1981a,b). In these storms positive CGs were produced from the anvil, while the main cores were still dominated by negative CG lightning (Holle et al. 1994). The positive CG flashes in these types of events tend to occur over large areas during the course of several hours; therefore they tend to have relatively low positive flash densities ($< 0.01$ km$^{-2}$ h$^{-1}$, Stolzenburg 1994). Although CG lightning activity during the mature phase of non-severe thunderstorms (described above) are characterized by a predominance of negative CG flashes, a growing body of evidence tends to suggest that severe thunderstorms producing large hail (diameter > 2 cm) and sometimes tornadoes may be dominated by high densities ($> 0.01$ km$^{-2}$ h$^{-1}$, Stolzenburg 1994) of positive CG flashes for extended periods of time (> 30 minutes) during the mature phase (e.g., Rust et al. 1985; Seimon 1993; MacGorman and Burgess 1994; Stolzenburg 1994; Carey et al. 1997; Carey and

Rutledge 1998). In these severe thunderstorms, the positive CG lightning flashes may be located in clusters in or around the convective core as opposed to the anvil region.

The mechanism by which positive ground flashes in severe storms dominate over negative ground flashes is unclear. Current hypotheses offered to explain the occurrence of high positive cloud-to-ground flash densities in mature thunderstorms fall into one of three categories: (1) the tilted-dipole, (2) the enhanced lower positive charge (sometimes referred to as an inverted dipole), and (3) precipitation "unshielding".

The tilted-dipole hypothesis is one in which the normal thunderstorm dipole (positive charge located over negative charge) is tilted, such that the upper positive charge carried on ice crystals is displaced laterally relative to the lower negative charge (deposited on graupel and hail particles) as a result of storm relative winds. This tilting of the dipole effectively "unshields" the upper positive charge center, allowing the direct transfer of positive charge to ground from great heights in the cloud.

The second hypothesis for explaining positive CG lightning in severe thunderstorms involves the development of an enhanced lower positive charge region (or inverted dipole) located beneath the negative charge center. Under certain thermodynamic conditions, the rebounding processes which results in negative charge being deposited on graupel and hail particles (positive charge on the smaller ice particles) can be reversed. This causes negative charge to be deposited in the upper portions of the storm as ice crystals are carried aloft in storm updrafts. The resulting positive charge deposited on graupel and hail particles leads to the development of the lower positive charge center. If the magnitude of the lower positive charge is greater than that of the

upper level charge center(s) then conditions would be favorable for positive cloud to ground discharges.

The third hypothesis, precipitation "unshielding", offered by Carey and Rutledge (1998), suggests that intense precipitation leads to a large precipitation current which removes charge from the negative charge center, thereby "unshielding" the upper level positive charge center. As in the tilted-dipole hypothesis once this "unshielding" occurs, conditions are favorable for positive CG lightning. This mechanism is attractive in the sense that it is also consistent with the paucity of negative CGs in these events. In other words, the lower negative charge center is reduced by precipitation currents, not by lightning.

This study will examine the co-evolving microphysical, and electrical characteristics of significant lightning producing storms in northeastern Colorado using the CSU-CHILL multiparameter radar and cloud-to-ground (CG) lightning data. The measured polarimetric variables will provide information on the size, shape, orientation, and thermodynamic phase of hydrometeors. This information will enable us to infer bulk-hydrometeor types and mixing ratios in these storms. We will focus on determining the three-dimensional distribution of various hydrometeor types in these storms (especially during periods of electrical transition from one CG polarity to another) in an effort to better elevate the hypotheses discussed above.

This thesis will also present a regional climatology of cloud-to-ground lightning based on data obtained from the National Lightning Detection Network (NLDN). This regional climatology will examine the spatial and temporal variations in CG lightning activity within the area of interest (Fig. 1.1). It will further provide insight into how

lightning characteristics (positive and negative peak currents and multiplicity) change as a function of positive CG fraction within a thunderstorm or "convective element" within the same area.

1.2 Data Description

Cloud-to-ground (CG) lightning data used in our regional climatology of CG lightning, and in each of our multiparameter radar-based case studies was collected by the National Lightning Detection Network (NLDN), and furnished to Colorado State University through the NASA Marshall Space Flight Center - Distributed Active Archive Center (MFSC-DAAC) for post-analysis. Polarimetric radar observations of four electrically active thunderstorms occurring on 2 June 1997, 1 July 1998, 2 July 1998 and 21 July 1998 were collected and archived by the CSU-CHILL Doppler radar, an 11 cm multiparameter radar located near Greeley, CO (Fig. 1.2). Each of the cases were selected for analysis because at some point in their lifetime they exhibited the following characteristics over a 30 minute period, within a 25 km × 25 km area: (1) over 50% of the CG lightning was of positive polarity and (2) each event contained a positive flash density greater than or equal to a value of 0.03 flashes $km^{-2}$ $h^{-1}$. The second criteria is a modification of the flashes $km^{-2}$ $h^{-1}$ lower bound offered by Stolzenburg (1994) to define significant positive flash densities in severe thunderstorms. Specifics of this modification, and supporting justification are discussed further in Section 3.5.

Using the multiparameter data collected from the CSU-CHILL radar we are able to discriminate between several hydrometeor types by applying a bulk hydrometeor identification matrix (Doviak and Zrnic, 1993; Straka and Zrnic, 1993; Carey and

Rutledge, 1998). We are then able to estimate the volumes of each hydrometeor type throughout the lifetime of each storm. These estimations, when coupled with the lightning data, provide insight into storm electrification processes as related to changes in the microphysics of the evolving thunderstorms.

This thesis is organized into six chapters. Following this introductory chapter, Chapter 2 presents a discussion of multiparameter radar theory, followed by a brief overview of thunderstorm electrification theory, and a discussion on previous research of positive CG producing storms. Chapter 3 will discuss the data and methodology used throughout this thesis, followed by a presentation of our regional climatology of cloud-to-ground lightning in Chapter 4. Observations and trends in CG lightning, along with our multiparameter analysis of four separate cases are then presented in Chapter 5. Concluding remarks, including suggestions for future research, are presented in Chapter 6.

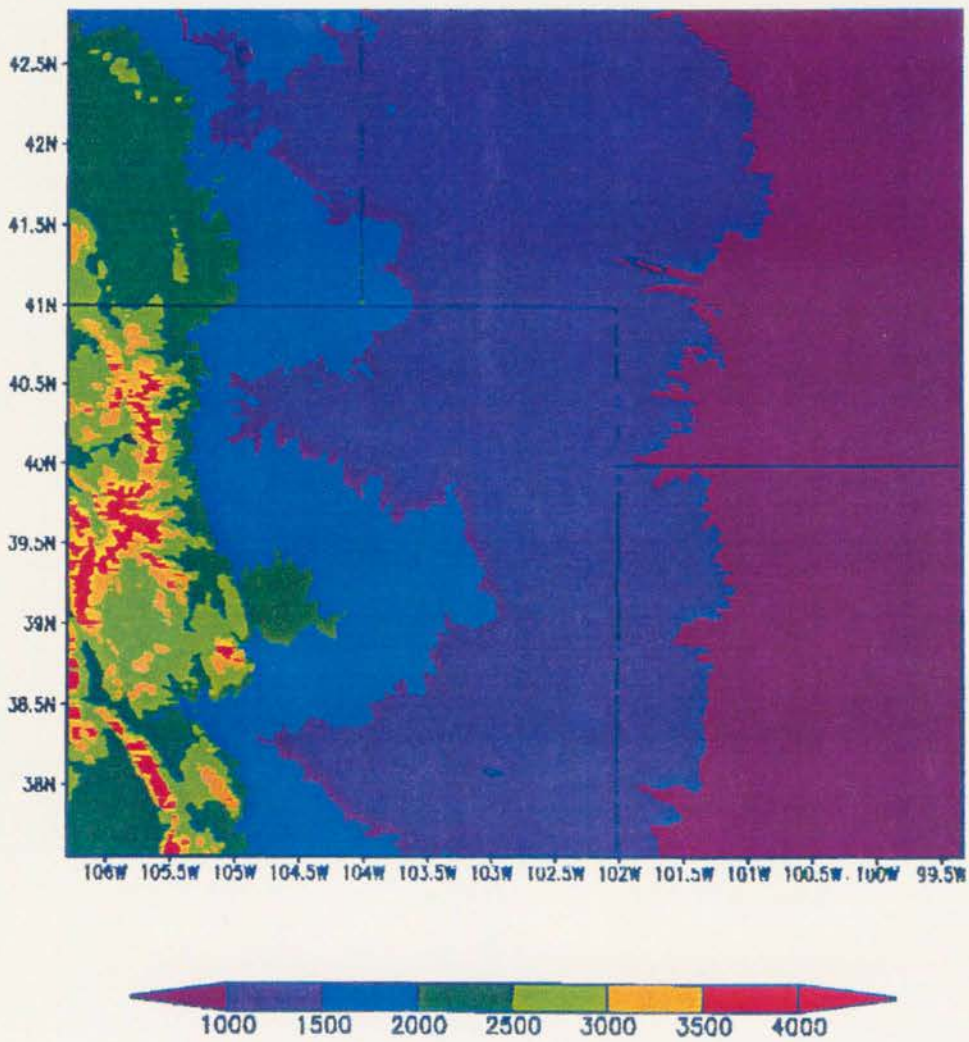


Figure 1.1: Topographic base map of the area included in our regional climatology of cloud-to-ground lightning.

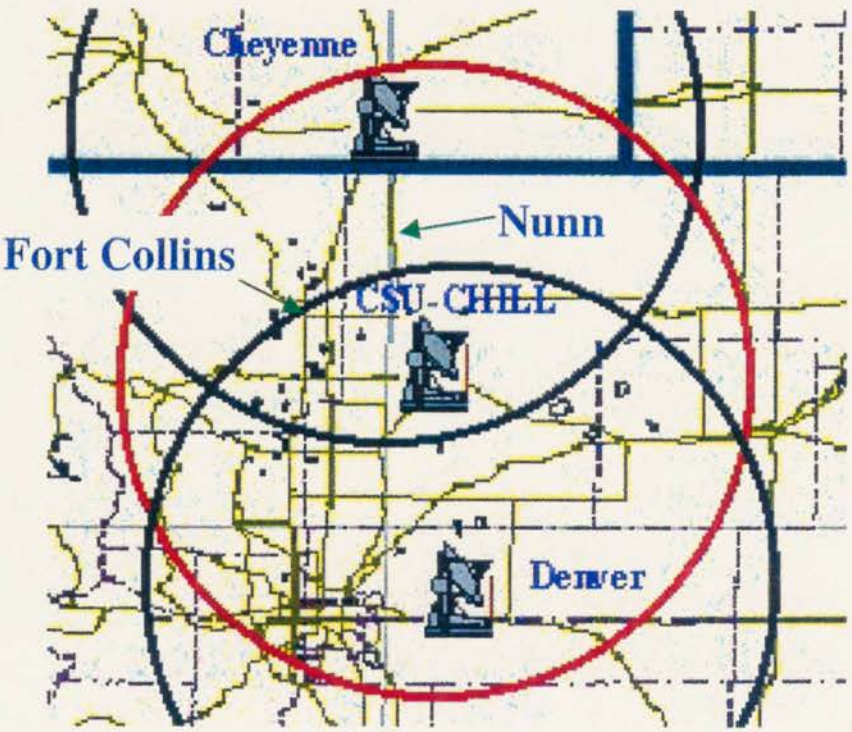


Figure 1.2: Schematic base map of the CSU-CHILL area. The red circle denotes the 100 km range ring of the CSU-CHILL radar, and the black circles denote the 100 km range rings of the Cheyenne, WY and Denver, CO WSR-88D radars.

# CHAPTER 2

# BACKGROUND THEORY

In this chapter we present a brief discussion of multiparameter radar theory, which will serve as the basis for our radar analyses. Additionally, we will discuss thunderstorm electrification theory and provide an overview of previous research on positive CG producing storms, as relevant to the present study.

## 2.1 Multiparameter Radar Theory

Unlike traditional Doppler weather radar which transmits and receives electromagnetic radiation strictly in one polarization plane, a multiparameter radar is capable of transmitting and receiving both horizontally and vertically polarized radiation. Specifically, the CSU-CHILL multiparameter radar, a dual linearly polarized S-band (2.725GHz or 11cm) Doppler radar, alternately transmits horizontally and vertically polarized electromagnetic radiation, and simultaneously detects both polarization states via dual receivers. The multiparameter variables measured by the radar include horizontal reflectivity ($Z_h$), radial velocity ($V_r$), differential reflectivity ($Z_{dr}$), linear depolarization ratio (LDR), correlation coefficient at zero lag $\rho_{hv}(0)$, and differential phase ($\Psi_{dp}$). Although not directly measured by the radar, an additional variable, specific differential phase ($K_{dp}$), can be estimated by filtering the total differential phase ($\Psi_{dp}$) through suitable filtering methods (e.g. Hubbert et al., 1993, Hubert and Bringi, 1995), thus obtaining $\phi_{dp}$, the propagation differential phase. The specific differential phase,

$K_{dp}$, is then obtained from the range derivative of $\phi_{dp}$. When used in conjunction with one another, these variables provide additional information pertaining to hydrometeor size, shape, orientation and thermodynamic phase; enabling inferences on bulk-hydrometeor types as well as improved rain and hail rate estimations (Doviak and Zrnic, 1993; Balakrishnan and Zrnic, 1990 a,b; Zrnic et al., 1993).

Reflectivity is a measure of the amount of power backscattered by individual radar volumes. Under Rayleigh conditions (i.e. particles much smaller than the wavelength of incident radiation), reflectivity depends on the sixth power of the hydrometeor diameter:

$$Z_{h,v} = \{ \pi^5 / \lambda^4 | K |^2 \} D_{h,v}^6 \qquad [mm^6 m^{-3}] \qquad (2.1)$$

where $Z_{h,v}$ is the horizontally and vertically polarized reflectivity factors, respectively, $\lambda$ is the wavelength of incident radiation, $| K |^2$ is the dielectric factor, and $D_{h,v}$ are the horizontal and vertical particle diameters. Of the polarized electromagnetic radiation that is transmitted only a minute portion is backscattered to the receiver. The backscattered radiation may have a component with the same polarization as the incident radiation (co-polar return; denoted by $Z_{hh,vv}$ where the first subscript indicates the polarization state of the transmitted radiation, and the second subscript the polarization state of the received radiation). In addition to the co-polar return, there may also be a component that is polarized orthogonal to the incident radiation, the cross-polar return; denoted by $Z_{hv,vh}$.

Differential reflectivity ($Z_{dr}$) is a measure of the reflectivity-weighted mean axis ratio of hydrometeors, and is a good indicator of particle shape and orientation. $Z_{dr}$ is the logarithmic ratio of the horizontal to vertical co-polar reflectivity factors, defined as:

$$Z_{dr} = 10\log_{10} (Z_{hh}/Z_{vv}) \quad [dB] \qquad (2.2)$$

Since differential reflectivity is a measure of mean oblateness, it is useful in discriminating between large raindrops and hail/graupel particles due to the pronounced differences in shape and orientation between the particle types. Pruppacher and Beard (1970) found that raindrops with diameters larger than 1mm are deformed into oblate spheroids, due to aerodynamic forces, with the preferred orientation of their major axis in the horizontal direction. Therefore, $Z_{dr}$ is positive for raindrops larger than about 1mm in diameter, and increases for larger drop sizes (Fig 2.1). Hail and graupel on the other hand tend to be more spherically symmetric, or exhibit random tumbling motions, leading to $Z_{dr}$ values near zero. Further, because $Z_{dr}$ is reflectivity-weighted, it is also sensitive to the dielectric factor and the size of the scattering hydrometeor. Since the dielectric constant of water particles is higher than that of ice particles (0.93 as opposed to 0.197) a raindrop with the same size and shape of a graupel particle will have a higher differential reflectivity than the graupel particle.

The correlation coefficient at zero lag ($\rho_{hv}(0)$) is a measure of the correlation between horizontally and vertically polarized waves at zero time lag, and depends on the orientation and shape of hydrometeors. For precipitation composed entirely of a single hydrometeor type (i.e. pure rain or pure hail), $\rho_{hv}(0)$ typically exceeds 0.97 (Balakrishnan and Zrnic, 1990); $\rho_{hv}(0)$ drops as the size spectrum of the precipitation particles in the radar pulse volume broadens (shapes become more irregular) or if both raindrops and ice particles coexist in the pulse volume, creating a broad distribution of particle shapes and sizes. Since hailstones are considerably larger, and usually more irregularly shaped than raindrops, $\rho_{hv}(0)$ falls below 0.94 - 0.96 when centimeter-sized hail is mixed with rain. A

minimum in $\rho_{hv}(0)$ occurs when both ice and rain make more or less equal contributions to the total reflectivity of the radar pulse volume.

Linear Depolarization Ratio (LDR) is defined as the ratio of the cross-polar return ($Z_{vh}$) to the co-polar return ($Z_{hh}$), and is defined as:

$$LDR = 10\log_{10}(Z_{vh}/Z_{hh}) \qquad [dB] \tag{2.3}$$

The cross-polar return will be zero for any particle whose major or minor axis is aligned with, or orthogonal to, the polarization of the incident radiation; thus LDR approaches negative infinity in these situations. A cross-polar return (depolarization) arises when a target is non-spherical, and its axis of symmetry is preferentially canted relative to the incident polarization plane. This happens, for example, when oblate particles wobble as they fall, or for hydrometeors of irregular shapes (i.e. hail with protrusions). LDR is also strongly tied to the effective dielectric constant of the hydrometeor (i.e. surface wetting increases the depolarization). For rain, canting is typically small, therefore LDR values typically range from –27 to –34 dB. Low-density graupel has a smaller dielectric constant than that of rain, so LDR values are typically < -30 dB (Doviak and Zrnic, 1993). Melting aggregates provide a water coating which will increase the dielectric constant, while at the same time tend to exhibit random tumbling motions as they fall; thus increasing the depolarization leading to LDR values $\geq$ –20 dB.

Differential phase ($\Psi_{dp}$) is defined as:

$$\Psi_{dp} = \phi_{dp} + \delta \qquad [^\circ \text{ km}^{-1}] \tag{2.4}$$

where $\phi_{dp}$ is the differential propagation phase, and $\delta$ is the backscatter differential phase. The differential propagation phase is defined as $\phi_{dp} = \phi_{hh} - \phi_{vv}$, where $\phi_{hh,vv}$ are the cumulative phase shifts for horizontally and vertically transmitted and received

polarized radiation during the round trip from the radar to the resolution volume and back. Differential propagation phase is a result of propagation through an anisotropic medium such as rain. For Rayleigh conditions, $\delta = 0$, however when the radar resolution volume contains particles large enough ($\geq 0.75$ cm for $\lambda = 11$ cm) to scatter in a Mie regime, $\delta$ becomes non-zero and must be considered. In practice, the $\delta$ contribution is separated from $\phi_{dp}$ through the use of filtering techniques (Hubbert et al., 1993).

The specific differential phase ($K_{dp}$) is calculated from the range derivative of $\phi_{dp}$. Once the filtering process described above is applied to $\Psi_{dp}$ to remove the contribution from $\delta$, $K_{dp}$ can be calculated using finite differencing techniques. Measurements of $\phi_{dp}$ at two different ranges, $r_1$ and $r_2$ can be used to calculate $K_{dp}$ as follows:

$$Kdp = 1/2\ d\phi_{dp}/dr \equiv [\phi_{dp}(r_2) - \phi_{dp}(r_1)]/2(r_2 - r_1) \quad [^\circ\ km^{-1}] \qquad (2.5)$$

Isotropic hydrometeors such as hail produce equal phase shifts for either polarization, so that any phase shift is due to anisotropic particles in the volume, such as oblate raindrops. As a result, $K_{dp}$ is only affected by oblate rain in a rain-hail mix (Fig. 2.2). Because $K_{dp}$ is basically insensitive to hail, this variable provides improved estimations of rain rate (compared to Z-R estimations), even in mixed-phase environments. Specific differential phase can be used in conjunction with horizontal reflectivity to separate contributions of rain and hail to total reflectivity, thus allowing for estimates of hail rates in addition to rain rates (Balakrishnan and Zrnic, 1990b; Carey and Rutledge, 1998; Lang, 1997).

## 2.2 Thunderstorm Electrification

Although the exact processes by which thunderstorms become electrified and ultimately lower charge to the surface of the Earth is still debated, there are two well developed competing theories. These theories can be classified into two broad categories: (1) the convective theory (Vonnegut, 1963; Wagner and Telford, 1981), and (2) the precipitation theory centered on the non-inductive charging (NIC) mechanism (e.g., Takahashi, 1978; Jayaratne et al., 1983; Saunders et al., 1991).

The convective theory proposes that warm air currents (updrafts) carry positively charged ions released from the Earth's surface into the developing thunderstorm. As these ions pass through the cloud they attach to cloud water droplets (Chiu and Klett, 1976) and continue to disperse throughout the storm. While these positively charged particles move through the cloud they begin to attract negatively-charged ions, situated in the upper troposphere, to the cloud's periphery. The negative ions also attach to water droplets and become entrained into the cloud where convective downdrafts transport them toward the Earth's surface (Vonnegut, 1963). This descending negative charge would lead to the development of a positive dipole, and further result in the incorporation of more positive ions into the lower portions of the cloud, which are then transported into the cloud thus creating a positive feedback cycle. This model, however, does not explain the tripole charge structure of thunderstorms, nor can it produce lightning on time scales similar to those of developing thunderstorms (Williams, 1989). This theory also does not seem to account for the pronounced electrical activity that is associated with mixed-phase precipitation.

Precipitation theories, on the other hand, exchange charge between particles in various thermodynamic states by non-inductive (Takahashi, 1978; Saunders et al., 1991) and inductive (Illingworth and Latham, 1987) processes. To date, the non-inductive charging mechanism appears to be the most promising method of thunderstorm electrification (Williams, 1989). It has been shown in laboratory studies that significant charge transfer can occur when millimeter-sized graupel particles collide with smaller ice crystals (diameter ~ 100 μm) in the presence of supercooled water (Reynolds et al., 1957; Takahashi, 1978; Jayaratne et al., 1983; Saunders et al., 1991; Avila et al., 1998). It was found that the magnitude and sign of charge transferred to the rimer during these graupel/ice collisions is a function of temperature and liquid water content (LWC). Figure 2.3 shows the dependence of the charge transferred to the rimer on temperature and LWC. Smoothed contours connect points of equal magnitude with the shaded area representing the LWC and temperature which produced a negative charge on the rimer. Note that at temperatures warmer than $-10^{O}$C, the rimer is positively charged, regardless of LWC.

Figure 2.4 provides a schematic diagram of how the non-inductive model works. As graupel particles grow in the mixed-phase region of the thunderstorm (region B in Fig. 2.4), and are suspended by convective updrafts, small ice crystals are swept past the graupel and subsequently transported into the upper portions of the storm. Rebounding collisions between the graupel particles and the ice crystals, in this region, result in negative charge being deposited on the graupel particle, and positive charge on being deposited on the ice crystals. This process leads to the development of an electrical dipole, with positive charge situated over negative charge. Once the graupel's terminal

velocity exceeds the storm updraft speed, it will begin to fall towards the surface of the Earth. Graupel/ice crystal collisions occurring below the charge reversal temperature region A in Fig. 2.4), which is some threshold between $-10^{o}$C and $-20^{o}$C dependant on liquid water content (LWC), will result in the falling graupel particle becoming positively charged and the ascending ice crystals negatively charged. The rising ice crystals can contribute to the elevated negative charge region, while the descending graupel produce a small positive charge region below the main negative charge center. The result is the development of an electrical tripole model (with the negative charge region sandwiched between two positive charge regions) in good agreement with the observed tripole structure of thunderstorms (Williams, 1989).

## 2.3 Positive Cloud-to-Ground Lightning

Lightning is the most dangerous and frequently encountered weather hazard experienced each year. It is the second most frequent weather related killer in the United States (floods and flash floods are number one) with nearly 100 deaths and 500 injuries each year (Mogil et al., 1977; Lopez et al., 1995; Lushine, 1996). Monetary losses approach $4-5 billion annually (Fig. 2.5; National Lightning Safety Institute, 1998) as a result of this phenomenon.

Lightning consists of individual electrical discharges, called flashes. Each flash goes from point to point in the air (in-cloud, or IC), or from the air to the ground (cloud-to-ground, or CG). CG lightning can be further subdivided into two categories, those that lower negative charge to ground (negative CG) and those that lower positive charge to ground (positive CG). Typically, more than 90% of the warm season CG lightning is of

negative polarity (Fuquay 1982; Orville et al. 1987; Reap and MacGorman 1989; Orville 1994; Orville and Silver 1997). Curiosity regarding this scarcity of positive CGs has triggered many studies on the origin of these flashes.

As noted in Chapter 1, positive ground flashes have been identified in several different non-severe weather scenarios. In recent years, however, positive ground flashes have also been identified with tornadic supercells, as well as other severe storms (Reap and MacGorman, 1989; Curran and Rust, 1992; Branick and Doswell, 1992; Carey and Rutledge, 1998).

In a study of cloud-to-ground lightning during the 1985-86 warm season, Reap and MacGorman (1989) compared lightning data to manually digitized radar (MDR) data, along with severe storm reports, and found a correlation between the occurrence of severe weather and elevated rates of positive CG flashes. They found positive flash density to be directly related to radar reflectivity, and discovered the highest frequency of severe weather reports for a given positive flash density were large hail reports, followed by wind damage and finally, tornadoes (Fig. 2.6).

Branick and Doswell (1992) studied the outbreak of several tornadoes stretching from southern Oklahoma into Nebraska and found a relationship between supercell structure and lightning ground strike polarity. Lightning data collected during these events revealed that the storms occurring from north-central Oklahoma into central Nebraska we dominated by positive CGs, while storms to the south by negative CGs. The tornadoes, and positive CGs, occurring in the northern storms were observed to occur in areas free of significant precipitation - associated with low-precipitation (LP) supercells. Conversely, tornadoes, and negative CGs, occurring in the southern storms

had significant precipitation within the mesocyclone regions - associated with high-precipitation (HP) supercells. LP supercells are characterized by the horizontal displacement of their primary updrafts and downdrafts, thus explaining the lack of precipitation within the mesocyclone region of the storm. The shear which causes the displacement of these drafts also causes the positively charged upper anvil region of the storm to be displaced laterally from the lower negative charge hence causing a tilted dipole (Brook et al., 1982). It is thought that the tilted dipole, and resulting "unshielding" of the upper charge region, led to the high positive flash densities in these LP storms. Branick and Doswell (1992) suggest that a validated relationship between positive CG frequency and supercell type could be used in an operational context to aid in the issuance of severe weather warnings; they caution however that the use of such a relationship is contingent on whether or not the correlation between elevated positive CG rates and supercell type can be demonstrated "routinely and reliably".

Curran and Rust (1992) observed the same relationship as Branick and Doswell (1992) in an isolated severe thunderstorm. They found that positive CG flash rates in this storm peaked during the LP stage and decreased to almost zero shortly after the storm had transitioned to the supercell stage.

In contrast to the findings of Branick and Doswell (1992) and Curran and Rust (1992), Carey and Rutledge (1998) found positive ground strikes to dominate during supercell, multi-cell, and squall-line structures, showing that positive CG lightning is not a "unique" signature of LP supercells. They deduced that the common characteristic of most storms dominated by positive CG lightning is storm severity (i.e. the presence of large hail and possibly tornadoes). The analysis of Carey and Rutledge (1998) found

(1) positive CG lightning to be negatively correlated in time with large hail, as peaks in large hail typically reached the surface 20-35 minutes prior to a broad maxima in positive CG lightning, (2) the majority of positive CG lightning struck ground in regions of light rain with little or no hail, (3) maxima in positive CG lightning flash rate tended to occur coincident, or just after the collapse of high-reflectivity convective cores, and (4) clusters of positive CG lightning were observed to occur with the rapid increase in the surface mass flux of the storm. These findings lead Carey and Rutledge (1998) to propose the precipitation "unshielding" hypothesis (discussed in Chapter 1) as a possible explanation for the elevated positive CG characteristics observed in this storm.

Clearly positive CG lightning appears to be associated with some severe weather events, but obviously this is a "one way" correlation. In addition to Branick and Doswell (1992), MacGorman and Burgess (1994) also emphasized that the correlation between positive CG lightning and severe storms is valid only in the forward direction, noting that severe weather frequently occurs in storms dominated by negative flashes as well. It is clear that more studies of positive CG producing severe storms need to be done in an effort to further explain this correlation. This thesis will contribute in this manner, and help to better elevate the hypotheses discussed in Chapter 1, specifically the tilted dipole hypothesis, the enhanced lower positive charge (or inverted dipole) hypothesis, and the precipitation "unshielding" hypothesis.

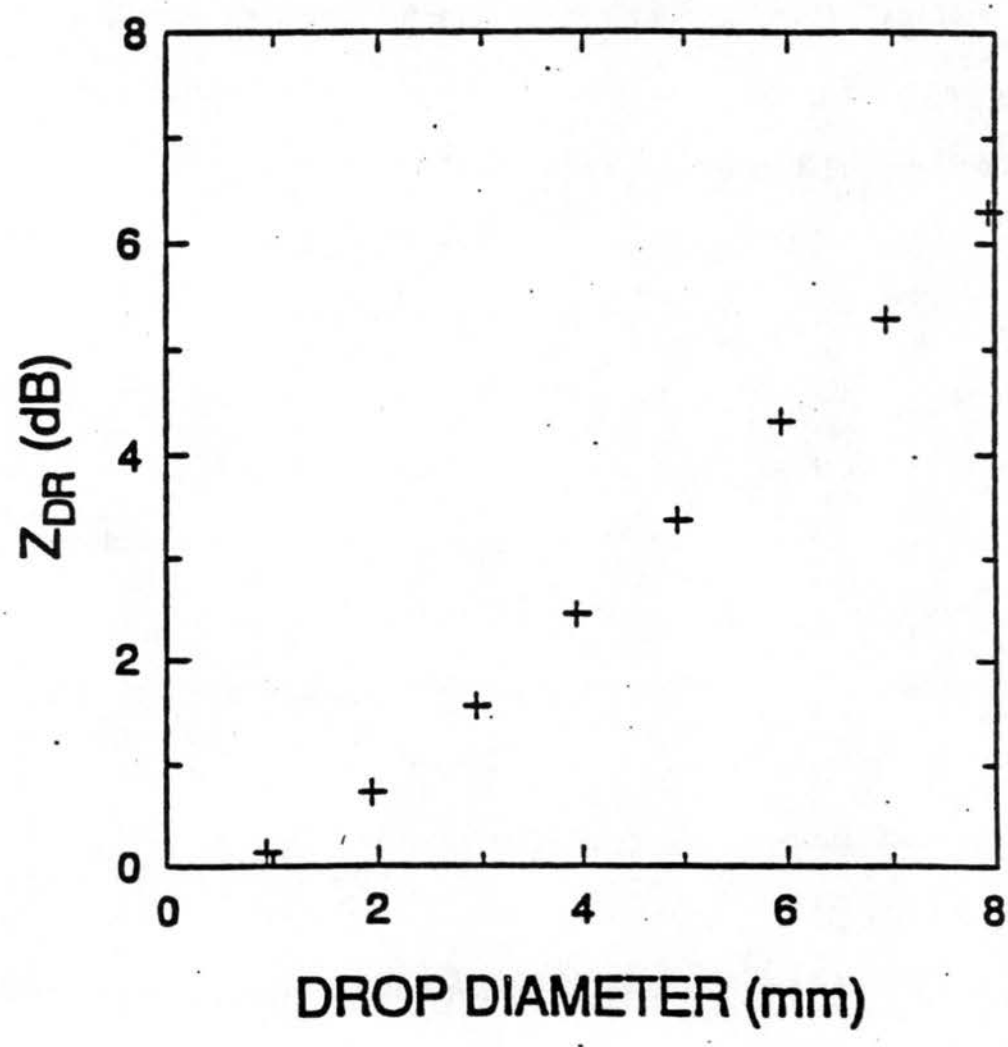


Figure 2.1: Calculations of $Z_{dr}$ in dB as a function of drop diameter for the drop-size shape relationship of Beard and Chuang (1987). Calculations use the scattering theory of Gans (1912).

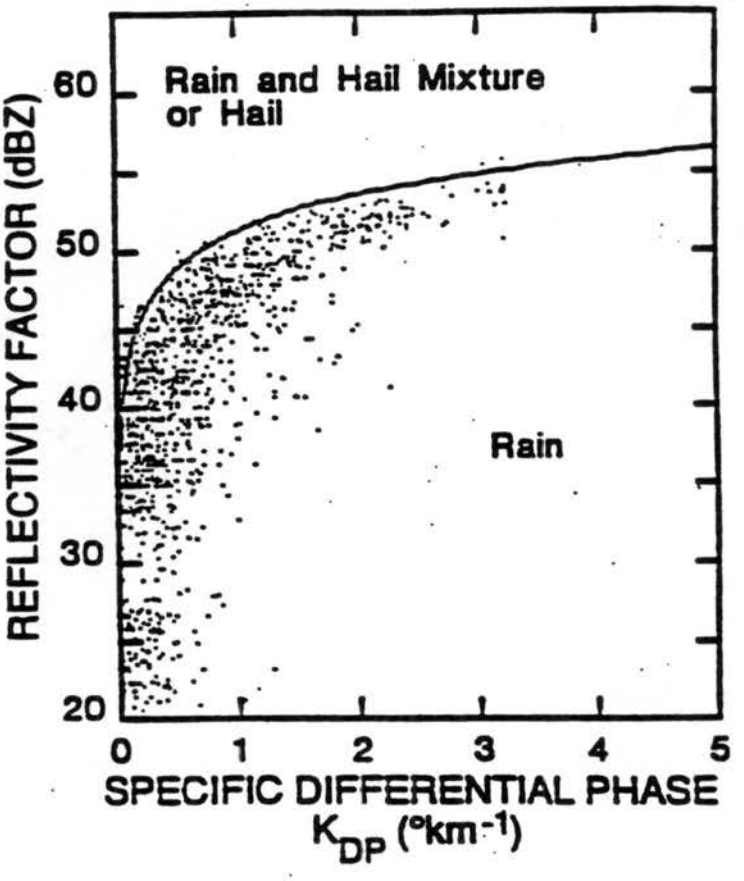


Figure 2.2: Scatter plot of Z-$K_{dp}$ of about 1400 radar measurements for an Oklahoma rainstorm on 10 June 1986. The empirical boundary between rain and mixed phase of hail is shown in a solid line. Z is an average of reflectivity factors at horizontal ($Z_h$) and vertical ($Z_v$) polarizations. (Adapted from Balakrishnan and Zrnic, 1990)

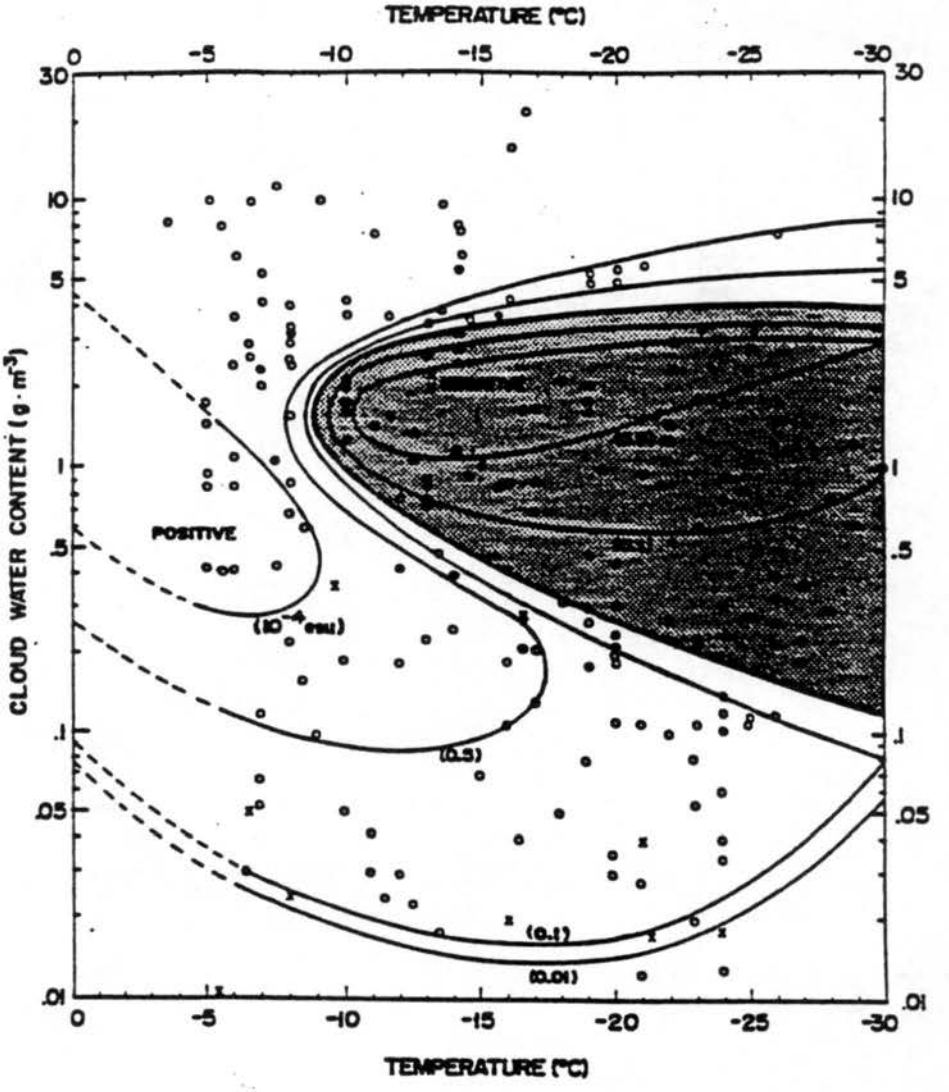


Figure 2.3: Electrification of rime as a function of temperature (°C) and cloud water content (g $m^{-3}$) for the laboratory experiments of Takahashi (1978). Solid circles depict negative charge, open circles positive charge, and crosses uncharged cases. The shaded area represents negative rime charging. The amount of electric charge of rime, on a single collision with an ice crystal, is shown in units of $10^{-4}$ esu.

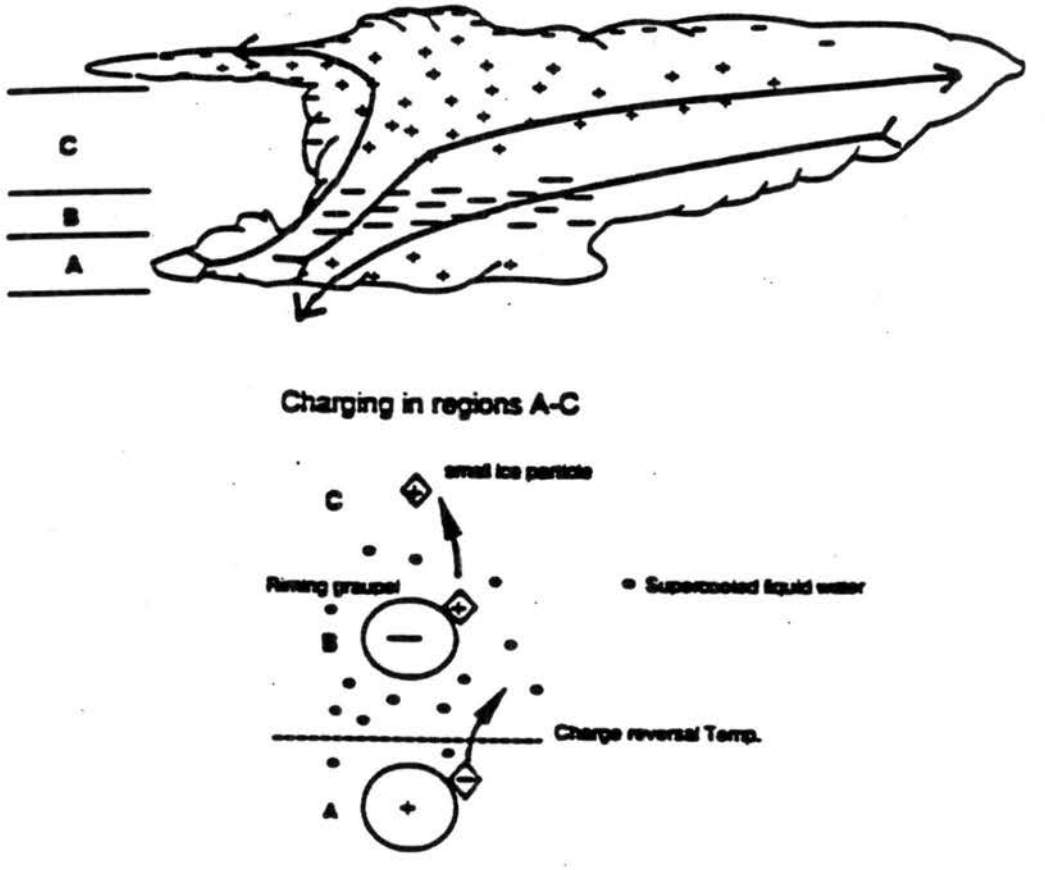


Figure 2.4: Illustration of the non-inductive charging process for a graupel/ice crystal collision in the presence of supercooled liquid water. See text for detailed explanation.

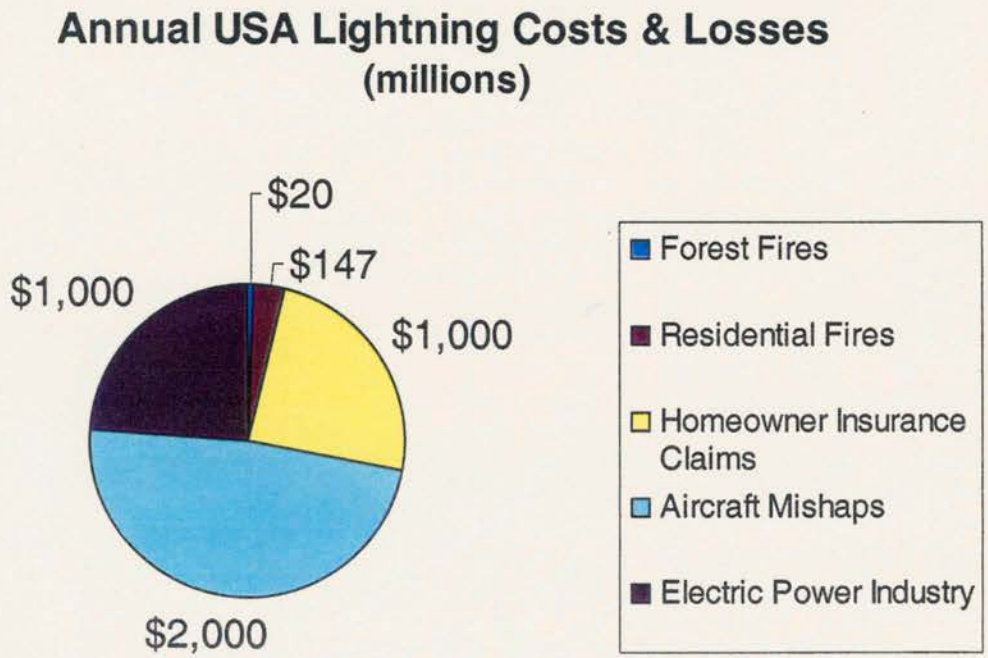


Figure 2.5: Annual monetary losses across the contiguous United States due to lightning. (Adapted from the National Lightning Safety Institute, 1988)

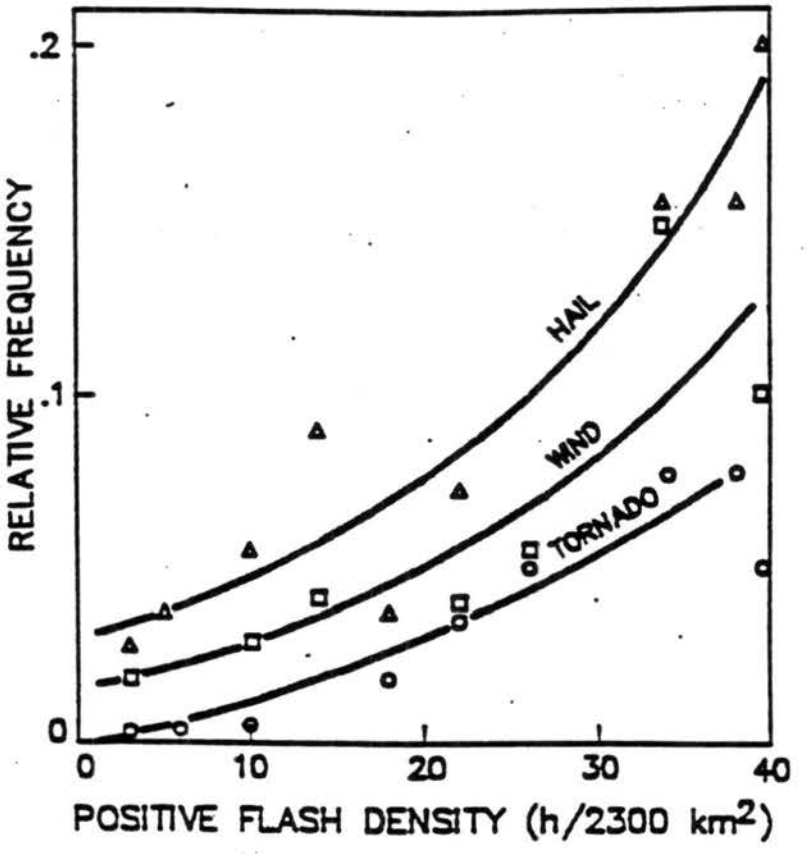


Figure 2.6: Fraction of grid blocks (relative frequency) containing large hail, damaging winds, or tornadoes as a function of positive flash density. (Adapted from Reap and MacGorman, 1992)

# CHAPTER 3

# DATA AND METHOD

## 3.1 Overview

In this chapter we discuss the data sets and methodology used in this study. We describe the lightning and radar data used in this study in Sections 3.2 and 3.3, respectively. Methods used in our regional climatology of cloud-to-ground lightning, case study selection, and radar analyses are then described in Sections 3.4, 3.5, and 3.6, respectively.

## 3.2 Lightning Data

The lightning data used in this study was acquired and processed by the National Lightning Detection Network (NLDN), under the control and management of Global Atmospherics, Inc. (GAI), of Tucson, AZ. The NLDN records the time, location, polarity, signal strength and multiplicity (number of return strokes) of CG flashes detected over the contiguous U.S. (Cummins et al. 1995, 1996, 1998). The NLDN is comprised of 105 electromagnetic sensors (Fig. 3.1), a satellite communications system, and a central processor (Fig. 3.2). In 1995 the NLDN underwent a network-wide upgrade in order to (1) increase the location accuracy of CG flashes and (2) increase the detection efficiency (Fig. 3.3) of low peak current CG flashes down to 5kA (Cummins et al. 1998). Results from Zajac (1998) and other studies indicate that the upgrade did succeed in increasing the detection of low peak current CG flashes; both mean positive and negative

peak currents showed lower values between 1995 (post-upgrade) and 1994 (pre-upgrade). While the findings listed above were expected from the upgrade, the detection of a large population of low peak current positive CG flashes over localized areas was not anticipated. It has been suggested that low peak current positive CG flashes on the order of a few kiloamps are false detections of IC lightning (e.g., Lopez et al. 1991). Some researchers have proposed using a 7kA peak current threshold for positive CG lightning in order to eliminate the false detection of IC lightning (P. Krehbiel, personal communications, 1998); we are electing to utilize this threshold in our subsequent analysis (described in Sec. 3.4).

### 3.3 Radar Data

The radar data used in this study was collected by the 11cm Colorado State University (CSU) CHILL multiparameter Doppler radar. System characteristics for the radar are given in Table 3.1. For each of the case studies presented in this thesis the CSU-CHILL radar measured the radial velocity ($V_r$), horizontal reflectivity ($Z_h$), differential reflectivity ($Z_{dr}$), differential phase ($\Psi_{dp}$), linear depolarization ratio (LDR), and correlation coefficient at zero-lag between horizontally and vertically polarized waves ($\rho_{hv}(0)$).

A sector scanning scanning strategy was used by the CSU-CHILL during the data collection for each of the cases studied in this thesis. Full volume coverage of each storm with preservation of good temporal resolution (~ 5 minutes or less) was typically achieved. Individual elevation sweeps were typically spaced 1° or less, with azimuthal limits such that most or all of the echo exceeding 30 dBZ was observed. At times, the

size and proximity of the storm required spatial resolution to be sacrificed in order to maintain good temporal resolution. In such events the radar may not have scanned to the top of the echo volume ("topped" the storm), or it may have used a more restrictive azimuthal range and therefore may not have sampled the horizontal extent of the storm at each elevation sweep. Specific instances in which spatial resolution was sacrificed will be discussed on a case by case basis in Chapter 5.

## 3.4 Methodology: Regional Climatology of Cloud-to-Ground Lightning

Since the purpose of developing this regional climatology is to determine storm scale lightning characteristics, as opposed to individual stroke statistics, a gridded analysis was performed on NLDN data within the area of interest (AOI; Fig. 1.1) for the summers (May–Aug) of 1996, 1997, and 1998.

The LLP signal strength values recorded by the NLDN were first converted from LLP units to peak current in kiloamps (kA) (Eqn. 3.1) using the estimates of Idone et al. (1998a) and Cummins et al. (1998).

$$I_{peak} = 0.185 \bullet I_{LLP} \quad \text{(kA)} \tag{3.1}$$

After converting signal strength to peak current we determined the optimum spatial and temporal resolutions to be used. To do this, three different gridding schemes were tested on a subset of the data (summarized in Table 3.2). It was found that the averaged values for each grid box varied significantly between the three different gridding schemes (Fig. 3.4a), however when the data were normalized by the total number of grid boxes, the results showed the same trends regardless of the gridding scheme

(Fig. 3.4b). These findings were consistent for the averaged values of positive and negative peak currents and multiplicity. They were, however, not applicable in the case of the flash density frequency distributions (Fig. 3.5).

Figure 3.6 illustrates why normalizing the flash density data for each gridding scheme does not result in similar trends in the frequency distributions for each resolution. Basically, it is a result of the scaling used between the gridding schemes. For example, if in a 60 minute period only one lightning strike was detected in a given 50km × 50km area, the flash density associated with that single strike would be 0.0004 flashes $km^{-2}$ $hr^{-1}$ when computed using the 50km × 50km / 60 minute gridding scheme. That same strike would also fall into a single 25km × 25km grid box, as well as a 10km x 10km grid box. The flash densities associated with a single stroke at the 25km × 25km / 30 minute and 10km × 10km / 15 minute resolutions are 0.0032 and 0.04 flashes $km^{-2}$ $hr^{-1}$, respectively. In order to get meaningful frequency distributions for resolutions other than 50km × 50km / 60 minutes, we must modify the distribution bins using the flash density associated with one flash per grid box as our lower limit.

These findings indicate that regardless of the gridding scheme used, we can expect the same general results once the appropriate lower limit is selected for flash densities. It was therefore determined that the 25 km × 25 km / 30 minute gridding scheme provided the optimum resolution for capturing/identifying storm-scale lightning characteristics.

Upon final selection of the gridding scheme, the complete NLDN data set was gridded, yielding over 9 million grid boxes analyzed (Table 3.2). For each grid box, positive and negative flash densities were calculated and used to determine the positive

CG fraction. Averaged positive and negative peak current and multiplicity values were also calculated for each grid box.

After gridding the data, three-dimensional frequency distributions were generated for each parameter (peak current, multiplicity and density, each as a function of percentage of positive CG fraction) and analyzed in an effort to aid in the lightning characterizations. Further, maps of each gridded parameter were also generated to aid in our analysis.

## 3.5 Methodology: Case Study Selection

As outlined in Chapter 1, it has been suggested by some researchers that severe thunderstorms may be characterized by greater than 50 percent positive CG fraction, coupled with high flash densities of positive strikes. Stolzenburg (1994) suggested using a positive flash density of 0.01 flashes $km^{-2}\ hr^{-1}$ as the "significant" flash density threshold. This threshold seems to be applicable to our 50km × 50km / 60 minute gridding resolution (equivalent to 25 flashes per grid box), however it needed to be modified for our 25km × 25km / 30 minute gridding scheme. We found that in the case of the former, 8.5% of the grid boxes containing lightning met the two criteria offered by Stolzenburg. We then analyzed the 25km × 25km / 30 minute resolution data to determine what flash density threshold, when coupled with the requirement for greater than 50% positive CG fraction, would partition 8.5% of the grid boxes and found this to be equal to a value of 0.03 flashes $km^{-2}\ hr^{-1}$, or 9 flashes per grid box. All grid boxes were then analyzed to see if they met the following criteria:

(1) spatially located within 100km range of the CSU-CHILL multiparameter radar,

(2) contained greater than 50% positive CG fraction, and (3) contained a positive flash density greater than or equal to a value of 0.03 flashes $km^{-2} hr^{-1}$. This analysis, summarized in Table 3.3, yielded a total of 49 days in which at least 1 significant grid box was found, totaling 139 significant grid boxes in all. Since some days had multiple grid boxes occurring, which may or may not be spatially and/or temporally correlated to one another, complete time-series animations of the NLDN data were generated (1 image every 30 minutes). A subjective analysis was then performed to identify the number of significant cases; our analysis identified a total of 68 significant cases. We then continued our subjective analysis, identifying a total of 16 cases that contained at least one significant electrical transition as described in Chapter 1. We then cross referenced the 16 identified potential cases with the data archives at the CSU-CHILL and found that there were only 4 instances in which detailed radar data was available; 2 June 1997, 1 July 1998, 2 July 1998 and 21 July 1998.

## 3.6 Methodology: Radar Analysis

Radar data from CSU-CHILL radar for each case study were edited using the Research Data Support System (RDSS) software developed at the National Center for Atmospheric Research (NCAR; Oye and Carbone, 1981). Most ground clutter and unwanted clear air echo were removed by thresholding on $Z_h$ (removing data with $Z_h < 0$ dBZ) and $\rho_{hv}(0)$ (removing data with $\rho_{hv}(0) < 0.7$). The threshold value for $Z_h$ seems appropriate since the reflectivity-rain rate relationship (Z-R relationship) used for light rain in this study (Jones, 1955) corresponds to a rain rate much less than 1mm $h^{-1}$, thereby eliminating any significant impact to precipitation measurements made in this

study (to be discussed later). Similarly, the thresholded value used for $\rho_{hv}(0)$ is well below any value seen in precipitation data (Carey and Rutledge, 1998; Lang, 1997) thus also minimizing any negative impacts in our analysis. As necessary, manual editing of the data was performed to eliminate remaining ground clutter and clear air echos.

Despite the overall sensitivity of the CSU-CHILL radar, drift in the transmitter trigger delay can cause positive or negative variations (or biases) in $Z_{dr}$ to occur (Butler, 1998). If not accounted for, this bias could significantly impact the discrimination of various hydrometeor types based on their $Z_{dr}$ value (to be discussed later). We expect the anvil region of a storm to contain small ice crystals and aggregates, whose median $Z_{dr}$ values should be near 0 dB. In order to determine the $Z_{dr}$ bias for each case study, several histograms of $Z_{dr}$ values in the low-reflectivity anvil regions were generated. If the median $Z_{dr}$ value was different than $0 \pm 0.2$ dB (P. Kennedy, personal communications) a bias was assumed, and the data were adjusted accordingly.

Once all editing had been completed and $Z_{dr}$ biases determined, a low-pass filter was applied to the range profile of $\Psi_{dp}$ to remove high frequency fluctuations in range due to backscatter differential phase ($\delta$), retaining the overall trend in $\phi_{dp}$ (Hubbert et al., 1993). Specific differential phase ($K_{dp}$) was then calculated by applying a finite differencing approximation (Eqn. 2.5).

All polarimetric variables (to include the newly generated $K_{dp}$ field) were then interpolated from polar to Cartesian coordinates using the REORDER software package, also developed at NCAR. The gridding scheme used a Cressman filter (Cressman, 1959), with a variable radius of influence. For the filtering process, azimuthal spacing was assumed to be 1°, the half-power width provided by the CHILL antenna. Elevation

spacing was also set to be 1°, because most elevation sweeps were spaced 1° or less apart. Grid resolutions of 1 km in the horizontal and 0.5 km in the vertical direction were used.

Once all data were gridded, a hydrometeor identification matrix (Table 3.4, identical to the one used by Carey and Rutledge, 1998, with one exception) was applied to each grid box in the analysis region. This matrix employs the use of $Z_h$, $Z_{dr}$, LDR, $K_{dp}$ and $\rho_{hv}(0)$ to partition each grid box below the freezing level, into one of the following categories: (1) small hail (diameter < 2 cm), (2) small hail mixed with rain, (3) large hail (diameter > 2 cm), (4) large hail mixed with rain, and (5) rain only. Above the freezing level, the same variables were used to distinguish between hail (diameter > 1 cm), graupel/small hail, and vertically oriented ice crystals ($T \leq -20°C$). The discrimination between hail and graupel/small hail was not included in the matrix developed by Carey and Rutledge (1998), and such a discrimination is difficult to justify. Here we have to rely heavily on radar reflectivity, and to some extent LDR, to discriminate between hail and graupel/small hail. Since we are above the freezing level we can assume that the ice particles are dry (Carey, 1995), therefore the primary difference between the two types of ice that we are trying to discriminate are size and density. If we recall the dependence of radar reflectivity on the particle diameter (Eqn. 2.1) we see that, for a given particle concentration, decreasing particle size would lead to decreasing values of radar reflectivity. Our lower reflectivity boundary for the discrimination of large hail (diameter > 1 cm) above the freezing level is $Z_h \geq 55$ dBZ. We would expect graupel and smaller hail to be present in higher concentrations than large hail, this will have a positive effect on $Z_h$ as discussed above. However, in most instances, the decrease in particle diameter

will have a larger negative effect on $Z_h$, therefore we chose $Z_h < 55$ dBZ as our upper boundary for the discrimination of graupel/small hail. This is not to say that graupel and small hail will not exist at reflectivities greater than or equal to 55 dBZ, especially during period of high concentrations. If anything, the use of this upper boundary would lead to underestimation of graupel and small hail above the melting level as opposed to over estimations. Our choice of LDR $\leq$ -26 dB, as compared to > -26 dB for hail (diameter > 1 cm), is based on the fact that we would expect the large, denser hail to be more irregularly shaped (i.e. more protuberances) and fall in more of a wobbling motion, causing canting of the major and minor axis. Also, as previously stated, the density of hail is higher than that of graupel; the higher density ice leads to a higher dielectric factor.

In addition to distinguishing between the presence of the hydrometeor types identified above, this thesis also used the polarimetric variables to calculate near-surface rain and hail rates, enabling us to estimate storm-total mass fluxes for each hydrometeor type.

Rain and hail rates were calculated through the following algorithm, identical to the one used by Lang (1997) and summarized in Table 3.5. If the specific differential phase at a grid point is above the noise level, 0.25° $km^{-1}$, then $K_{dp}$ is used to calculate the rain rate through the following equation (Sachidananda and Zrnic, 1987):

$$R(K_{dp}) = 40.683 \bullet (K_{dp})^{0.866} \qquad mm\ h^{-1}. \qquad (3.2)$$

If Kdp < 0.25° $km^{-1}$, then a reflectivity-rain rate relationship from Jones (1955) is used to calculate the rain rate:

$$Z_h = 486 \bullet R(Z_h)^{1.37} \qquad mm\ h^{-1}. \qquad (3.3)$$

If this rain rate is between 1 and 20 mm $hr^{-1}$, then it is used in the flux calculation described below. If the Z-R relationship gives a rain rate greater than 20 mm $hr^{-1}$, then it is assumed that the reflectivity is almost entirely due to hail, and no rain rate is calculated at that grid point. Instead, we must determine the portion of the total reflectivity that is due to rain and subtract that from the total reflectivity to get the amount of reflectivity due to hail.

$$Z_{total} = Z_{rain} + Z_{hail} \qquad mm^6\ m^{-3}. \qquad (3.4)$$

To do this we use $K_{dp}$ to determine the reflectivity factor (in $mm^6\ m^{-3}$) due to rain at a grid point by substituting the $K_{dp}$-R relationship from Sachidananda and Zrnic (1987) into the Z-R relationship from Jones (1955). Substituting Eqn. 3.1 into Eqn. 3.2,

$$Z_{rain} = 77899 \bullet K_{dp}^{1.186} \qquad mm^6\ m^{-3}. \qquad (3.5)$$

Once isolated, we determine if $Z_{hail}$ is within 7 dB of $Z_{rain}$. If so, then the hail rate is assumed negligible, after Balakrishnan and Zrnic (1990b). If the hail rate is assumed to be non-negligible, we use a hail-reflectivity relationship (Carey and Rutledge, 1998; based on the Cheng and English, 1983, hail size distribution) to determine the actual hail rate in mm $h^{-1}$, liquid equivalent.

$$H(K_{dp}, Z_{hail}) = 88.0 / \exp[5.38 \times 10^{-6} Z_{hail} \{K_{dp}\}^{-0.297}] \qquad mm\ h^{-1} \qquad (3.6)$$

With the rain and hail rates calculated at each grid point in our analysis region, the next step was to calculate the precipitation fluxes of both rain and hail. Fluxes were computed by summing all precipitation rates over the horizontal analysis region at a specific level in the storm. We chose to compute the fluxes at a height of 0.5 km AGL since this level was typically the lowest level in the gridded radar volumes.

Although careful effort was made to ensure that the partitioning of the five-dimensional space of $Z_h$, $Z_{dr}$, $K_{dp}$, LDR, and $\rho_{hv}(0)$ lead to eight separate and distinct hydrometeor types, multiparameter radar measurements are not unique. This means that more than one hydrometeor mix could give the same set of multiparameter radar measurements; thus leading to the potential for misidentification of hydrometeor types in our analysis. Further, using polarimetric variables used to derive rain rates, as described above, can have some error associated with it. Although, as described in Chapter 2, the use of $K_{dp}$ provides a superior estimate of rain rates, variations in the drop size distribution along with radar estimation errors can lead to rain rate errors on the order of 10-20% (Chandrasekar et al., 1990). Rain rates derived from Z-R relationships are prone to errors of 30-40% (on the low end) when rain rates are greater than 20 mm $h^{-1}$, due to the possibility of hail contamination which would lead to over-estimation of the true rain rate. For rain rates less than 20 mm $h^{-1}$, however, Z-R derived rain rates have errors comparable to those of $K_{dp}$ derived rain rates. Further, hail rate calculations are also prone to error. The computation of $Z_{rain}$ used in Eqn. 3.4 to isolate $Z_{hail}$ is subject to errors on the order of a few dBZ (Doviak and Zrnic, 1993). The hail size distribution used in our algorithm (Cheng and English, 1983) can also introduce error into our calculations as it may not always be valid. Further, our algorithm assumes Rayleigh scattering by hail, which may not always be the case, especially in the case of large, wet hail.

| CSU-CHILL Radar Characteristic | Value |
|---|---|
| Wavelength (cm) | 11 |
| Antenna diameter (m) | 8.5 |
| 3 dB beamwidth (°) | 1.0 |
| Peak power (kW) | 800 |
| Pulse length/2 (m) | 150 |
| Pulse repetition frequency (Hz) | 1000 |
| Number of samples | 128 |
| Receiver noise power (dBm) | -115 |
| Maximum range (km) | 150 |

Table 3.1: CSU-CHILL radar characteristics.

Spatial and Temporal Gridding Resolutions

| Spatial Resolution | | | Temporal Resolution | Total # of Grid Boxes |
|---|---|---|---|---|
| **km x km** | **Lat x Lon** | **# of Grid Boxes in AOI** | **(minutes)** | **M,J,J,A 1996/97/98** |
| 10 x 10 | $0.0899^{o}$ x $0.1179^{o}$ | 3,481 | 15 | 123,310,944 |
| 25 x 25 | $0.2249^{o}$ x $0.2944^{o}$ | 529 | 30 | 9,369,648 |
| 50 x 50 | $0.4497^{o}$ x $0.5928^{o}$ | 121 | 60 | 1,071,576 |



Table 3.2: Spatial and temporal gridding resolutions used in our regional climatology of cloud-to-ground lightning.

**Summary of NLDN Gridded Analysis**

| | |
|---|---|
| Case Days Identified: | 49 |
| "Significant" Grid Boxes Identified: | 139 |
| "Significant" Cases Identified: | 68 |
| Potential Cases Identified: | 16 |
| Cases in which detailed radar data was available: | 4 |

Table 3.3: Summary of our gridded NLDN analysis. A case day is defined as a day in which one or more "significant" grid boxes was identified; a "significant" grid box is one which met the following criteria: (1) located within 100 km of the CSU-CHILL radar, (2) contained > 50% positive CG fraction, and (3) contained a positive flash density $\geq 0.03$ flashes $km^{-2}$ $hr^{-1}$; "significant" cases denotes the total number of individual cases idntified; potential cases are those significant cases that contained at least one significant electrical transition.

Bulk-Hydrometeor Identification Using Multiparameter Radar Data

| Hydrometeor Type | $Z_h$ (dBZ) | $Z_{dr}$ (dB) | LDR (dB) | Kdp (° $km^{-1}$) | $\rho_{hv}(0)$ |
|---|---|---|---|---|---|
| **T ≥ 0°C** | | | | | |
| 1. Small hail (D < 2 cm) | ≥ 50 | ≤ 0.5 | < -18 | < 0.5 | > 0.96 |
| 2. Small hail and rain | ≥ 50 | < 1.0 | -27 to -20 | ≥ 0.5 | ≤ 0.98 |
| 3. Large hail (D > 2 cm) | ≥ 55 | ≤ 0.5 | ≥ -18 | < 0.5 | ≤ 0.96 |
| 4. Large hail and rain | ≥ 55 | < 1.0 | ≥ -20 | ≥ 0.5 | ≤ 0.96 |
| 5. Rain | ≤ 60 | > 0.5 | ≤ -27 | ≥ 0.5 | ≥ 0.97 |
| **T < 0°C** | | | | | |
| 6. Hail (D > 1cm) | ≥ 55 | < 0.5 | > -26 | < 0.5 | > 0.97 |
| 7. Graupel and small hail | < 55 | < 0.5 | ≤ -26 | < 0.5 | > 0.97 |
| **T ≤ -20°C** | | | | | |
| 8. Vertically oriented ice crystals | ≤ 40 | not used | not used | < -0.25 | not used |

Table 3.4: Bulk hydrometeor identification matrix using CSU-CHILL multiparameter data. (Adapted from Carey and Rutledge, 1998)

**Overview of precipitation rate calculations**

| | |
|---|---|
| If $K_{dp} \geq 0.25\ ^{\circ}km^{-1}$:<br>$R(Kdp) = 40.683 * (Kdp)^{0.866}$ | (Sachidananda and Zrnic, 1987) |
| If $K_{dp} < 0.25\ ^{\circ}km^{-1}$ and $1\ mm\ hr^{-1} < R(Zh) < 20\ mm\ hr^{-1}$<br>$Z_h = 486 * R(Z_h)^{1.37}$ | (Jones, 1955) |
| Hail ($mm\ hr^{-1}$ liquid equivalent):<br>$H(K_{dp}, Z_{hail}) = \frac{88.0}{\exp[5.38 \times 10^{-6} Z_{hail}\{K_{dp}\}^{-0.297}]}$ | (Carey and Rutledge, 1998) |

Table 3.5: Overview of algorithm used to calculate rain and hail rates from CSU-CHILL multiparameter data.


Figure 3.1: NLDN sensor types and locations after the 1995 upgrade. (After Graham et al., 1997).

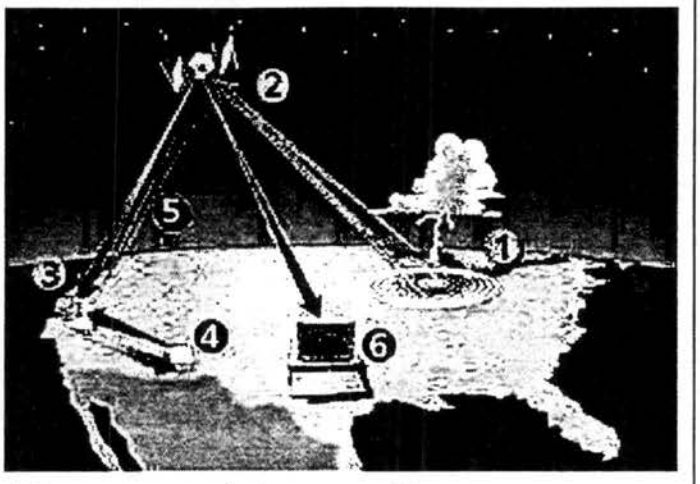


1.Sensors transmit data to satellite
2.Satellite relays information to earth station
3.Data is transmitted to NCC via land-lines
4.NCC processes data
5.Processed data is relayed back to satellite
6.Lightning data is displayed within seconds of occurrence

Figure 3.2: Schematic depicting primary components and operations of the NLDN. (GAI, 1998)

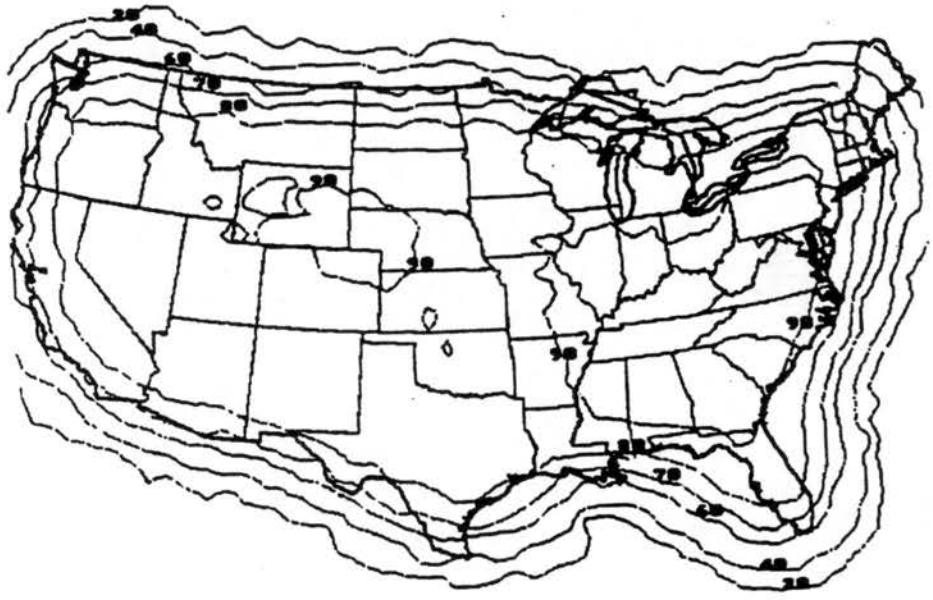

Figure 3.3: Projected NLDN detection efficiency after the 1995 NLDN upgrade. (After Cummins et al., 1995)

a)

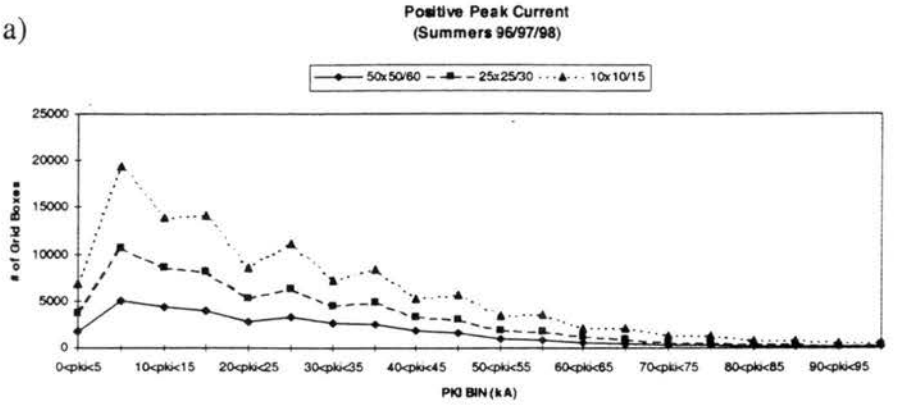


b)

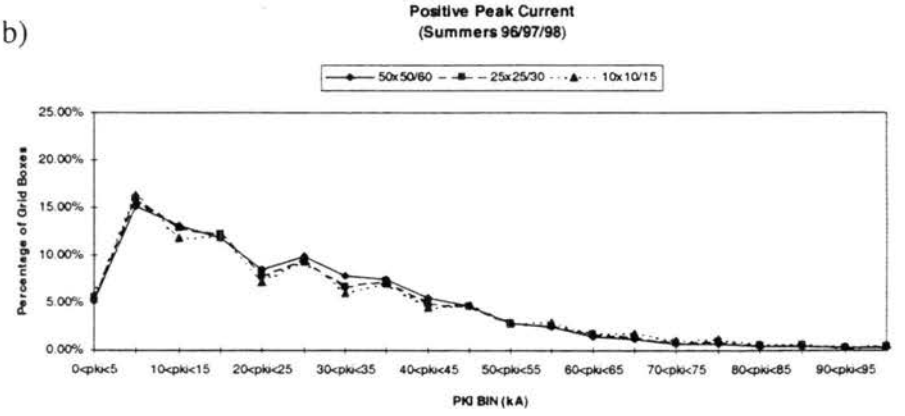


Figure 3.4: (a) Comparison of frequency distributions of positive peak current values obtained from three separate gridding schemes. (b) Comparison of frequency distributions in (a), normalized by the total number of grid boxes.

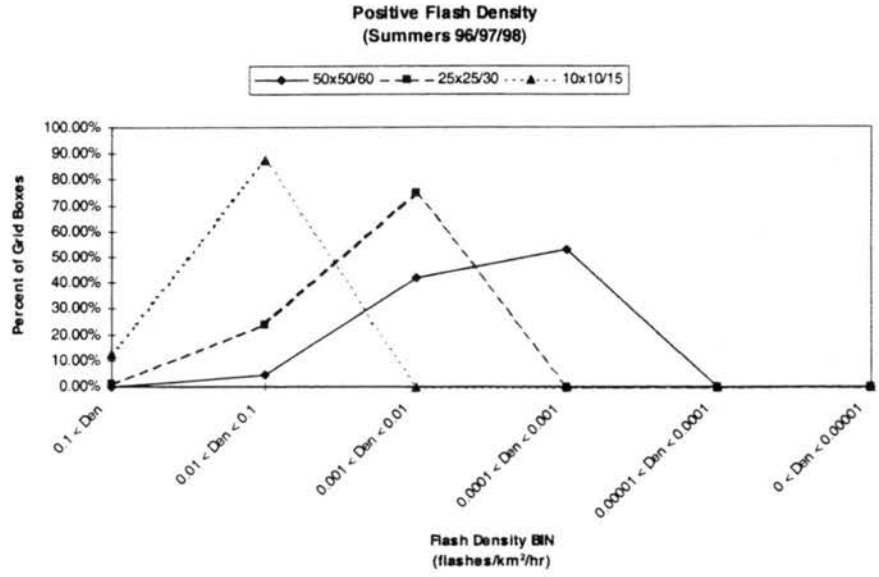


Figure 3.5: Comparison of frequency distributions of positive flash density values obtained for three separate gridding schemes, normalized by the total number of grid boxes.

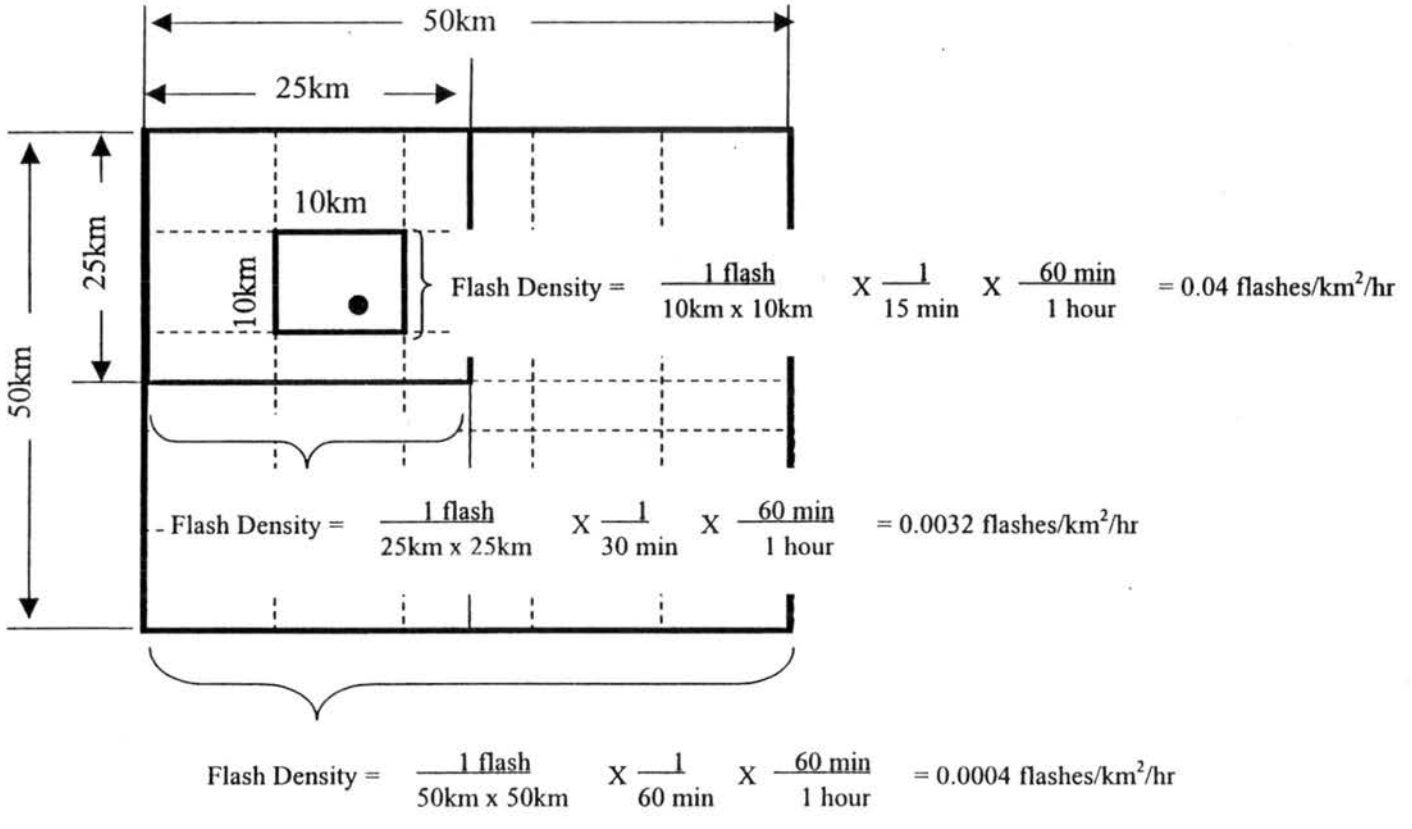


Figure 3.6: Explanatory diagram depicting a single lightning strike within a 50 km x 50 km grid box in a one hour period. Due to the different spatial and temporal resolutions, this single flash would have a different flash density associated with it for each gridding resolution, as depicted above.

# CHAPTER 4

# REGIONAL CLIMATOLOGY

# OF CLOUD-TO-GROUND LIGHTNING

## 4.1 Overview

Each year an average of over 21 million cloud-to-ground (CG) lightning strikes are recorded by the National Lightning Detection Network (NLDN) across the contiguous United States (Fig. 4.1). Of these 21 million CG lightning strikes, less than 10% (1.7 million) are of positive polarity, that is, flashes that deliver positive charge to ground (Orville 1994; Orville and Silver, 1997). Our summer season regional analysis (summarized in Tables 4.1 and 4.2) found that an average of nearly 500,000 CG flashes are detected within the area of interest (AOI; Fig. 1.1) each year, between the months of May and August (2.3% of the annual U.S. average). Further we found that over 65,000 of these strikes (13.1%) were of positive polarity. Following the methodology outlined in Section 3.3, this chapter presents our regional, summer season climatology of cloud-to-ground lightning from 1996-98 (May-Aug). Our climatology is separated into an examination of the diurnal variations in CG lightning (Sec. 4.2) and the spatial and temporal variations in positive (Sec. 4.3) and negative (Sec. 4.4) CG lightning activity. Section 4.5 describes some of the interrelated characteristics of positive and negative CG lightning as we transition from low to high positive CG fraction.

## 4.2 Diurnal Variations in Cloud-to-Ground Lightning

Obviously CG lightning activity is infrequent and episodic in nature. Thus, the diurnal cycle of CG lightning frequency does not represent CG lightning activity on any given day during these summer months, rather it indicates the *tendency* for summer season CG lightning activity to occur at a specific time during the day.

Figure 4.2a shows normalized frequency distributions of the diurnal variations in the occurrence of grid boxes containing positive and negative CG lightning strokes. The peak time of occurrence of positive CG lightning is at 2000 MDT, lagging the occurrence of peak negative CG lightning by 3 hours (1700 MDT). Similarly, figure 4.2b shows a comparison of normalized frequency distributions based on our gridded analysis. Here, the peak time of occurrence of "significant" grid boxes (grid boxes containing greater than 50% positive CG fractions with positive flash densities greater than or equal to 0.03 flashes $km^{-2}$ $hr^{-1}$, discussed in Sec. 3.4) is at 1900 MDT, lagging the peak occurrence for all grid boxes containing CG lightning by 2 hours. These findings are consistent with those of Zajac (1998) who found that positive CG lightning activity lags negative CG lightning activity by 0 to 2 hours over most, but not all regions, of the contiguous United States.

## 4.3 Positive Cloud-to-Ground Lightning Activity

Figures 4.3a-d show the spatial, summertime, distribution of percent positive CG lightning averaged over all three summers (Fig. 4.3a), as well as each individual summer (Fig. 4.3 b-d). Although the spatial distribution of the percentage of positive CG lightning within a grid box shows some variability from year to year, we tend to see the

same general trend; note the west to east gradient showing an increase in the average positive CG fraction, in a grid box, as one moves eastward from the lee of the Rockies.

Figure 4.4a shows a frequency distribution of the, non-thresholded, percent positive CG lightning within a grid box over the entire period of interest. The predominant feature to note in this figure is the bimodal character; nearly 75% of all grid boxes had a positive CG fraction of 25% or less, while over 20% had positive CG fractions greater than 75%. To ensure these findings were not a result of a predominance of grid boxes containing single strokes (which would lead to a positive CG fraction of either 0 or 100 percent, depending upon polarity of the flash) we reanalyzed the data, thresholding on the total number of strokes contained in the grid box. Figure 4.4b shows a normalized comparison of the results of thresholding the data based on 1 or more, 2 or more, 4 or more, and 10 or more strikes per grid box. Each threshold results in the same bimodal character in the distribution. These findings lead us to conclude that the storms sampled were either dominated by a low positive CG fraction ($\leq 25\%$) or a high positive CG fraction ($> 75\%$), with no apparent transition in the intermediate ranges.

### *4.3.1 Summer Season Positive Cloud-to-Ground Flash Density*

Figures 4.5a-d depict spatial distributions of the positive CG flash density for all three summers combined (Fig. 4.5a; flashes $km^{-2}$/3 summers) as well as each individual summer (Fig. 4.5b-d; flashes $km^{-2}$/summer). Positive flash densities show significant spatial variability from year to year, but when we look at our three-summer composite (Fig. 4.5a), we see a southwest to northeast gradient with increasing flash densities to the

northeast. These findings indicate that the positive flash densities in summertime thunderstorms should increase as we move leeward of the Rockies.

### *4.3.2 Mean Positive Peak Current.*

Figure 4.6a shows the spatial distribution of the mean positive peak current, averaged over the summer months of 1996-98. Here again we see a west to east gradient with increasing average positive peak current lee of the Rockies, with a regional maximum found in southern Nebraska. Spatial distributions for each individual summer period (Fig. 4.6b-d) show similar trends.

Figures 4.7a-d show three-dimensional frequency distributions of the average positive peak current within a grid box as a function of percent positive CG fraction for each of the four different positive flash density thresholds (1 or more, 2 or more, 4 or more and 10 or more positive flashes per grid box) similar to those described above for total flash density. Regardless of the threshold, "convective elements" (defined as a single grid box) with lower positive CG fractions have a lower mode in the positive peak current distribution. As we increase the positive CG fraction, the mode begins to increase in value. The magnitude of the mode increase, as we increase positive CG fraction, is threshold dependent as is evident when comparing the frequency distributions. The higher the minimum flash count per grid box, the higher the average peak current associated with the mode. Figure 4.8 better illustrates this increase by comparing normalized frequency distributions (over all percent positive CG bins) of the average positive peak currents.

### *4.3.3 Mean Positive Multiplicity*

Figures 4.9a-d show spatial distributions of averaged positive CG multiplicity for all three summers (Fig. 4.9a) and each individual summer (Fig. 4.9b-d). Again we see significant variations in the distribution and magnitude of averaged positive CG multiplicity, but typically values are less then 1.2 returns strokes per grid box. One dominant feature that is consistent within all four figures are the elevated multiplicity values along the western portion of the area of interest. These areas of elevated multiplicity values are located in areas of higher, complex terrain (see Fig. 1.1), and are consistent with the findings of Lopez and Holle (1986).

Three-dimensional frequency distributions of positive CG multiplicity (Fig. 4.10a-d) show that regardless of the positive CG fraction within the grid box, the predominant multiplicity is 1, with a very narrow distribution. As the minimum number of positive flashes per grid box increases, (progress from Figs. 4.10a to 4.10d) we see that the distribution of positive multiplicity values narrows even further, with over 95% of the grid boxes having a multiplicity value of 1.

## 4.4 Negative Cloud-to-Ground Lightning Activity

As previously mentioned, nearly 90% of all summertime lightning detected within our region of interest lowers negative charge to ground. This section will focus on describing the typical characteristics of the negative CG flashes.

### *4.4.1 Summer Season Negative Cloud-to-Ground Flash Density*

Figures 4.11a-11d show spatial distributions of the negative CG flash density for all three summers combined (Fig. 4.11a; flashes $km^{-2}$/3 summers) as well as each individual summer (Fig. 4.11b-d; flashes $km^{-2}$/summer). Unlike the positive CG flash densities discussed in section 4.3.1 (Fig. 4.5a-d) the negative flash densities tend to show similar spatial distributions regardless of the individual summer examined. The predominant feature on these maps is the "bulls-eye" in flash density values located in central Colorado. This peak in flash densities is most certainly topographically related (see Fig. 1.1), co-located with the location of Pike's Peak (elev. 3400m).

### *4.4.2 Mean Negative Peak Current.*

Figure 4.12a shows the spatial distribution of the mean, negative peak current, averaged over the summer months of 1996-98. Again we see some variability from summer to summer (Fig. 4.12b-d) but the trend is the same. That is, a northwest to southeast gradient exists with average negative peak currents increasing to the southeast as we move away from the Rockies. Here the regional maximum is found on the Nebraska – Kansas border, with an absolute magnitude over one half that of the mean positive peak current map (Fig. 4.6a).

Figures 4.13a-d show three-dimensional frequency distributions of the average negative peak current within a grid box as a function of percent positive CG fraction for each of the four different negative flash density thresholds (1 or more, 2 or more, 4 or more and 10 or more negative flashes per grid box) similar to those described for positive flash density. We find that regardless of the threshold, "convective elements" with a

lower positive CG fraction have a larger (more negative) mode in the average negative peak current distribution. Also contrary to our findings in section 4.3.2 we note that as we increase the positive CG fraction the mode tends to decrease (become less negative). We find that regardless of the threshold, the mode value of the average negative peak current remains in the –15 to –20 kA bin (Fig. 4.14).

### *4.4.3 Mean Negative Multiplicity*

Figures 4.15a-d show spatial distributions of averaged negative CG multiplicity for all three summers (Fig. 4.15a) and each individual summer (Fig. 4.15b-d). Again we see significant variations in the distribution and magnitude of averaged negative CG multiplicity with values ranging from as low as 1 return stoke to as high as 2.8 return strokes per grid box. These maps all show elevated multiplicity values along the Front Range, lee of the Rockies with maximum values located in north central Nebraska.

Three-dimensional frequency distributions of negative CG multiplicity (Fig. 4.16a-d) are much more interesting than those shown for positive CG multiplicity (Fig. 4.10a-d). Here we see that for all grid boxes containing *at least one* negative CG (Fig. 4.16a), the average multiplicity value associated with the mode is 1, regardless of the positive CG fraction. As the positive CG fraction increases, the distribution of multiplicity values narrows, converging on a value of 1. When we examine frequency distributions for grid boxes containing *more than one* negative CG (Fig. 4.16b-d) a different mode begins to emerge. Now the multiplicity value associated with the mode is 2, but this value is dependent upon the positive CG fraction within the grid box. For grid boxes dominated by negative CGs (low positive CG fraction) the multiplicity value

associated with the mode is 2, as we increase the positive CG fraction the mode shifts over to a value of 1. Despite the shift in modes from 2 to 1 the composite frequency distribution over all positive CG fraction bins (top horizontal plot on Fig. 4.16b-d) has a mode associated with a negative multiplicity value of 2, dominated by the grid boxes containing lower positive CG fractions. This is consistent with previous statements as to the general rarity of positive CG flashes compared to negative CG flashes.

## 4.5 Interrelated Characteristics of Positive and Negative Cloud-to-Ground Lightning

This section serves as an overall summary of our regionally averaged lightning statistics, providing an inter-comparison of positive and negative CG lightning as the positive CG fraction increases within a "convective element".

We found that grid boxes with low positive CG fractions had relatively low positive peak currents and relatively high negative peak currents. As the positive CG fraction increased, the positive peak current tended to increase while the negative peak current tended to decrease in strength. Examining the CG multiplicity, we found that regardless of the positive CG fraction, the average number of positive return strokes is 1, with a very narrow distribution. Multiplicity for negative flashes did not follow this same behavior. Instead, the negative CG multiplicity characteristics changed significantly from a mode of 2 for low positive CG fractions (< 50% for grid boxes containing 4 or more negative CG flashes), to a mode of 1 for higher positive CG fractions (> 50%). Further, we found that the distribution in the negative CG multiplicity narrowed as we increased the positive CG fraction in the "convective element".

This regional climatology of CG lightning (as detected by the NLDN) has helped us to better describe how CG lightning characteristics (multiplicity and peak current) for each polarity (positive and negative) change as the percentage of positive CG lightning changes. This climatology has also served as the foundation from which to select cases for further, detailed investigation, including mulitparameter radar observations. Chapter 5 will present these analyses.

Cloud-to-Ground Lightning for 1996 – 98 ( May – Aug)

| Month | Total Flashes | | | Positive Flashes | | |
|---|---|---|---|---|---|---|
| | **1996** | **1997** | **1998** | **1996** | **1997** | **1998** |
| May | 48,996 | 31,680 | 53,062 | 11,265 | 4,985 | 18,382 |
| June | 92,803 | 161,960 | 58,032 | 15,282 | 24,993 | 13,518 |
| July | 148,349 | 177,861 | 203,826 | 20,730 | 19,953 | 24,929 |
| August | 159,826 | 170,801 | 186,942 | 18,770 | 11,822 | 11,162 |
| Summertime Total | 449,974 | 542,302 | 501,862 | 66,047 | 61,753 | 67,991 |
| | | 498,046 (average) | | | 65,264 (average) | |

Table 4.1: Regional cloud-to-ground lightning statistics for 1996 - 98 (May – Aug).

Monthly and Summer Season Percentage Positive Cloud-to-Ground Lightning for 1996 – 98

| Month | Percent Positive | | |
|---|---|---|---|
| | **1996** | **1997** | **1998** |
| May | 22.99% | 15.74% | 34.64% |
| June | 16.47% | 15.43% | 23.29% |
| July | 13.97% | 11.22% | 12.23% |
| August | 11.74% | 6.92% | 5.97% |
| Summer Season Average | 14.68% | 11.39% | 13.55% |



Table 4.2: Monthly and summer season percentage positive cloud-to-ground lightning for 1996 – 98 (May – Aug).

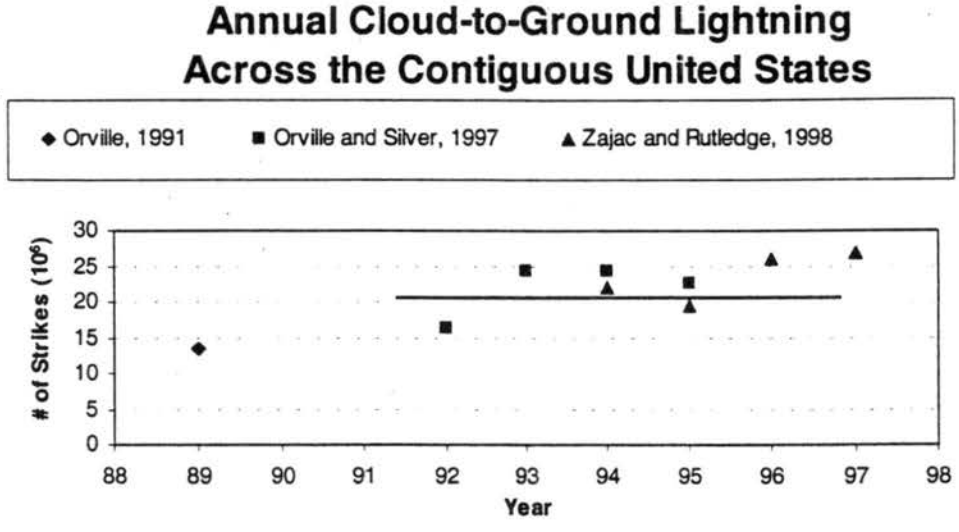


Figure 4.1: Summary of values of annual cloud-to-ground lightning across the contiguous United States as found in the literature. The annual average is depicted by the horizontal line on the graph.

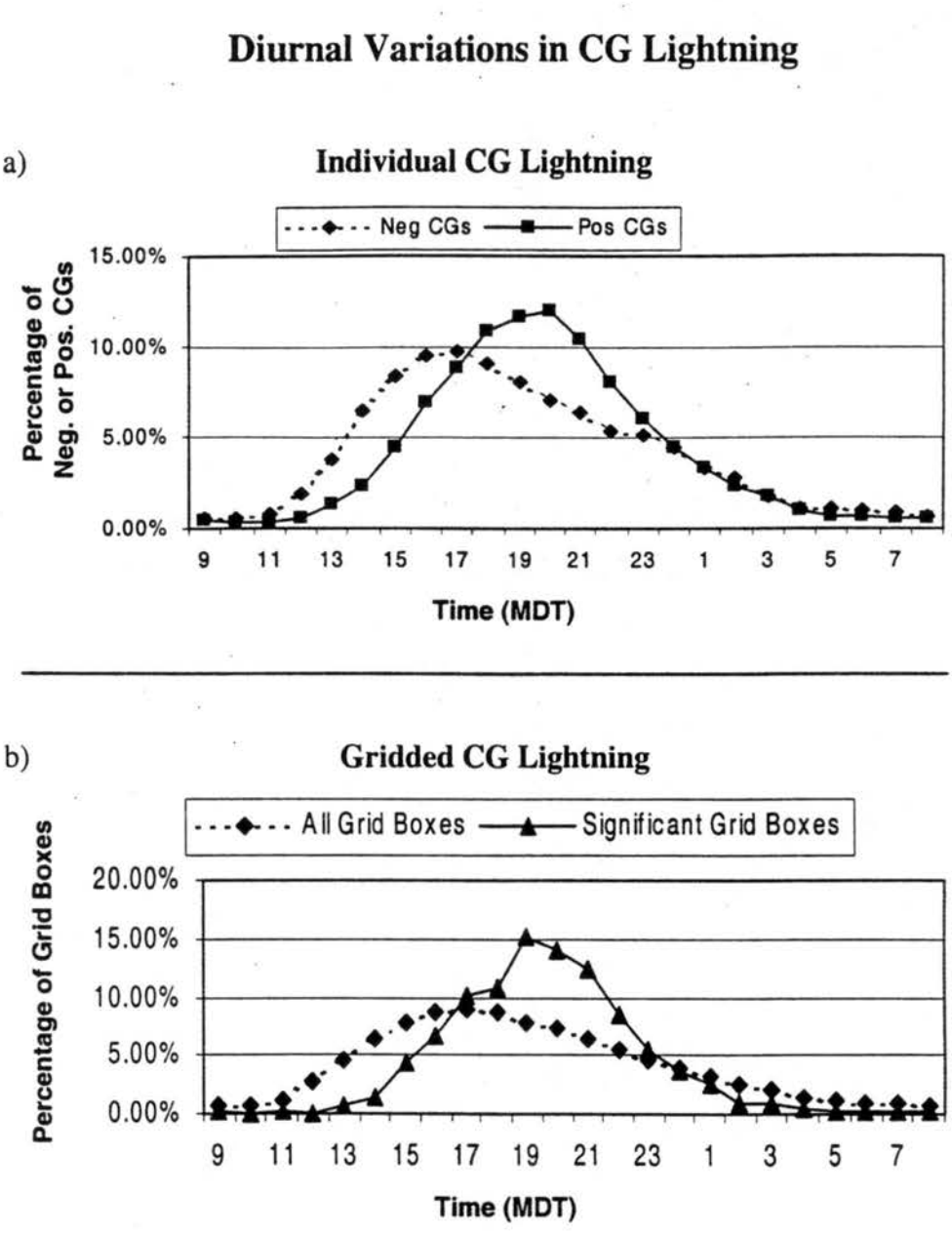


Figure 4.2: Frequency distributions of diurnal variations of (a) individual positive and negative cloud-to-ground lightning and (b) gridded cloud-to-ground lightning. Significant grid boxes are defined as those whose positive CG fraction is 50% or greater, accompanied by positive flash densities greater than or equal to 0.03 flashes $km^2$ $hr^{-1}$.

## Average Percent Positive CG Lightning

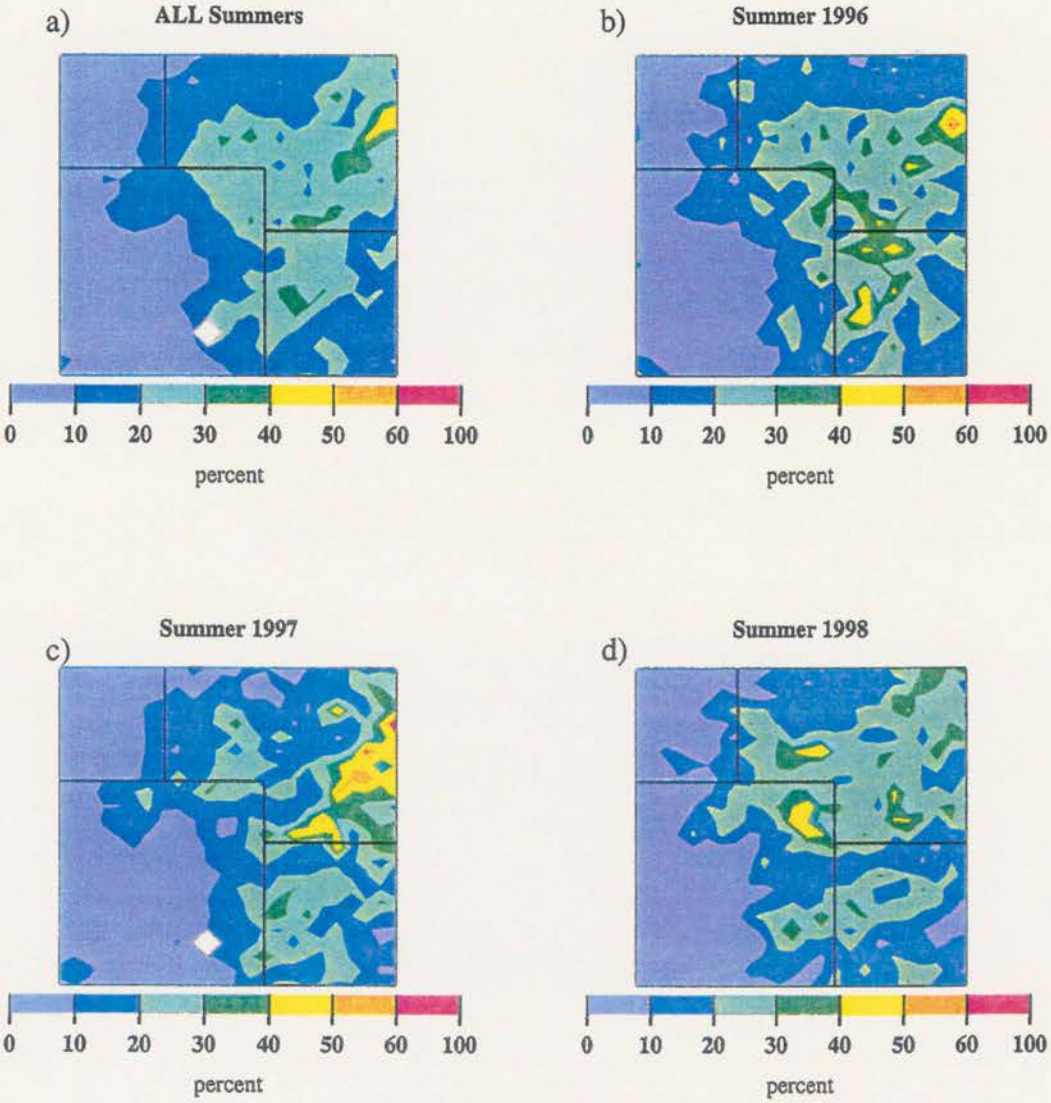


Figure 4.3: Spatial distribution of the average percentage of positive CG lightning within a grid box averaged over (a) all three summers, (b) the summer of 1996, (c) the summer of 1997, and (d) the summer of 1998.

a)

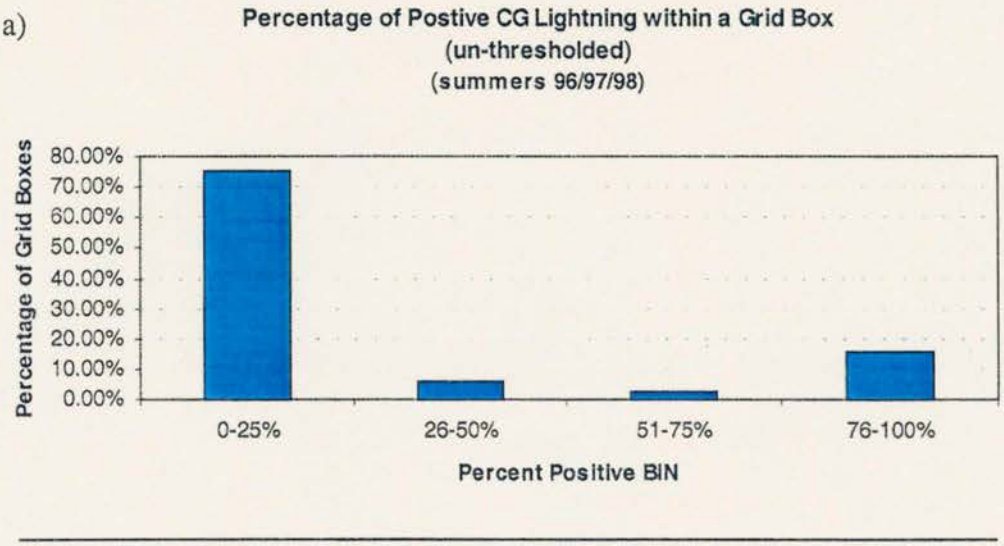


b)

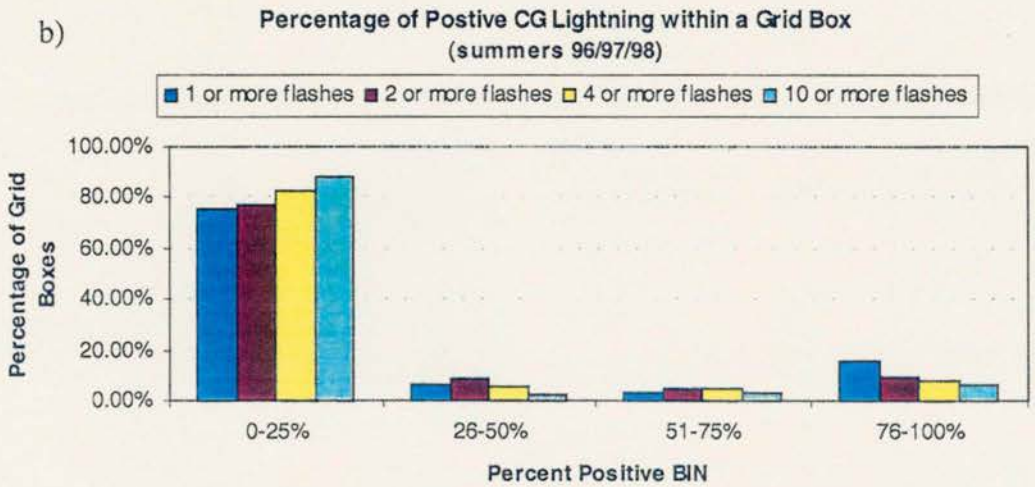


Figure 4.4: Frequency distributions of (a) non-thresholded average percent positive CG lightning within a grid box regardless of flash density for the entire period of record, and (b) the thresholded average percent positive CG lightning within a grid box based on requirements for 1, 2, 4, and 10 or more strikes per grid box, respectively. Both plots have been normalized by the total number of grid boxes.

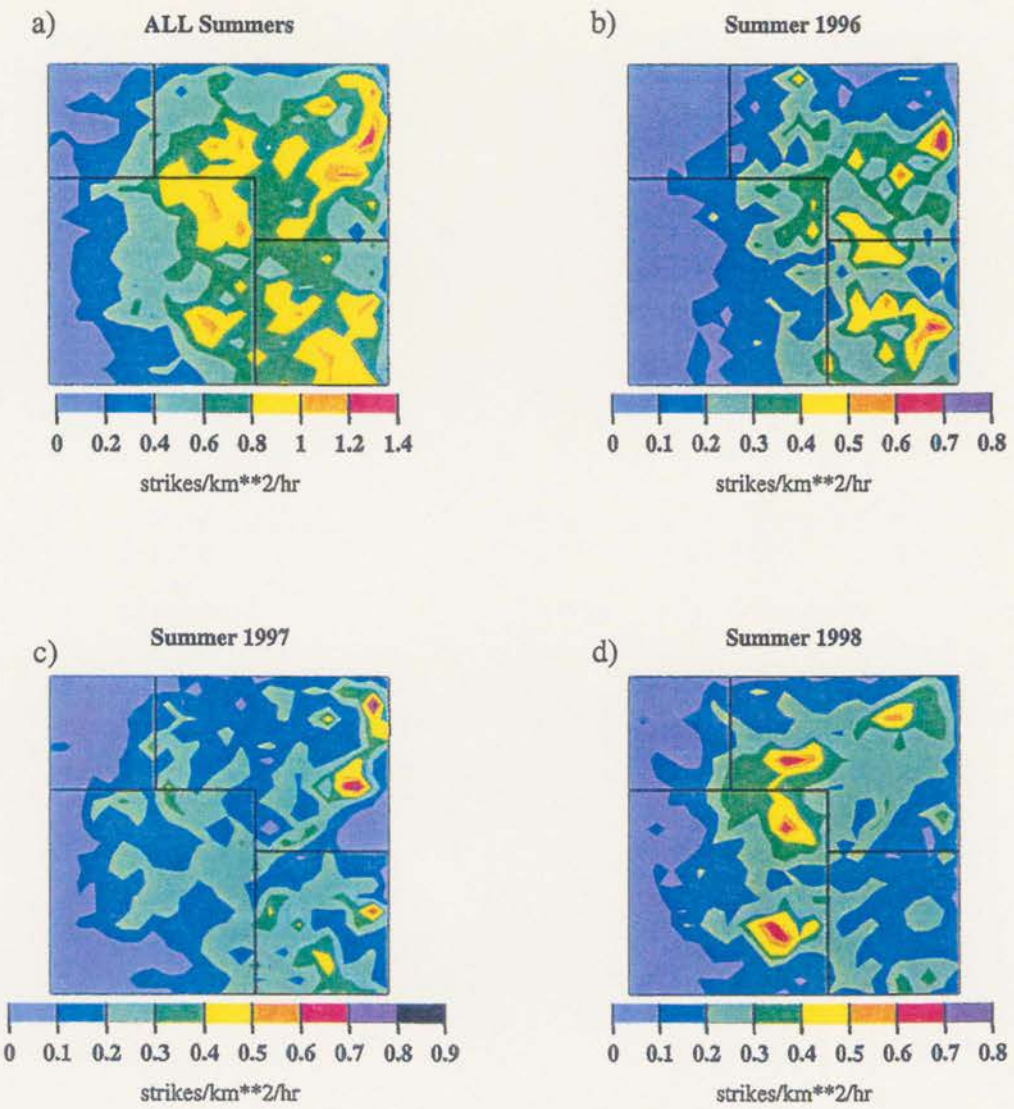


Figure 4.5: Spatial distribution of the average positive CG flash density within a grid box for (a) all three summers (cumulative), (b) the summer of 1996, (c) the summer of 1997, and (d) the summer of 1998.

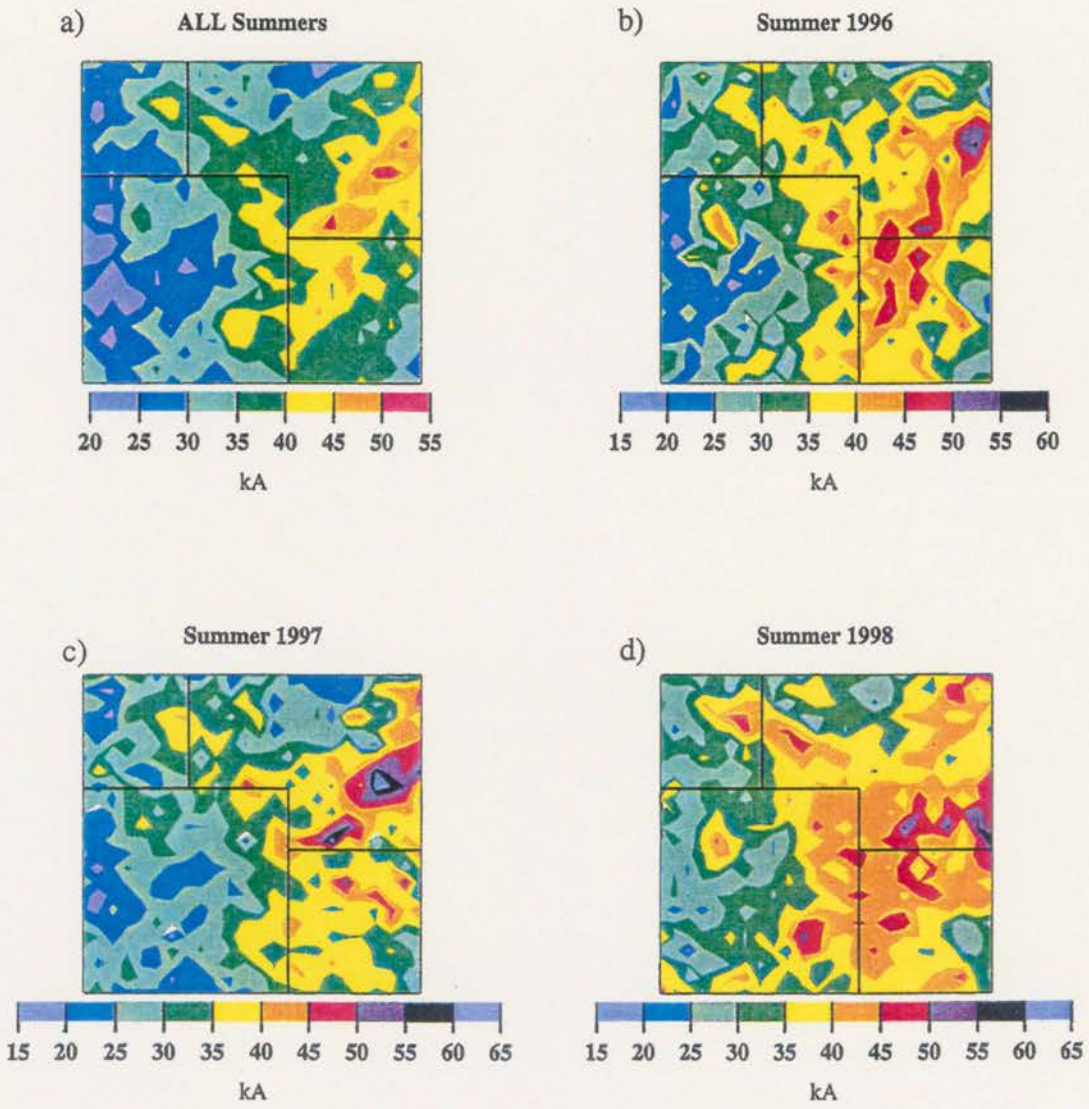


Figure 4.6: Spatial distribution of the average positive CG peak current within a grid box averaged over (a) all three summers, (b) the summer of 1996, (c) the summer of 1997, and (d) the summer of 1998.

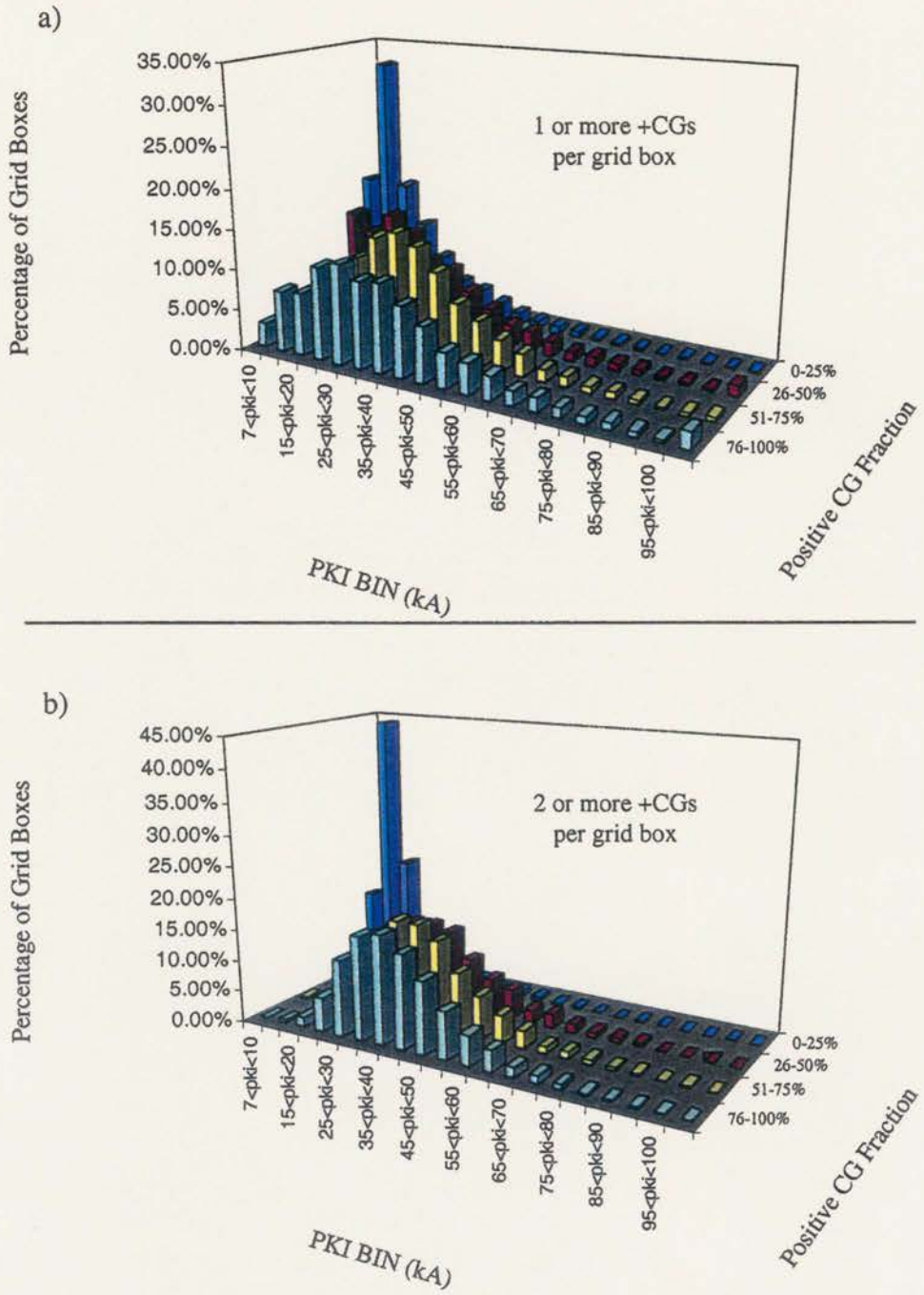


Figure 4.7: Normalized three-dimensional frequency distributions of average positive peak current as a function of positive CG fraction for grid boxes containing (a) one or more positive CGs per grid box and (b) two or more positive CGs per grid box.

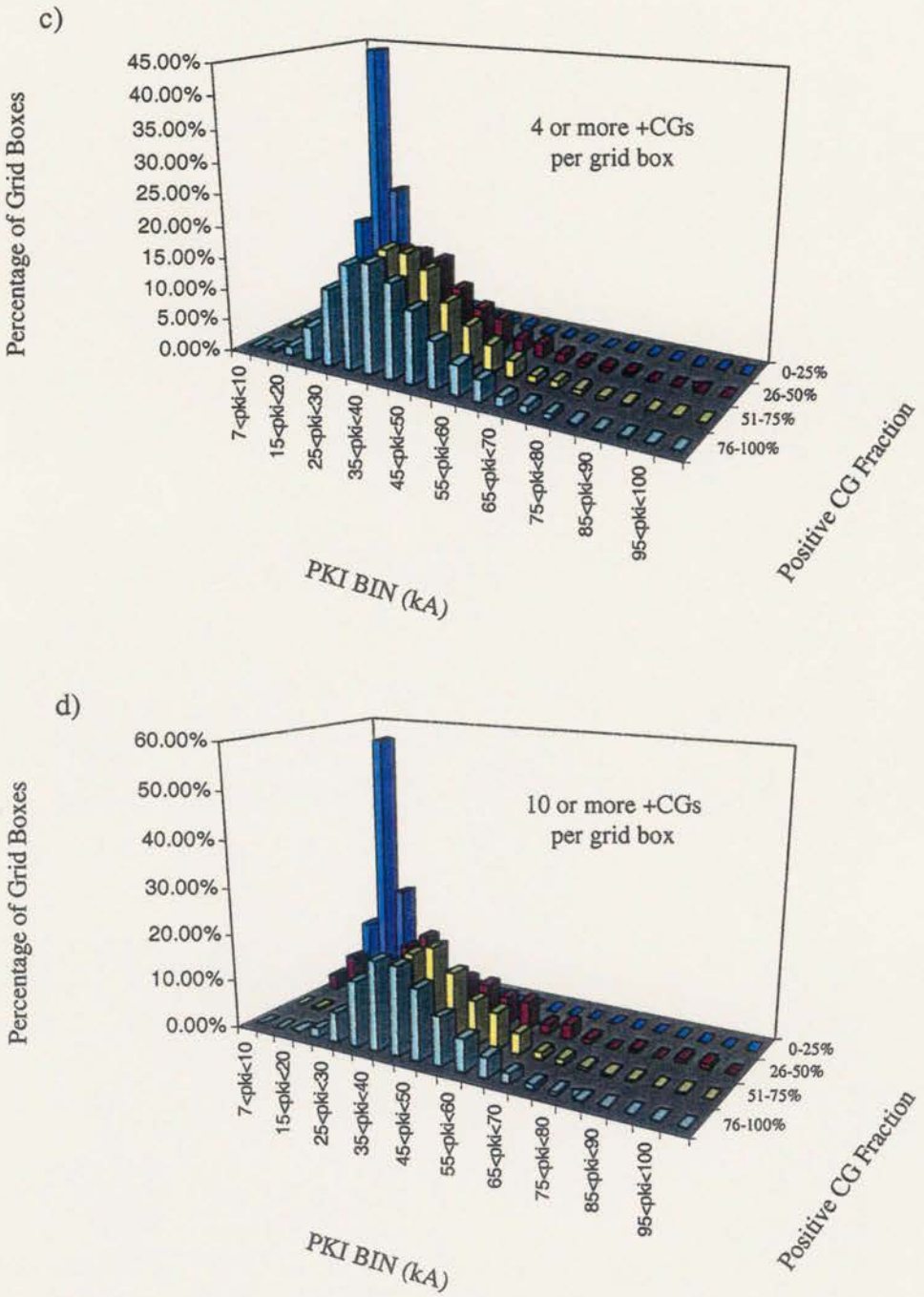


Figure 4.7: Normalized three-dimensional frequency distributions of average positive peak current as a function of positive CG fraction for grid boxes containing (c) four or more positive CGs per grid box and (d) ten or more positive CGs per grid box.

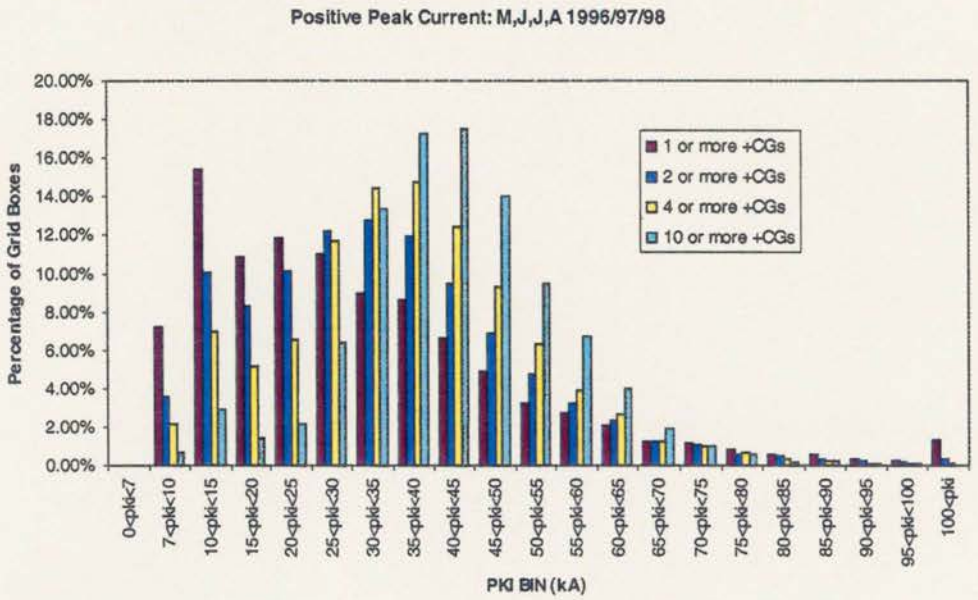


Figure 4.8: Comparison of normalized frequency distributions of average positive peak current for four separate positive flash density thresholds (1, 2, 4, and 10 or more positive flashes per grid box).

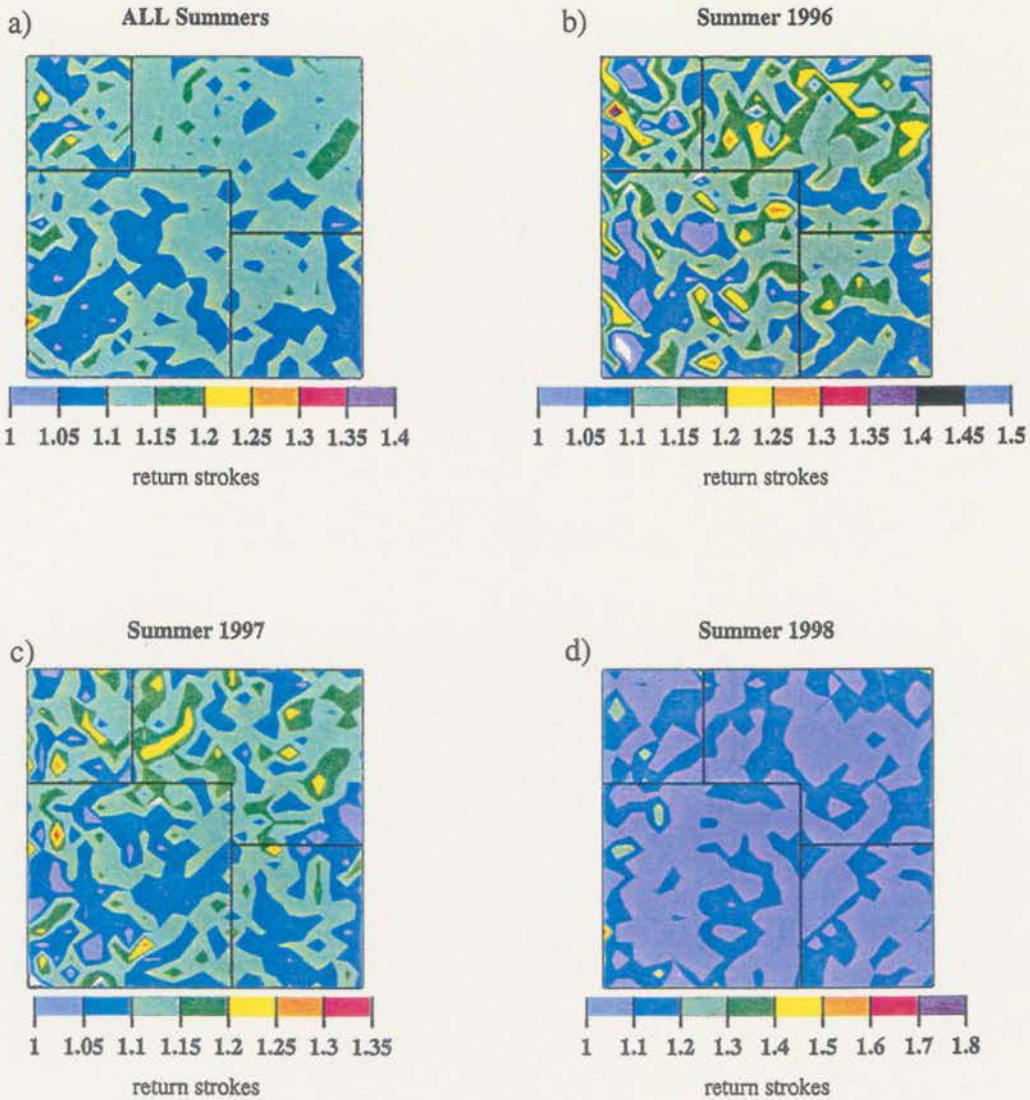


Figure 4.9: Spatial distribution of the average positive CG multiplicity within a grid box averaged over (a) all three summers, (b) the summer of 1996, (c) the summer of 1997, and (d) the summer of 1998.

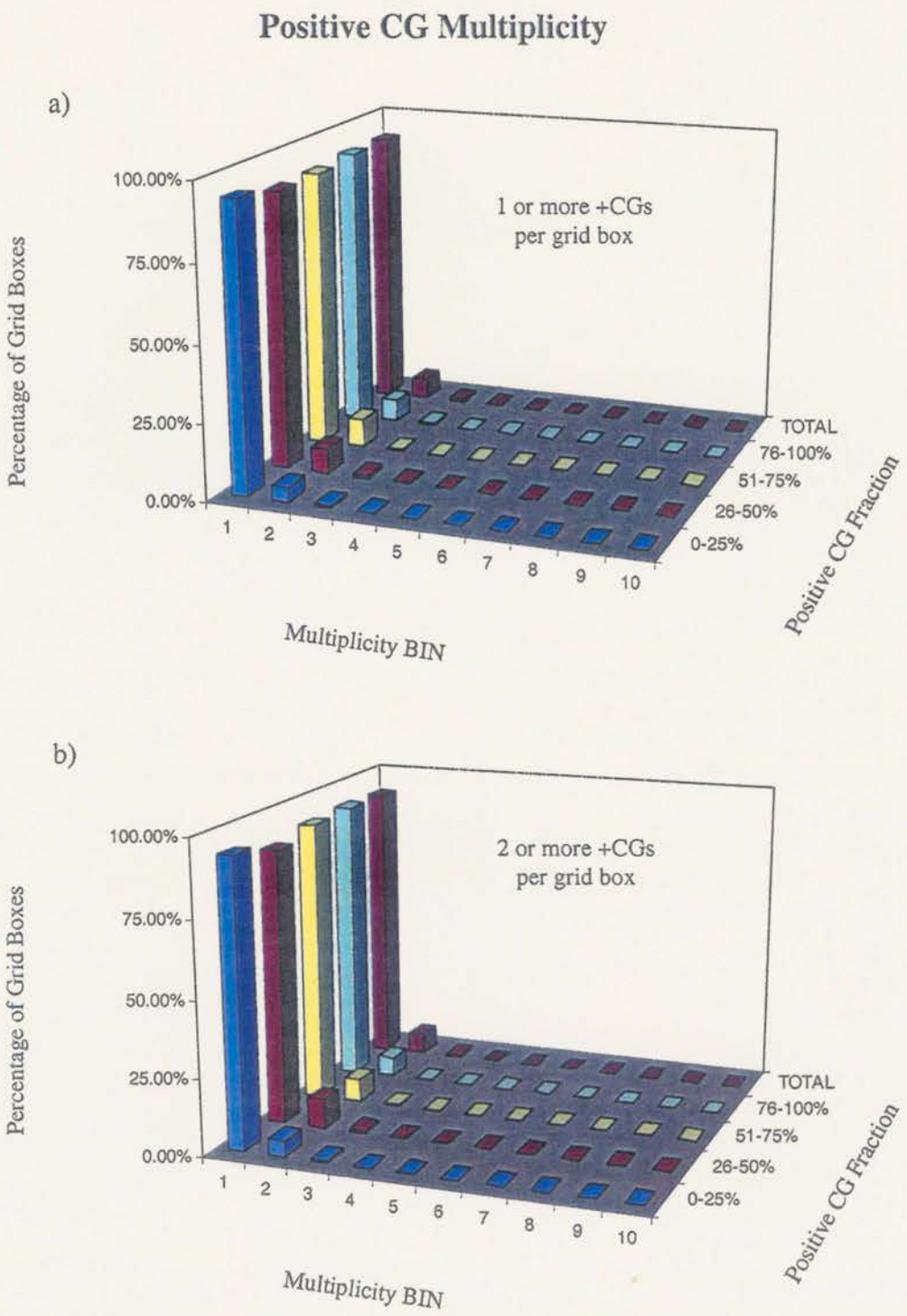


Figure 4.10: Normalized three-dimensional frequency distributions of average positive CG multiplicity as a function of positive CG fraction for grid boxes containing (a) one or more positive CGs per grid box and (b) two or more positive CGs per grid box.

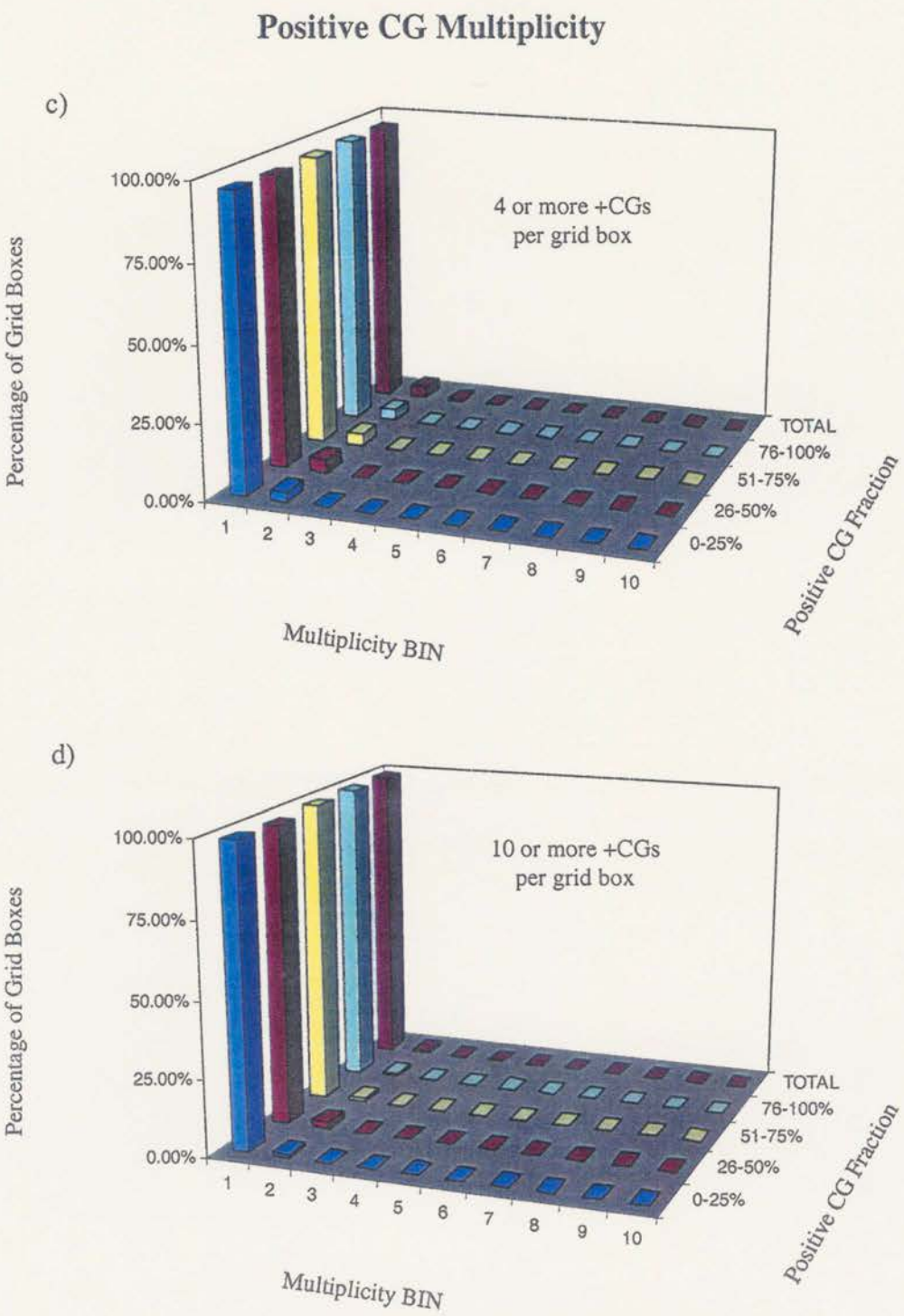


Figure 4.10: Normalized three-dimensional frequency distributions of average positive CG multiplicity as a function of positive CG fraction for grid boxes containing (c) four or more positive CGs per grid box and (d) ten or more positive CGs per grid box.

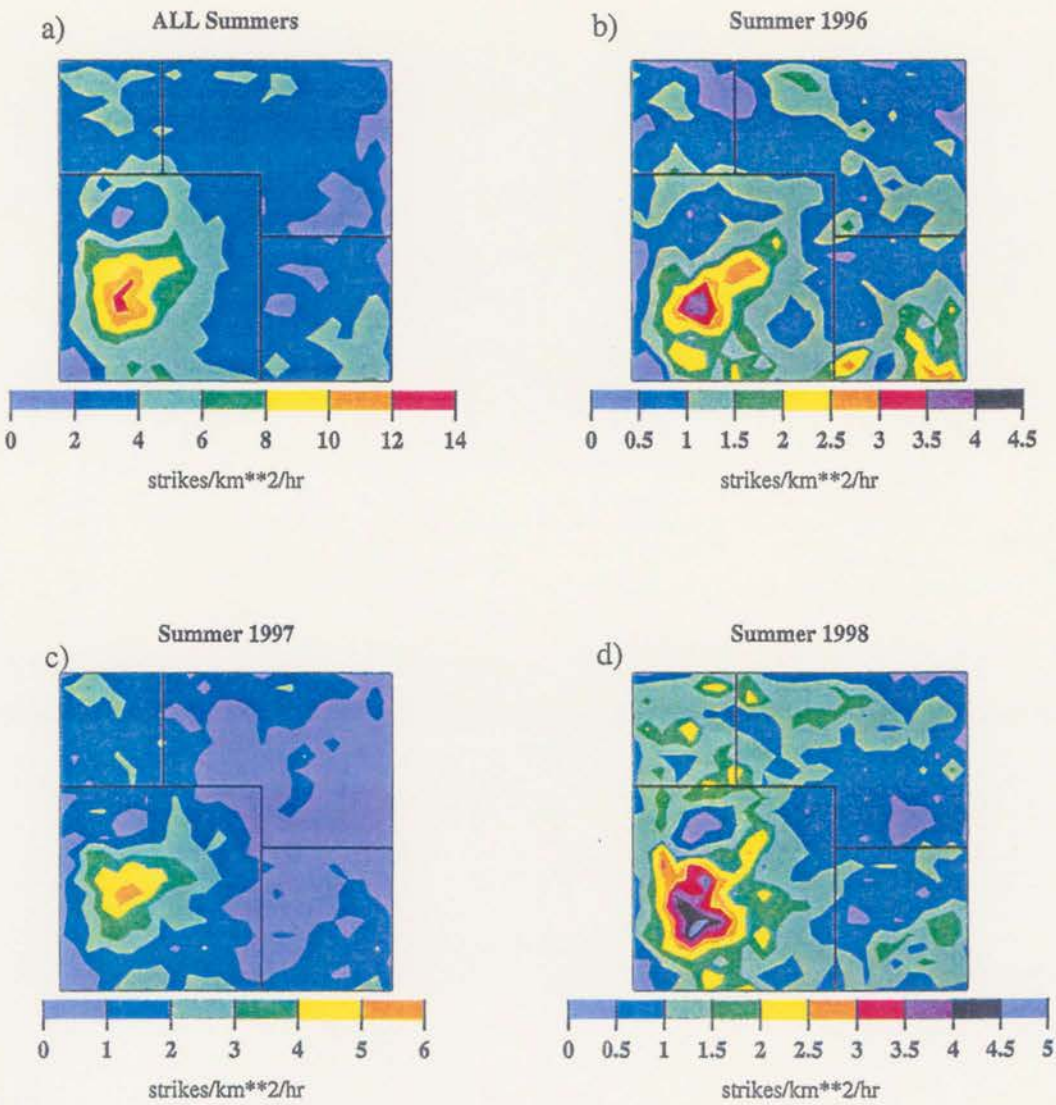


Figure 4.11: Spatial distribution of the average negative CG flash density within a grid box averaged over (a) all three summers, (b) the summer of 1996, (c) the summer of 1997, and (d) the summer of 1998.

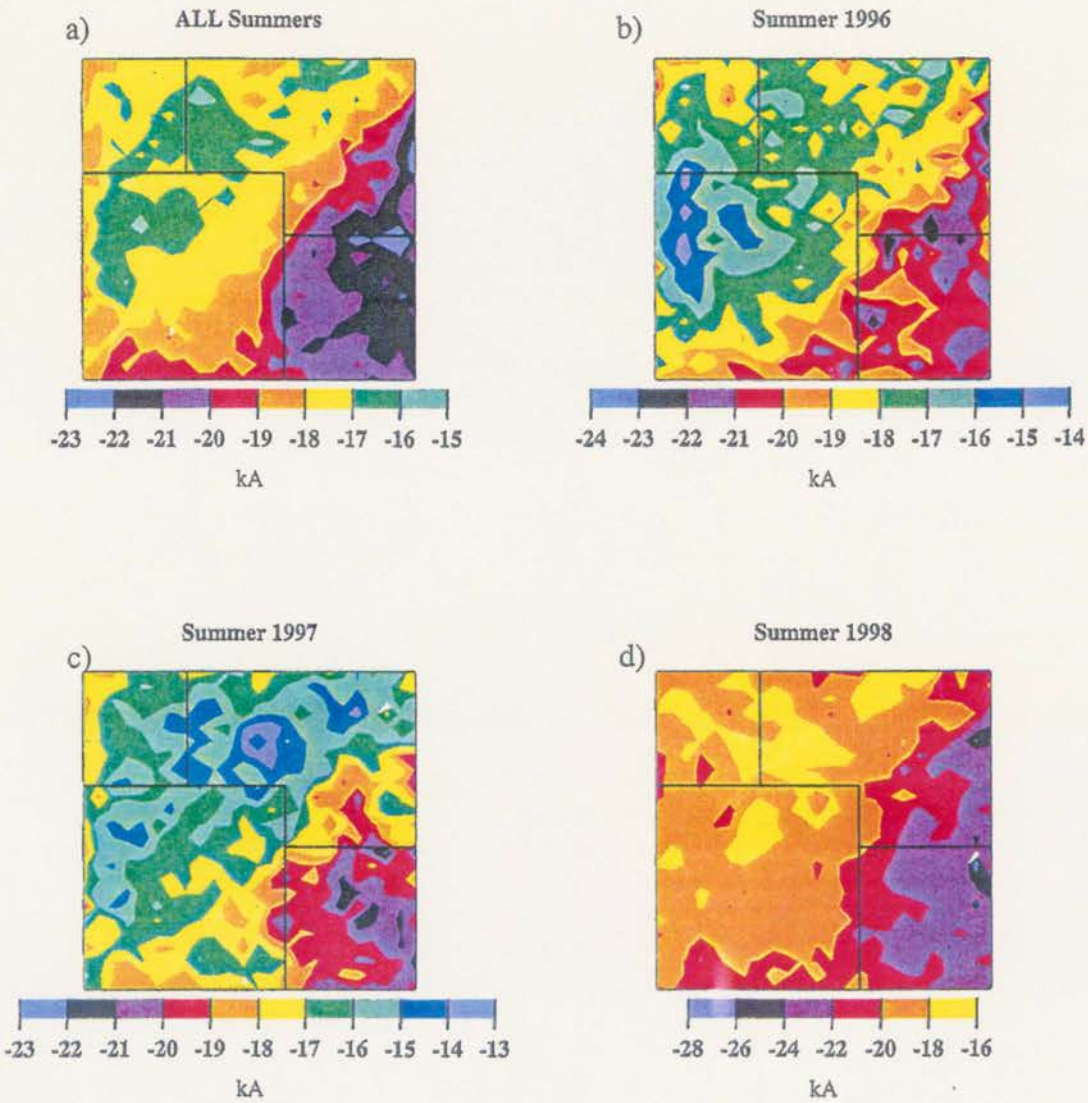


Figure 4.12: Spatial distribution of the average negative CG peak current within a grid box averaged over (a) all three summers, (b) the summer of 1996, (c) the summer of 1997, and (d) the summer of 1998.

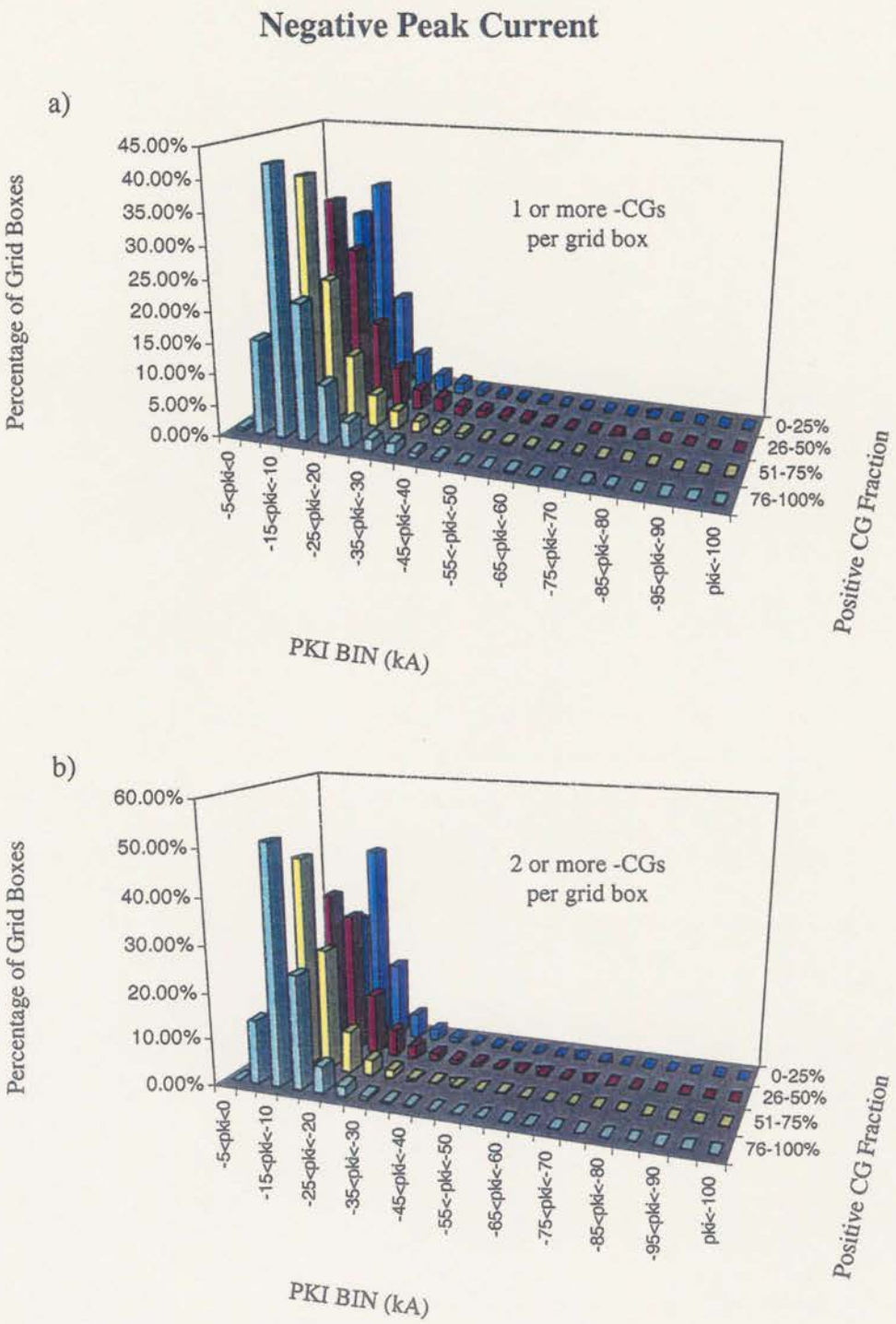


Figure 4.13: Normalized three-dimensional frequency distributions of average negative peak current as a function of positive CG fraction for grid boxes containing (a) one or more negative CGs per grid box and (b) two or more negative CGs per grid box.

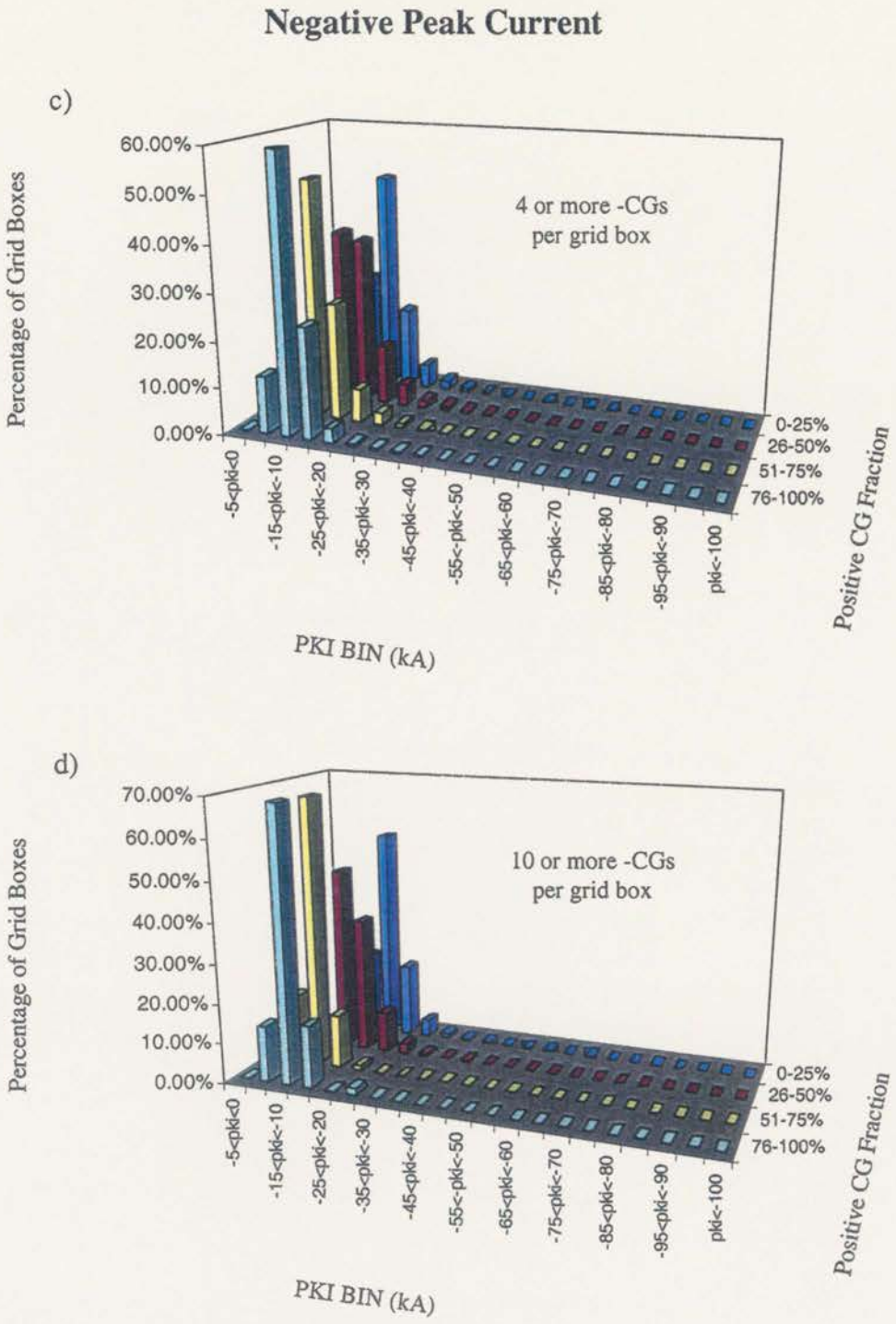


Figure 4.13: Normalized three-dimensional frequency distributions of average negative peak current as a function of positive CG fraction for grid boxes containing (c) four or more negative CGs per grid box and (d) ten or more negative CGs per grid box.

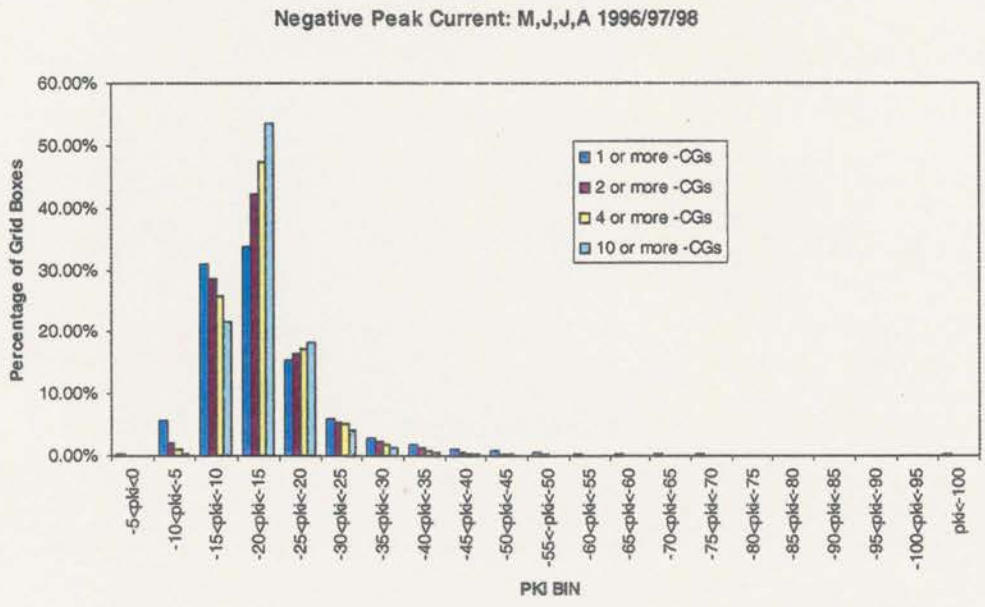


Figure 4.14: Comparison of normalized frequency distributions of average negative peak current for four separate positive flash density thresholds (1, 2, 4, and 10 or more negative flashes per grid box).

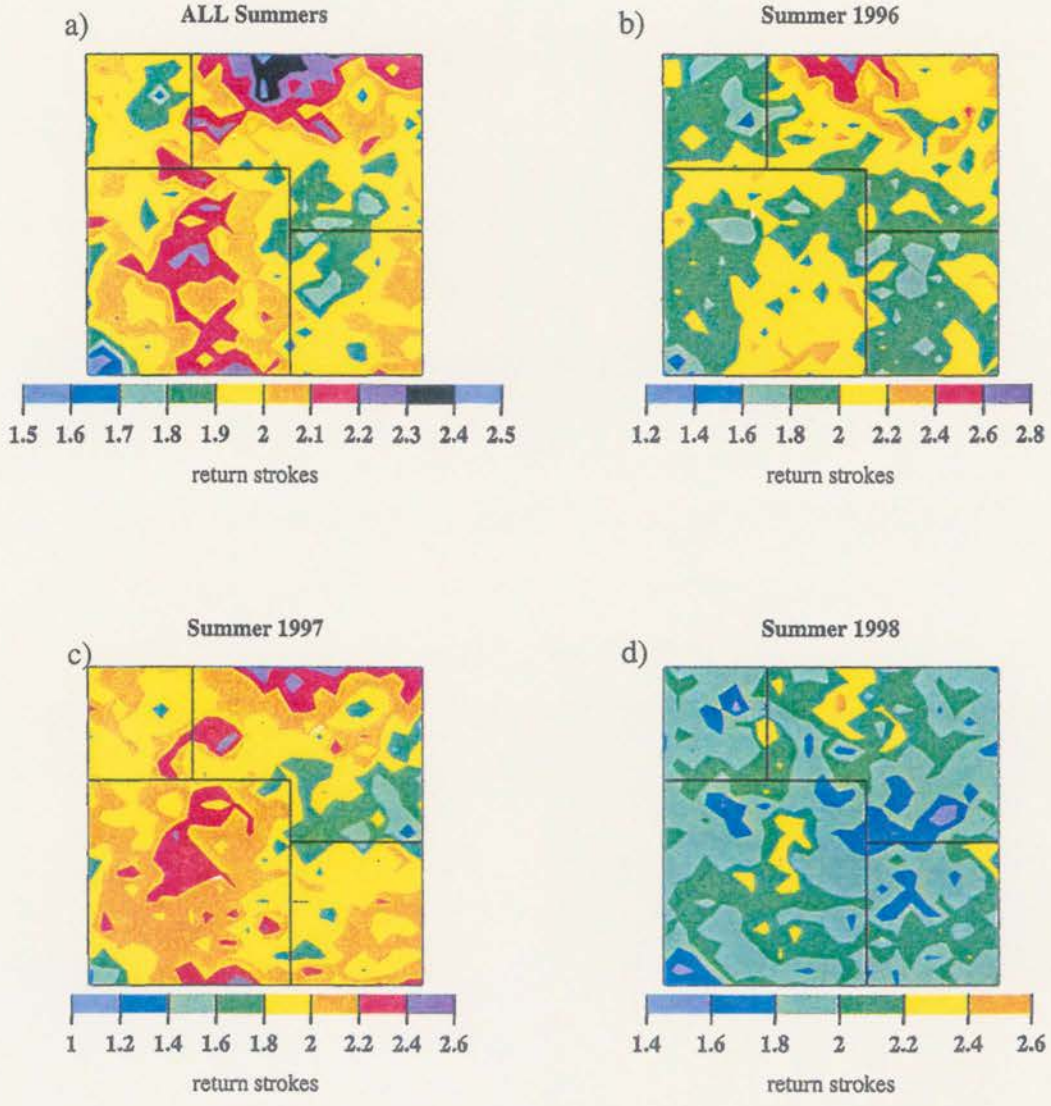


Figure 4.15: Spatial distribution of the average negative CG multiplicity within a grid box averaged over (a) all three summers, (b) the summer of 1996, (c) the summer of 1997, and (d) the summer of 1998.

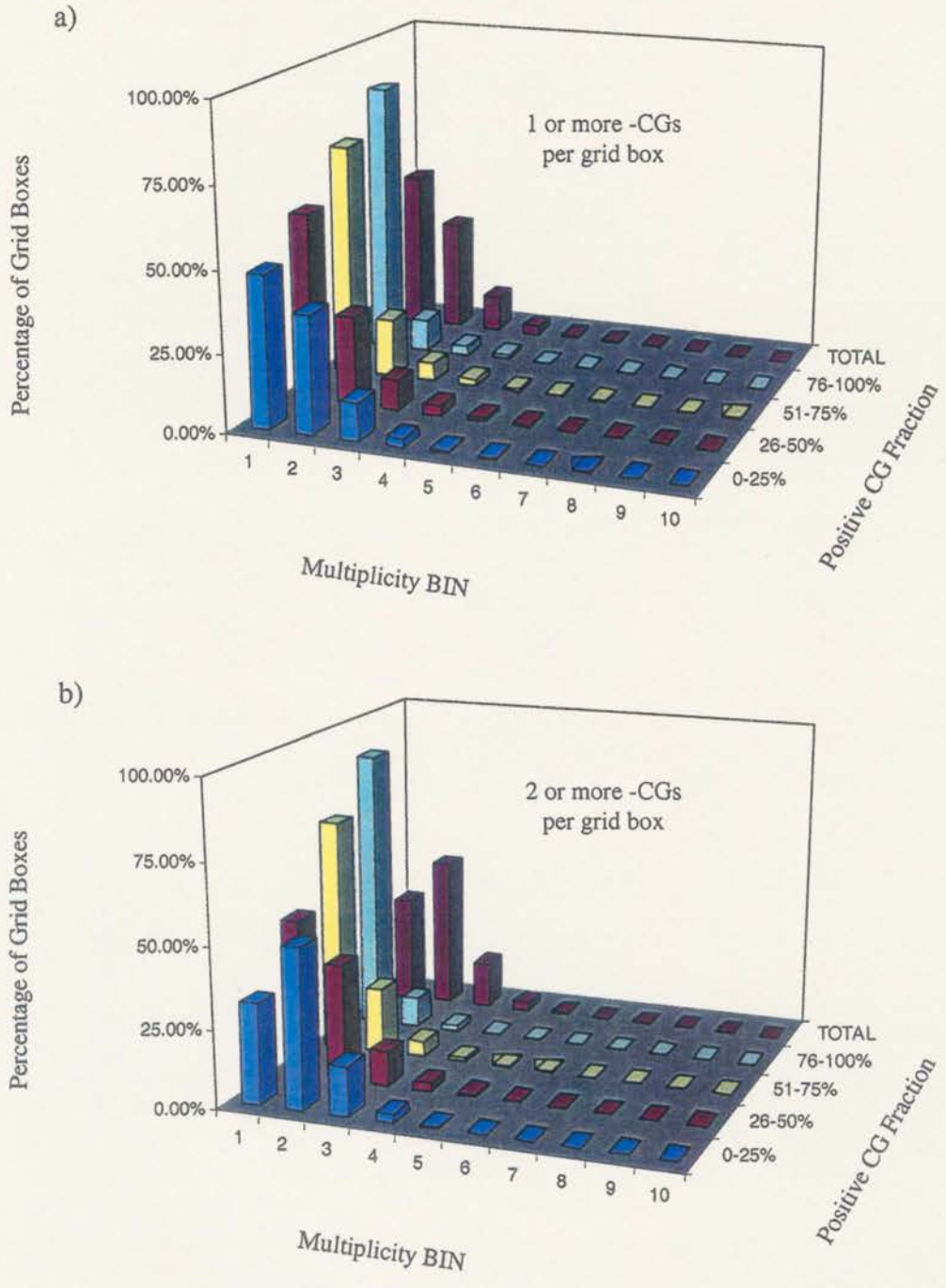


Figure 4.16: Normalized three-dimensional frequency distributions of average negative CG multiplicity as a function of positive CG fraction for grid boxes containing (a) one or more negative CGs per grid box and (b) two or more negative CGs per grid box.

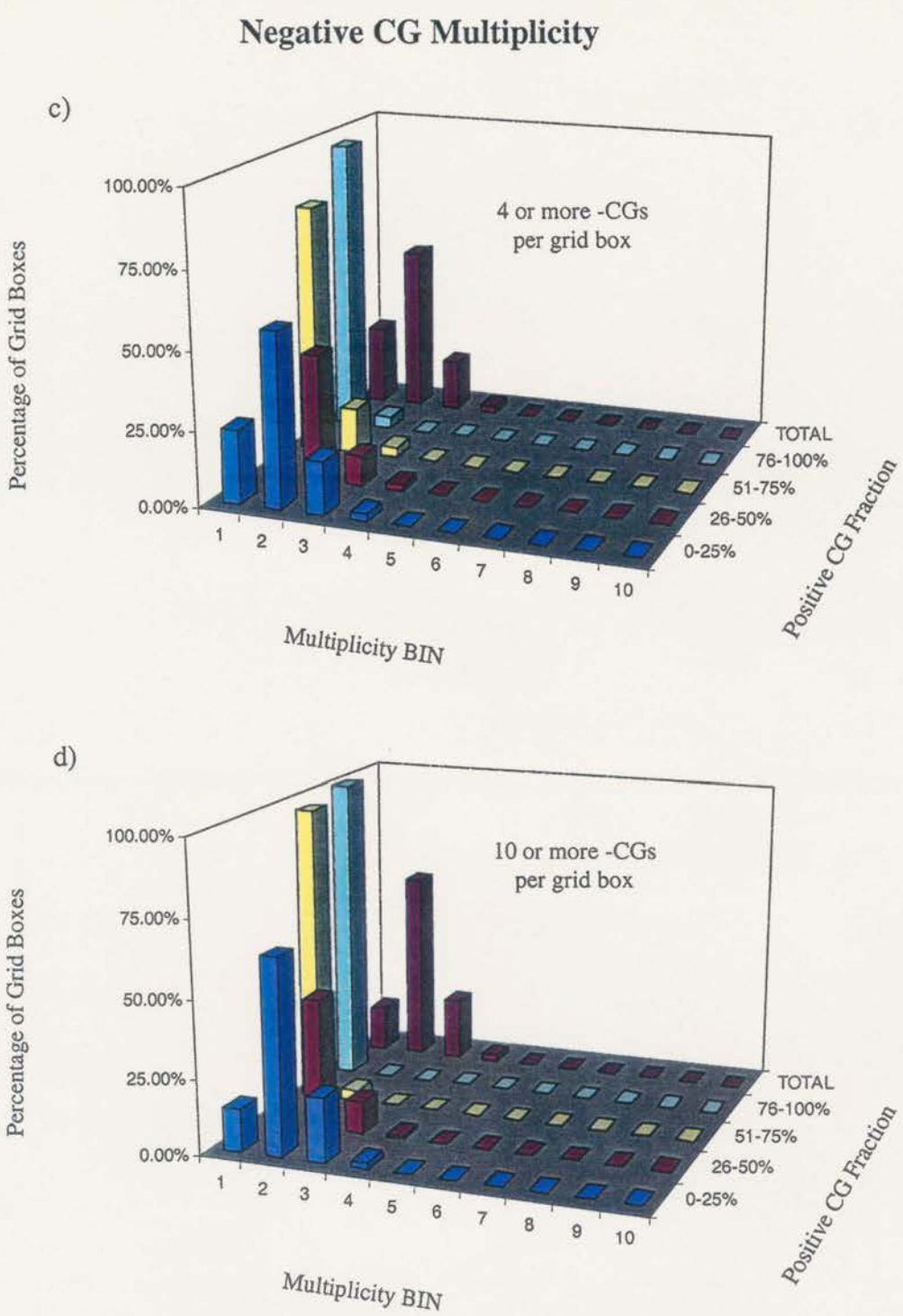


Figure 4.16: Normalized three-dimensional frequency distributions of average negative CG multiplicity as a function of positive CG fraction for grid boxes containing (c) four or more negative CGs per grid box and (d) ten or more negative CGs per grid box.

# CHAPTER 5

# ANALYSIS OF SELECTED CASES STUDIES

In this chapter we examine the co-evolving microphysical and electrical characteristics of four different storms observed along the Front Range of northeastern Colorado. Each of these cases were selected for examination because at some point in their lifetime they were observed to have been dominated by greater than 50% positive CG fraction, coupled with significant positive flash densities (> 0.03 flashes $km^2$ $hr^{-1}$) based on the output resulting from our regional climatology of cloud-to-ground lightning strikes. The 2 June 1997 storm will be discussed in Section 5.1, followed by the 1 and 2 July 1998 storms in sections 5.2 and 5.3, respectively. Our final case, 21 July 1998, will be discussed in section 5.4. In each of these sections we will focus our efforts on investigating periods in which electrical transitions were evident. Section 5.5 will provide an overall summary of our findings, highlighting any repeatable trends appearing in the data.

As a matter of convention, cloud-to-ground (CG) flash rates (expressed in flashes $min^{-1}$) are calculated by averaging the number of flashes detected in a five-minute period. Although it would be more representative to call these values averaged 5-minute flash rates, we have elected to use the convention described above. Additionally, in our discussions of small hail (< 1 cm) and graupel volumes above the melting level (category 7 in Table 3.4), for brevity, the term graupel volume will be used in lieu of graupel and

small hail volume. It is important to note that this term will be applied only to volumes above the melting level. Below the melting level, the term small hail (category 1 in Table 3.4) is used to describe ice particles with diameters < 2 cm, regardless of density, and regardless of the fact that the small hail located beneath the melting level may in fact be a result of graupel aloft, descending below the melting level. A final term that appears throughout our discussions is "electrical transition". This term is meant to describe a transition in the dominant CG polarity of the storm, particularly from negative to positive.

## 5.1 2 June 1997

Our first case study occurred on 2 June 1997, and produced a total of 433 positive CG lightning strokes over our period of interest (1317 – 1756 MDT). During most of this timeframe, positive CG strokes were the dominant polarity, with a total of three transitions in CG polarity evident.

### *5.1.1 Overview of Storm Electrical Characteristics and Transitions*

Figure 5.1 shows a time-series plot of 5-minute NLDN CG flash rates, along with averaged 1-minute flash rates, for each polarity. Notice that this storm was dominated by positive CG lightning for nearly 4 hours, (1330 - 1715 MDT). Only around 1440 MDT were the 5-minute flash rates dominated by negative polarity flashes. This storm was initially dominated by negative CG lightning, but shortly after the initial radar volume, transitioned to positive polarity domination (transition 1). Specifically, at 1330 MDT positive CGs began exhibiting a pulsing characteristic with peak flash rates as high at 4.4

$min^{-1}$ and as low as 1 $min^{-1}$. This pulsing continued throughout our observational period, but positive flash rates were highest prior to 1440 MDT (transition 2). In fact, a total of 158 positive flashes were detected over the 70 minute time period (averaging 2.3 flashes $min^{-1}$) prior to the transition to lower positive flash rates. During this time period, negative CG flash rates were typically less than 1 $min^{-1}$, averaging 0.5 flashes $min^{-1}$ (36 flashes) over the same 70-minute time frame. At 1440 MDT negative CG flashes dominated the 5-minute NLDN flash rates, after which positive CG flashes resumed domination at an average of 1.7 $min^{-1}$ over the next 150 minutes (1445 - 1715 MDT). After 1715 MDT, the storm transitioned to being dominated by negative CG flashes (transition 3).

A summary of CG lightning statistics for this storm can be found in Table 5.1. Note that, consistent with our findings in Chapter 4, the mean positive peak current is on the order of 32 kA, with a mean negative peak current value of –12.8 kA. In an effort to determine how average peak current and multiplicity values changed with the percentage of positive CG lightning we calculated the percentage of positive CG lightning that occurred during the timeframe of each individual radar volume. Average positive and negative peak current and multiplicity values were then calculated for CGs occurring within each radar volume. Results of these calculations are presented in Figure 2(a-d), and show agreement with our findings in Chapter 4; average positive (negative) peak currents increasing (decreasing) with increasing positive CG fraction, with positive CG multiplicity showing slight increases with increasing positive CG fraction (still focused on a value of one), and negative CG multiplicity values decreasing. The reason that average positive peak current values show only a slight increase with positive CG

fraction is due to the small number of data points in which positive CG fraction was less than 50%.

*5.1.2 Overview of Storm Evolution and Structure*

To provide an overview of the general storm evolution throughout the period, Fig. 5.3(a-j) shows a series of horizontal cross-sections of reflectivity (dBZ) obtained from the CSU-CHILL radar at 0.5km AGL; these cross-sections are spaced approximately 30 minutes apart.

During the first hour of full volume sector scans this storm propagated to the southeast with low-level reflectivities typically in excess of 65 dBZ, peaking at 1404 MDT with a core of nearly 72 dBZ (Fig. 5.3b). After this time, reflectivity values rapidly decreased to less than 60 dBZ by 1433 MDT (Fig. 5.3c). The southerly component of the propagation of this storm then ceased and the system began moving due east as it began to re-intensify. Over the next hour, this storm moved approximately 45 km to the east, crossing the LTER Nunn field office shortly after 1520 MDT. Radar operators received in-situ reports from the field office of pea to "good marble" sized hail and high winds. Mud reportedly splashed onto the roof on the north side of the building. Over the next 20 minutes the development and intensification of a "V-notch" on the southeastern flank of the intensifying storm occurred (Fig. 5.3e, x = -4 km, y = 40 km; 5.4a;). This "V-notch", also known as a "hook echo", is a classic tornado vortex-signature (TVS). Examination of gridded velocity data (Fig. 5.4b, x= 0 km, y= 48 km) indicates gate-to-gate shear, with inbound velocities in excess of 15 m/s, and outbound velocities near 10 m/s immediately to the east. Although no confirmed reports of tornadoes were associated with this storm,

a long-lived rotating cloud base was reported shortly after the 1520 MDT field office passage located several miles further south on Weld County Road 37. At 1538 MDT (Fig. 5.4a) the storm was at peak intensity, with a well developed "hook echo" and reflectivities near 73 dBZ. After this point, the storm slowly weakened as it continued to the east. After 1600 MDT the storm began to take on more of an east-west orientation, with additional development having taken place along the trailing outflow boundary by 1633 MDT. By 1640 MDT the system had evolved into a broad convective line with the 40 – 50 dBZ contour extending some 60 km in the east-west direction. Following this broadening of the storm complex, several mergers and cell splits were observed to occur, with the end result being a supercell with peak low-level reflectivities of 70 dBZ located approximately 40 km east of the radar (Fig. 5.3j).

*5.1.3 Comparison of Lightning and Bulk Precipitation Rates*

Upon examination of the surface fluxes during the period of interest (Fig. 5.5 a-c), we noticed a relatively steady state of the total mass flux with a slight increase from 1317 - 1445 MDT, primarily due to rain. Upon further examination, we do note a peak in the surface hail mass flux (Fig. 5.5c) at approximately 1440 MDT, 20 minutes after the peak in positive CG flash rates observed at 1420 MDT. Extending our analysis beyond the transition to lower positive CG flash rates (1445 MDT) we begin to see trends that would support the precipitation "unshielding" hypothesis offered by Carey and Rutledge (1998) (hypothesis 3 outlined in Chapter 1). In general, positive CG flash rates pulsed along with the surface rain mass flux, with peaks in positive CG flash rates associated with relative peaks in rain mass flux values. For example, a relative peak in surface rain

mass fluxes can be seen at 1450 MDT (Fig. 5.5b), followed by a peak in 5-minute positive CG flash rates at 1515 MDT (25 minutes later). This same trend is again repeated, with a shorter time scale, with the observation of a peak in rain mass flux at 1530 MDT, followed by a positive CG peak from 1535 - 1540 MDT. The next significant peak (in CGs) was observed at 1645 MDT, nearly coincident with the large peak in rain mass flux. Following this last significant pulse, positive CG flash rates begin to diminish while surface rain mass flux values continue to increase.

Although surface hail mass fluxes are subject to large errors and must be interpreted with caution, as discussed in Chapter 3, examination of these fluxes (Fig. 5.5c) show trends linking elevated positive CG flash rates to peaks in surface hail mass flux values. Specifically, observed peaks in positive CG flash rates (1420, 1540 and 1645 MDT) appear to precede peaks in the surface hail mass flux by anywhere from 10 to 25 minutes (1440, 1605, and 1710 MDT, respectively).

To investigate the spatial relationship between positive CG lightning and storm structure, we present frequency and cumulative percentage histograms of rain rates which occurred at each of the 433 positive ground strike locations (R) and maximum rain rates which occurred within 10 km of each positive ground stroke ($R_{max}$). We will also discuss positive CG strike location with respect to hail rates, but this discussion will be in relative terms, since hail rate estimations are subject to large errors.

As can be seen in Fig. 5.6, a large fraction (64%) of positive CG flashes were situated in regions of light rain ($\leq$ 20 mm $hr^{-1}$) while 28% of flashes occurred in moderate rain (20 – 60 mm $hr^{-1}$). Only 8% occurred in areas of heavy rain ($\geq$ 60 mm $hr^{-1}$). The distribution of peak rain rate within 10 km is very flat with relative maxima at 10, 30, 70,

100, 140, 160 and 180 mm $hr^{-1}$, suggesting that many positive ground strokes are within a convective scale distance (10 km) of a sometimes intense precipitation shaft.

Similar analyses were accomplished for both hail rates at the ground strike location and maximum hail rates within 10 km of the positive ground strike. The results from these analyses indicate that a very small percentage of the positive CG flashes come to ground in areas of significant hail rates, and that nearly 25% of the positive CG flashes occurred within a convective scale distance (10 km) from a hail shaft.

### *5.1.4 Identification of Bulk Hydrometeor Types*

Following the procedures outlined in Chapter 3, results from our hydrometeor partitioning indicate a good mix of hydrometeor types throughout the storm. If an inverted dipole were indeed present during this event (although we are unable to determine if a reversal of the primary charge dipole occurred) our observations may lend credence to this hypothesis to explain the occurrence of positive CG flashes. If a typical thunderstorm dipole were present, however, our findings may then lend credence to the precipitation unshielding hypothesis offered by Carey and Rutledge (1998). Unfortunately, we had no measurements of the charge structure in the storms we studied.

Prior to the observed transition from high positive CG flash rates to lower flash rates (1440 MDT) our hydrometeor partitioning (below the melting level; Fig. 5.7) indicated the presence of large hail, large hail mixed with rain, small hail, and small hail mixed with rain. After the transition, however, we noted the absence of large hail, with a significant reduction in the volume of large hail mixed with rain, leading to a predominantly small hail/rain mix (1445 – 1600 MDT). Consistent with our findings in section 5.1.4, after approximately 1600 MDT we began to see a dramatic increase in the storm volume beneath the melting level that contained pure rain.

Recall from our discussions on non-inductive charging in Chapter 2 (Sec. 2.2), that for a typical thunderstorm dipole (positive charge situated over negative charge) graupel/ice collisions occurring beneath the charge reversal temperature, which is some threshold between –10 °C and -20 °C (depending on liquid water content), will result in the graupel particle becoming positively charged with negative charge being imparted to the ascending ice crystals. This mechanism would lead to the development of an area of enhanced positive charge beneath the main negative charge center, providing a downward bias for generation of negative CG lightning. Upon examination of time-height cross-sections of small hail below the melting level (Fig. 5.8), along with graupel above the melting level (Fig. 5.9), we find elevated volumes of the former occurring minutes after observing elevated volumes of graupel above the melting level. Specifically, we observe elevated volumes of graupel at T > -20 °C, which may be beneath the charge reversal level depending upon LWC, preceding elevated volumes of small hail beneath the melting level by anywhere from 5 to 15 minutes. More importantly, these peaks in graupel volume precede observed peaks in positive CG flash rates by anywhere from (10 - 25 minutes).

There are two arguments that may explain the peaks in positive CG flashes, as opposed to negative CG flashes, observed following peaks in graupel above the melting level. An inverted dipole, with negative charge situated over positive charge could explain the increase in positive CG flashes, associated with the increase in graupel aloft. Here, graupel particles, descending beneath the charge reversal level could obtain negative charge as a result of graupel/ice crystal collisions. This would then lead to the generation of an enhanced lower negative charge area, thus providing a downward bias for positive CG flashes. This applies if the graupel is suspended within an updraft. If the graupel is descending in a downdraft, then the charge reversal and NIC mechanisms would no longer apply, as precipitation in a downdraft would quickly scavenge cloud liquid water and suppress the presence of freshly nucleated ice crystals. A second, and more plausible, explanation for the observed peaks in positive CG lightning involves a normal thunderstorm dipole (positive over negative charge). Here, as the graupel above the melting level

descends it produces enhanced small hail volumes beneath the melting level. This small hail then proceeds to melt, resulting in a small hail/rain mix at the surface. Rather than creating a reversal in charge, the descending small hail and rain carries negative charge, thus depleting the primary negative charge center, increasing the likelihood of positive CG flashes.

Additional support can be added to this second explanation by looking at the time series of large hail (> 1 cm) above the melting level (Fig. 5.10). Here we find positive CG flash rates and large hail aloft to be anti-correlated, with peaks in large hail associated with depressions in the positive CG flash rates. The presence of large hail aloft may be indicative of wet growth at high liquid water contents (Williams et al., 1991) for which positive charging of the precipitation may occur. This statement, however, is a very loose assumption, as Saunders and Brooks (1992) argued that under wet growth conditions, ice crystals are more likely to adhere to hail and graupel particles, rather than rebound, thus decreasing charge separation under these conditions. Never the less, the presence of elevated liquid water content may enable the charge reversal mechanism to occur during these time frames, thus enhancing the depleted lower charge centers in the storm, suppressing the positive CG lightning during these times.

Although we are unable to determine if a reversal of the primary charge dipole (i.e. inverted dipole) occurred in this event, our observations may lend credence to this hypothesis if an inverted dipole were in fact present. If a typical thunderstorm dipole were present, our findings may then lend credence to the precipitation unshielding hypothesis offered by Carey and Rutledge (1998). However, these arguments must remain speculations since charge measurements were unavailable.

## 5.2 1 July 1998

Multiparameter observations of the 1 July 1998 storm began at 1803 MDT. Full volume coverage was conducted up to 2025 MDT. Cloud-to-ground (CG) lightning flash

rates were low throughout the first half of the storm, transitioning to high-density positive CG domination at 1945 MDT. Preliminary analysis performed by Lang and Rutledge (1999) during the low CG phase indicated that updraft speeds were as large as 40 m $sec^{-1}$. These strong updrafts were argued to have created an elevated dipole (MacGorman and Nielsen, 1991), thus favoring IC over CG discharges. Our subsequent analysis of this storm will be focused on the time frame following the low CG phase, and focused on the electrical transition marking the domination by positive CG lightning.

*5.2.1 Overview of Storm Electrical Characteristics and Transitions*

Figure 5.11 shows a time-series plot of 5-minute NLDN CG flash rates, along with averaged 1-minute flash rates for both lightning polarities. From approximately 1800 - 1900 MDT this storm exhibited characteristics similar to cases studied by Lang et al. (1999), storms being dominated by positive CG flashes at low flash rates (typically less than 0.4 flashes $min^{-1}$). After 1900 MDT, however, the storm began to transition from a low CG producer to a high CG producer with peak total flash rates over the next 40 minutes of observation approaching 3 flashes $min^{-1}$, predominantly dominated by negative CG flashes. Positive CG flashes began to dominate after 1940 MDT with positive flash rates peaking at 1 flash $min^{-1}$ for a 10 minute period, averaging 0.9 flashes $min^{-1}$ for the 20 minute period in which positive CG flashes were observed to dominate. Overall, the average positive CG flash rate from 1900 to 2005 MDT (65-minute period following the transition to high CG flash rates) was 0.6 flashes $min^{-1}$. We will focus our subsequent analysis during the time frame of the electrical transition observed at 1910 MDT, specifically 1856 - 2000 MDT (times of available full volume scans).

Cloud-to-ground lightning statistics for this storm can be found in Table 5.2. Again, consistent with our findings in Chapter 4, only this time for a lower density positive CG event, this storm had a mean positive peak current near 20 kA, with a mean negative peak current near –15 kA. Unlike our findings from the 2 June 97 case, the lightning characteristics (averaged positive peak current and negative CG multiplicity) for this storm do not seem to be consistent with our findings in Chapter 4. In Fig. 5.12(a-d) we see that both averaged positive and negative peak currents decrease with increasing percentage of positive CG lightning. Although not conclusive, this downward trend in average positive peak current is probably a function of the number of data points available; the large average positive peak current at 10% positive CG fraction is actually associated with a single positive CG with a peak current of 33.21 kA. If we were to remove this data point the overall trend in the data would be for the average positive peak current to increase with increasing positive CG fraction, the same trend would most likely result from additional data points. Also, most likely a result of the number of data points, we see an increasing trend in negative CG multiplicity with increasing positive CG fraction. The data point that is causing this upward trend is the result of 2 negative CG flashes with an average multiplicity of 4.5 return strokes.

### *5.2.2 Overview of Storm Evolution and Structure*

This section will characterize the significant features associated with the storm as it evolved during the period of interest. Horizontal cross-sections of reflectivity (dBZ) spaced approximately 15 minutes apart, are presented in Fig. 5.13(a-e).

When full volume scans of this storm began at 1803 MDT (Fig. 5.14) a maximum, low-level, reflectivity core (69 dBZ at 0.5 km AGL) was located approximately 40 km north of the CSU-CHILL radar. Over the next hour, this supercell maintained core reflectivity values above 60 dBZ while moving approximately 30 km to the southeast. All the while, this storm exhibited characteristics similar to those observed by Lang (1997), being dominated by positive CG flashes at low flash rates (typically less than 0.4 flashes $min^{-1}$).

At 1856 MDT (our first analysis volume) this supercell began to split, with a low-level reflectivity core (69 dBZ) located approximately 25 km NE of the CHILL radar (Fig. 5.13a; x = 18 km, y = 21 km), and a secondary core (> 50 dBZ) developing just to the north. By 1908 MDT (Fig. 5.13b) the right moving cell, continued its southeasterly progression, while the newly generated cell to the north moved slowly to the north-northeast. As the southern cell was the dominate of the two cells, azimuthal limits of the radar were decreased to ensure good temporal resolution of this cell; consequently, by the 1920 MDT volume scan (not shown), the northern cell was no longer being scanned.

By 1925 MDT (Fig., 5.13c), the primary cell had again split while 2 new cells (both in excess of 50 dBZ) began converging with the primary cell from the south and southeast. Additionally, we begin to see the development of a multi-cellular convective line (< 50 dBZ) to the north-northeast of the primary cell. Azimuthal limits of the radar were again adjusted, this time to include the most intense cells, as well as the developing convective line. Over the next 20 minutes several cell mergers occurred, with the most notable being at 1950 MDT with two cells having merged to create a 50 – 60 dBZ

contour extending some 25 km in the east-west direction, with two separate cores in excess of 60 dBZ.

To summarize storm evolution, this storm began as a single supercell that split a total of four different times during our observation. Further, this supercell also merged with several developing cells, the most notable being the brief 1950 MDT merger between cells 1 and 5, resulting in a broad, multi-cellular line, extending some 25 km in the east-west direction. This merger occurred during the same time frame in which positive CGs were observed to begin dominating the CG lightning strikes.

### *5.2.3 Comparison of Lightning and Bulk Precipitation Rates*

An examination of surface fluxes for this storm (Fig. 5.15a-c) reveals that the primary component of the storm total mass flux is the contribution made by the rain mass flux. Looking at the surface rain mass fluxes (Fig. 5.15b) during the period of interest (1856 - 2000 MDT) we see both positive and negative CG flash rates increase along with the increasing mass flux values. At approximately 1940 MDT, coincident with the peak in surface rain mass flux, the negative CG flash rates begin to plummet to 0.2 $min^{-1}$ by 1950 MDT. As the negative CG flash rates diminish we see an increase in the positive CG flash rate, peaking at 1955 MDT, 15 minutes after the observed peak in the surface rain mass flux. This observation is broadly consistent with the precipitation "unshielding" hypothesis, and will be explored further in the next section.

Upon investigation of the spatial relationships between positive CG ground strike locations and rain rates for this case (Fig. 5.16) we found that 60% of the positive CGs were situated in regions of light to moderate rain (24% light, 36% moderate), with 40%

of the positive CGs coming to ground in areas of heavy precipitation. Further our findings indicate that the majority (80%) of positive CG flashes were located within 10 km of some intense precipitation shaft. Although positive CGs in this storm seemed to have some higher rain rates associated with them, they were still typically void of high hail rates. In fact, over 75% of the positive CGs came to ground in areas of relatively light hail rates. On the other hand, nearly 75% of all positive CGs came to ground within 10 km of an intense hail shaft, contrary to our findings in case 1.

### *5.2.4 Identification of Bulk Hydrometeor Types*

Results of the hydrometeor partitioning for this case show enhanced volumes of large hail mixed with rain near the surface, occurring from the beginning of our period of interest, and ceasing prior to the 1935 MDT peak in total CG lightning (Fig. 5.17). This decrease in volume occurred some 25 – 30 minutes prior to the transition to positive CG domination at 1945 MDT. Time height cross-sections of individual hydrometeor types indicates that elevated volumes of small hail were present just beneath the melting level from roughly 1845 - 1930 MDT. All the small hail melted as it fell to the surface, leaving only the largest hail to be mixed with rain. Above the melting level, our analysis reveals a broad maximum in graupel volume (Fig. 5.19) prior to the transition to positive CG domination. This maximum persisted from approximately 1920 – 1935 MDT, the same time frame of the observed broad peak in negative CG flashes. Additionally, volumes of large hail (> 1 cm) above the melting level peak at about 1920 MDT, just prior to the increase in negative CGs. As discussed in section 5.1.5 the presence of large hail may be an indication of wet growth. Wet growth conditions would be expected to

provide ample LWC for charge reversal associated if rebounding collisions of graupel and ice particles beneath the primary negative charge center indeed occurred. The flurry of negative CGs following the peak in large hail above the melting level adds credence to the argument for an area of enhanced lower positive charge, which would provide a downward bias for negative CG discharges in a typical thunderstorm dipole.

The switch in the dominant polarity of the storm observed at 1945 MDT occurs 25 minutes after the peak in large hail volumes just discussed. Recall that the peak in the surface rain mass flux occurred approximately 5 – 10 minutes prior to this transition. We can speculate that the precipitation-laden downdraft of this storm rapidly depleted cloud liquid water, thus eliminating the lower positive charge region. Continued precipitation then scavenged negative charge from the lower portions of the storm providing more favorable conditions for positive CG flashes.

## 5.3 2 July 1998

Not 24 hours after the initiation of the previous case, a second storm exhibiting characteristics desirable for this study developed north-northwest of the CSU-CHILL radar. This storm started out being dominated by negative CG flashes, but quickly transitioned to domination by positive CG flashes, with a period of nearly 30 minutes in which negative CG lightning was non-existent.

### *5.3.1 Overview of Storm Electrical Characteristics and Transitions*

Figure 5.20 shows a time-series plot of 5-minute NLDN CG flash rates, along with averaged 1-minute flash rates for each polarity. This storm started out dominated by

negative CG lightning from 1730 - 1750 MDT, after which the negative CG flashes ceased. Positive CG flash rates rapidly increased to 1 flash $min^{-1}$ by 1805 MDT, followed by a rapid decrease over the following 5 minutes. Positive CG flash rates remained at 0.2 $min^{-1}$ for the next 15 minutes, with negative CG flashes non-existent. After 1820 MDT we begin to see both positive and negative CG lightning activity exhibit a pulsing characteristic, with positive CG flashes remaining dominant through then end of our period of interest. Overall, the average positive CG flash rate was 0.6 flashes $min^{-1}$ over the 50-minute period in which positive CG flashes were observed to dominate the CG lightning strikes. We will focus our subsequent analysis during the time-frame of the electrical transition observed at approximately 1755 MDT, specifically 1733 MDT - 1835MDT (times of available full volume scans).

Table 5.3 summarizes the CG lightning statistics for this storm, with Fig. 5.21(a-d) showing the results of our investigation into how the CG lightning characteristics are modified with increasing positive CG fraction. Again we see that the average positive peak current is larger than the average negative peak current for all flashes. When trends in peak current and multiplicity are examined, we find that the lack of data points again causes problems in interpreting the data, as one or two outlying points can significantly impact the linear trends. This problem will be resolved in Section 5.5 where we discuss the trends in the data using all four data sets, providing us with over 550 positive CG flashes, and 350 negative CG flashes. By combining all four data sets we will have a total of 93 volumes, over which we can calculate our positive and negative CG statistics.

*5.3.2 Overview of Storm Evolution and Structure*

To provide and overview of our third case study, Figure 5.22(a-f) shows a series of horizontal cross-sections of reflectivity (dBZ), each spaced approximately 10 – 15 minutes apart. At the time of the first volume scan (1733 MDT; Fig. 5.22a) the peak, low-level, reflectivity (0.5 km AGL) was 65 dBZ (cell 1). This storm remained, relatively, quasi-stationary during the first half hour of radar coverage with the center of the reflectivity core ( $\geq$ 63 dBZ) moving only 8 km to the southeast in a 30 minute time period. An interesting feature that appeared benign during this initial volume scan, but later developed into a convective line was the weak line of reflectivity ( $Z_h \leq 20$ dBZ) that extended from the northeastern edge of the storm (x = -10 km, y = 90 km) to the east-northeast, out of range of the radar. A weak core of reflectivity was apparent in this line with a 20 - 30 dBZ contour at x = 0 km, y = 92 km (cell 2). Cell 2 rapidly expanded, horizontally, but after 1744 MDT (Fig. 5.22b) began showing signs of dissipation. Examination of the velocity data associated with cell 2 is indicative of an outflow boundary propagating to the south. By 1754 MDT (Fig.5.22c) cell 2 had completely dissipated, with the outflow having contributed to the development of a secondary reflectivity core (cell 3) within the interior of the 30 - 40 dBZ contour of cell 1, extending to the northeast. By 1807 MDT (Fig. 5.22d) a well developed convective line had organized, and began moving more rapidly to the east. By 1816 MDT cell 1 had spilt, generating a 3rd reflectivity core (cell 4), while at the same time an unassociated cell (cell 5) had developed 25 km north-northeast of the CHILL radar site (50 km south of the convective line). Cell 4 rapidly dissipated, leaving cells 1 and 3 (both sharing a common 40 – 50 dBZ contour) at 1822 MDT (not shown), with cell 5 (to the south) rapidly

intensifying. Shortly after this time, the focus for data collection shifted to cell 5, thus degrading the spatial resolution of the convective line to the north (cells 1 and 3). As a result of this shift in scanning strategy, we will focus our analysis on the microphysical evolution of the storm up to this point. This new cell, however, eventually merged with the convective line, creating a multi-cellular line with a continuous 30 - 40 dBZ echo extending some 55 km in horizontal distance.

### *5.3.3 Comparison of Lightning and Bulk Precipitation Rates*

Upon examination of mass flux time-series plots associated with this storm (Fig. 5.23 a-c) we see that the total mass flux is fairly steady-state, with a broad peak observed to occur in and about the time of maximum positive CG flash rates (1805 MDT). Looking at the individual components of the total mass flux associated with this storm (rain and hail mass fluxes), we note that the rain mass flux (Fig. 5.23b) is the primary contributor to the total mass flux. Examining the hail mass flux (Fig. 5.23c) however, we find a peak in the hail mass flux approximately 10 minutes prior to the observed transition from negative to positive CG flash domination (1755 MDT), 20 minutes prior to the peak in positive CG flash rates.

Our investigation into the spatial distribution of positive CG lightning with respect to rain rates is presented in Figure 5.24. Similar to the 2 Jun 97 storm, positive CG lighting is this storm is also found to occur predominantly away from the precipitation cores. As can be seen in Fig. 5.24, the majority (59%) of the positive CG flashes were situated in regions of light rain, 36% in moderate rain, and only 5% in heavy rain. We also find that about 50% of the positive CGs fell within 10 km of intense

precipitation (> 60 mm $hr^{-1}$). Results from looking at positive CG strike locations and relative hail rates are also very similar to our findings in case 1, with only 6% of the positive CGs associated with significant hail rates (i.e. hail rates exceeding 2 mm $hr^{-1}$).

*5.3.4 Identification of Bulk Hydrometeor Types*

Results of our hydrometeor partitioning indicate that this storm produced a mixture of predominantly small hail mixed with rain near the surface (Fig. 5.25a), with small hail only just beneath the melting level (Fig. 5.25b). Not much in the way of rain only was detected during our observation period, although rain volumes did begin to increase near the end of the period of observation. A broad maximum in small hail volume below the melting level was apparent throughout the majority of our period of interest, with a peak in the volume of small hail mixed with rain near the surface from 1745 - 1750 MDT, 5 - 10 minutes prior to our electrical transition, 20 - 25 minutes prior to our peak positive CG flash rates (1805 MDT).

Above the melting level, our partitioning algorithm indicated two broad peaks in graupel volume (Fig. 5.25c), the first appeared from approximately 1755 - 1810 MDT, after the electrical transition of this storm. The second peak in graupel volume was observed between 1820 - 1830 MDT, the same time frame in which positive CG flash rates recovered from their brief (15 minute) suppression. Additionally, above the melting level we see a peak in large hail (> 1 cm) volume at 1745 MDT, 10 minutes prior to electrical transition, 20 minutes prior to peak positive CG flash rates Fig. 5.26.

Of additional interest is the 15-minute period (1810 - 1825 MDT) in which positive CG flash rates, dropped significantly, with only a total of 3 flashes detected

during this time frame. This is the same time frame in which the primary cell in this storm split (1807 MDT; Fig. 5.22d) and subsequently re-intensified some 15 minutes later (by the 1822 MDT volume). Coincident with the splitting of the primary cell, we see suppression in graupel volumes above the melting level, relative to the two broad maxima discussed above.

## 5.4 21 July 1998

The day of 21 July 1998 was characterized by widespread convection with echoes > 30 dBZ extending from 315 deg to 045 deg in azimuth at a range of 50 to 75 km from the CSU-CHILL radar. Coverage of the final storm examined during this study did not begin until 1632 MDT, at which point there were three well developed cores of reflectivity > 50 dBZ within an enclosed 40 dBZ contour .

### *5.4.1 Overview of Storm Electrical Characteristics and Transition*

Figure 5.27 shows a time series of the 5-minute NLDN flash rates, along with averaged 1-minute flash rates, for each polarity. As we can see, this storm was dominated by negative CG flashes during the first hour of observation (1630 - 1730 MDT) with peak negative flash rates of 3.2 $min^{-1}$, and average flash rates of 1.9 $min^{-1}$ during the one hour period (113 flashes). During this same time frame, positive CG flash rates were low, with a total of only 12 flashes over the entire 1-hour period (averaging 0.2 flashes $min^{-1}$). After 1730 MDT a sharp transition in the dominant polarity of flashes occurred, with positive CG flash rates increasing dramatically. Peak values were

2.2 $min^{-1}$, and averaged 1.9 flashes $min^{-1}$ over the next 35 minutes. Coincident with this ramp up in positive CG flashes, the production of negative CG flashes diminished markedly, with average values over the 35-minute time frame of 0.5 $min^{-1}$. We will focus our subsequent analysis during the time-frame of the electrical transition observed at 1730 MDT, specifically 1719 MDT - 1809MDT (times of full volume scans).

Cloud-to-ground lightning statistics for this case can be found in Table 5.4, with Fig. 5.28(a-d) showing the results of our investigation into how the CG lightning characteristics are modified with increasing positive CG fraction. Again we see that the average positive peak current is larger than the average negative peak current for all flashes. Despite the relatively few data points (compared to the 2 June 97 case), examination of the trends in peak current and multiplicity are very consistent with our findings in Chapter 4, and similar to those found for the 2 June 97 case. We see increasing (decreasing) positive (negative) average peak currents with increasing positive CG fraction, and decreasing negative multiplicity values, with positive multiplicity showing a slight increase, but still focused on a value of 1. The reason that the data from this case is more usable than those of the previous 2 cases (1 and 2 July 1998), is because there were a total of 215 lightning flashes from which to derive our statistics (80 positive CGs and 135 negative CGs). Cases 2 and 3 each had a total of less than 100 flashes from which to derive these same statistics. Again, these problems will be resolved in Section 5.5 where we discuss the trends in the data using all four data sets.

*5.4.2 Overview of Storm Evolution and Structure*

Early in the afternoon of 21 July 1998, data collection at the CSU-CHILL radar was focused on a thunderstorm complex, to the northwest of the radar site, that generated locally strong surface winds, hail and flooding rain. Due to the proximity of the storm to the radar, the azimuthal limits were set so as to ensure full volume coverage of this system as it moved to the east. It was not until 1632 MDT that the azimuthal limits of the radar were broadened so as to include the cells of interest in this study. Figure 5.29(a-g) provides an overview of the general storm evolution, with low-level horizontal cross-sections of reflectivity spaced approximately 15 minutes apart.

Our first full volume scan of the period was made at 1632 MDT (Fig. 5.29a), showing the position of three convective cores with reflectivities in excess of 50 dBZ, each sharing a common 40 – 50 dBZ contour. Several mergers and splits are observed to occur over the next 45 minutes with the end result being a broad multi-cellular convective line 60 km northeast of the CSU-CHILL radar spanning approximately 50 km from northwest to southeast (1719 MDT; Fig 5.29d); peak low-level reflectivites were measured at 54 dBZ in the southeastern portion of the line. Over the next 15 minutes, the convective line broadened as it slowly propagated away from the radar. Five separate reflectivity cores, in excess of 50 dBZ, are visible during the 1734 MDT volume scan (Fig. 5.29e), however the eastern most cell is 85 km from the radar, and quickly propagates out of range. It is during this volume scan in which we observe the transition to domination by positive CG flashes, primarily associated with the convective core located in the center of the convective line (approximately 50 deg azimuth). From this point on, positive CG flash rates remain elevated as the convective line continues to

propagate to the east, with the southern most cells beginning to dominate as the northern cells dissipate. At 1747 MDT (Fig. 5.29f) we see our first low-level reflectivity cores exceeding 60 dBZ (62 dBZ at x = 76 km, y = 26 km). By 1809 MDT (Fig. 5.29g), our last volume scan, two reflectivity cores in excess of 60 dBZ are present, both in the southern most portions of the convective line, each cell however is on the fringe of the radar resolution boundaries.

### *5.4.3 Comparison of Lightning and Bulk Precipitation Rates*

Upon examination of the surface fluxes during the period of interest (Fig. 5.30a-c), we note the significant change in hail flux near 1725 MDT (Fig. 5.30c). Before this time hail fluxes were insignificant, and CG flash rates were predominantly negative. After this time however, a marked increase in hail mass flux values occurred, as well as an increase in positive CG flash rates. These results are similar to the findings of Lang (1997) who observed positive CG flash rates to dominate during periods of elevated hail mass fluxes during a 12 July 1996 storm in NE Colorado. In our case, peaks in the positive CG flash rates appear to precede peaks in the surface hail fluxes by approximately 10 minutes. The surface rain mass flux rates (Fig. 5.30b) seem to be relatively steady state, only showing a gradual increasing trend toward the end of the period. During the time frame in which we are interested we did observe rain mass flux values increasing about 10 minutes prior to the transition to positive CG domination, with a relative peak 5 minutes prior to the transition.

Similar to our findings in cases 1 and 3, Fig. 5.31 shows that 50% of the positive CGs came to ground in areas of light rain, 37% in moderate rain, and only 13% in heavy

rain. Also, 69% of the positive CGs were located within 10 km of an intense precipitation shaft (> 60 mm $hr^{-1}$). Examining the relative hail rates, we find the same trends as in cases 1 and 3, with the bulk (95%) of positive CG strikes located in areas characterized by relatively low hail rates, with 35% being located within 10 km of a relatively intense hail shaft.

*5.4.4 Identification of Bulk Hydrometeor Types*

Results of our hydrometeor partitioning for our final case indicate that throughout its entire lifetime, the storm volume below the melting level was predominantly characterized by small hail mixed with rain (Fig. 5.32). During the 30 minute period surrounding the time of our electrical transition (approx. 1715 - 1745 MDT) we do see a slight increase in the presence of strictly small hail (category 1, Table 3.4; Fig. 5.33) just beneath the melting level, which eventually mostly melts as it falls to the surface, producing a rain hail mix. Above the melting level our partitioning detected no large hail (> 1 cm; category 6, Table 3.4), but did indicate the presence of an enhanced graupel volume aloft near the end or our observational period (after 1745 MDT; Fig. 5.34). Close inspection of the graupel volume time-series presented in Fig. 5.34 also reveals a relative peak in graupel volume at 1724 MDT, 6 minutes prior to the observed electrical transition.

In this particular case, we speculate that the lack of large hail aloft, may be indicative of the absence of wet growth. We could then argue that due to a lack of cloud liquid water, the charge reversal mechanism would not apply in this case. As in our other cases, the presence of small hail beneath the melting level, which eventually melts, and

falls to the ground in a rain/hail mix may lend support to the precipitation "unshielding" hypothesis. Examination of the data prior the time frame of interest indicates that small hail volumes just beneath the melting level were practically non-existent prior to the polarity transition (Fig. 5.33). In fact our first peak in small hail volumes occurs at approximately 1720 MDT, 10 minutes prior to positive CG domination in this case.

## 5.5 Summary and Discussion

This section will provide an overall summary of our findings in this chapter, highlighting any repeatable trends appearing in the data. We will also provide a discussion as to the applicability of each of the three hypotheses offered for explaining the occurrence of positive CG lightning in mature thunderstorms; specifically: (1) the tilted dipole, (2) the enhanced lower positive charge (or inverted dipole), and (3) the precipitation "unshielding" hypotheses.

### *5.5.1 Summary of Significant Trends*

Table 5.5 provides a summary of the 921 CG lightning flashes associated with these four events. Figure 5.35 shows how each of the CG lightning characteristics (average positive and negative peak current and average positive and negative CG multiplicity) is modified with the positive CG fraction. Overall, these findings are in very good agreement with those found in Chapter 4, with increasing (decreasing) positive (negative) peak currents associated with increasing positive CG fraction. CG multiplicity values also show trends in agreement with our previous findings.

Our analysis of four significant lightning producing storms has revealed some interesting relationships between the multiparameter radar inferred precipitation structure and positive CG lightning. The following points summarize the key findings in this chapter:

1) Overall, our findings (Fig. 5.36) indicate that the majority (59%) of the positive CGs associated with each of these cases were situated in regions of light rain ($\leq$ 20 mm $hr^{-1}$) while 22% of the flashes occurred in moderate rain (20 – 60 mm $hr^{-1}$). Only 19% of the positive flashes were situated in heavy rain ($\geq$ 60 mm $hr^{-1}$). Additionally, more than 90% of the positive CGs came to ground in areas of low-level reflectivities in excess of 20 dBZ (at 0.5 km AGL). Furthermore, these findings indicate that many of these lightning strikes are within a convective scale distance (10 km) of an intense precipitation shaft. Typically, positive CG flashes were also void of significant hail rates as well.
2) In the two cases in which large hail (> 1 cm) was detected above the melting level prior to the observed electrical transition (1 and 2 July 98), we found peaks in large hail aloft to precede peaks in positive CG flash rates by anywhere from 20 – 25 minutes. In our 2 June 97 case, large hail aloft was detected after the initial electrical transition to positive CG domination. Hence in that case large hail aloft was anti-correlated with positive CG lightning, with peaks in large hail volumes associated with suppressed (but still present) positive CG flash rates.
3) In three of the four cases studied we found elevated graupel and small hail volumes above the melting level preceded peaks in positive CG flash rates by anywhere from 15 – 25 minutes. The exception to this was the 2 July 98 case, where we noted two

broad peaks in graupel volume aloft, both collocated with peaks in positive CG flash rates. The absence of graupel aloft, between these two peaks was coincident with suppressed positive CG flash rates, and occurred during the same time frame as we observed the thunderstorm to split.

4) Additionally, the presence of small hail just beneath the melting level seems to be of significance with respect to electrical transitions and subsequent peaks in positive CG flash rates. With the exception of the long lived 2 June 97 case, each of the storms had peaks in small hail volumes located just beneath the melting level several minutes prior to the observed electrical transition, and subsequent peaks in positive CG flash rates. Further in each of the four cases peaks in the positive CG flash rates tend to lag peaks in the surface mass flux (rain, hail or both) by anywhere from 5 – 25 minutes.

*5.5.2 Discussion of Hypotheses*

As discussed in Chapter 1, a tilted dipole is a normal polarity dipole (positive over negative charge) in which the positive charge carried on ice crystals is tilted down-shear by storm relative winds from the precipitation shaft which carries negative charge, thus resulting in an electrical dipole that is tilted with respect to the vertical. The horizontal displacement of the positive charge center effectively "unshields" the positive charge from the surface of the earth. Such an arrangement of charge could then facilitate the occurrence of positive ground flashes. Some limited evidence for this mechanism can be found in our observations. Specifically, we note that a majority of positive CG flashes tended to occur in areas of light rain with little or no hail (Figs. 5.6, 5.31, and 5.36).

A larger portion of our findings, however, tend to negate the applicability of this hypothesis, for our cases. A large portion of the positive CGs were located within 10 km of an intense precipitation shaft of some sort, indicating that the positive CGs came to ground relatively close to the convective cores, rather than horizontally displaced as this hypothesis suggests. Also, some of the positive CGs were found in areas characterized by heavy precipitation (Fig. 5.16 and 5.36). Additionally, less than 5% of the postive CGs came to ground in areas characterized by weak low-level reflectivity ($\leq$ 10 dBZ at 0.5 km AGL) with increasing reflectivities aloft; indicative of the possibility of positive CGs emanating from the horizontally displaced anvil region of the storm. Furthermore, in each of the cases presented the occurrence of negative CG lightning was relatively depressed during the portion in which positive CGs were observed to dominate. The tilted dipole hypothesis does not explain the suppression of negative CGs, because if the dipole were merely tilted, one would not expect a preference for positive CG lightning since the negative charge center is still closer to the ground.

The second hypothesis offered for explaining positive CG lightning in mature thunderstorms involves the development of an enhanced lower positive charge region (or inverted dipole). Recall that under certain conditions, graupel and hail particles can obtain positive charge with ice crystals acquiring negative charge during a rebounding collision in the presence of supercooled cloud liquid water. The gravitational separation of these particles could facilitate the generation of a lower positive charge center. Williams et al. (1991) point out that most hailstones with diameters of 1 cm or larger would experience wet growth at moderate to high liquid water contents for which positive charging of the precipitation particle may occur. Williams et al. (1991) and

Williams (1995) suggest that the prevalence of wet growth conditions for riming hail may explain the presence of positive CG clusters in severe thunderstorms. However, the laboratory experiments of non-inductive charging by Saunders and Brooks (1992) suggest that charging of the rimer during wet growth conditions becomes negligible, as colliding particles would be more apt to adhere to one another rather than rebound.

The majority of our findings, however, tend to support the precipitation "unshielding" hypothesis offered by Carey and Rutledge (1998), where intense precipitation shafts lead to a large precipitation current which removes charge from the negative charge center, thereby "unshielding" the upper level positive charge center. As in the tilted-dipole hypothesis, once this "unshielding" occurs, conditions are favorable for positive CG lightning. Based on our findings, summarized in Sec. 5.5.1, we can argue that as small hail and graupel fall beneath the melting level, they bring with it negative charge from the lower portions of the storm. This descending ice mass creates enhanced volumes of small hail just beneath the melting level. Peak mass fluxes at the surface tend to follow the peaks in enhanced hail volumes, indicating that the small hail fell to the surface in the form of small hail and rain. Following the peaks in surface mass flux we typically see enhanced positive CG flash rates, and suppressed negative CGs. Peaks in the positive CG flash rates are typically achieved within 25 minutes of the observed peaks in surface mass flux. The suppression of negative CG lightning is explained by the transfer of negative charge to ground via a precipitation current, not by lightning itself.

**Cloud-to-Ground Lightning Statistics: 2 June 1997**

| *Statistic* | *Positive CG lightning* | *Negative CG lightning* |
|---|---|---|
| Count | 433 | 247 |
| Mean (kA) | 32.3 | -12.8 |
| Standard Deviation (kA) | 18.2 | 7.5 |
| Minimum (kA) | 7.4 | -62.9 |
| Maximum(kA) | 155.4 | -3.7 |

Table 5.1: Summary of CG lightning statistics for 2 June 1997 case study.

**Cloud-to-Ground Lightning Statistics: 1 July 1998**

| *Statistic* | *Positive CG lightning* | *Negative CG lightning* |
|---|---|---|
| Count | 31 | 57 |
| Mean (kA) | 19.8 | -15.4 |
| Standard Deviation (kA) | 15.2 | 6.4 |
| Minimum (kA) | 63.3 | -41.7 |
| Maximum(kA) | 7.4 | -8.31 |

Table 5.2: Summary of CG lightning statistics for 1 July 1998 case study.

**Cloud-to-Ground Lightning Statistics: 2 July 1998**

| *Statistic* | *Positive CG lightning* | *Negative CG lightning* |
|---|---|---|
| Count | 25 | 13 |
| Mean (kA) | 29.3 | -17.5 |
| Standard Deviation (kA) | 18.3 | 7.9 |
| Minimum (kA) | 90.8 | -29.5 |
| Maximum(kA) | 8.1 | -6.5 |

Table 5.3: Summary of CG lightning statistics for 2 July 1998 case study.

**Cloud-to-Ground Lightning Statistics: 21 July 1998**

| *Statistic* | *Positive CG lightning* | *Negative CG lightning* |
|---|---|---|
| Count | 80 | 135 |
| Mean (kA) | 41.4 | -16.2 |
| Standard Deviation (kA) | 28.7 | 7.3 |
| Minimum (kA) | 7.3 | -57.6 |
| Maximum(kA) | 166.7 | -5.7 |

Table 5.4: Summary of CG lightning statistics for 21 July 1998 case study.

**Cloud-to-Ground Lightning Statistics: All Cases**

| *Statistic* | *Positive CG lightning* | *Negative CG lightning* |
|---|---|---|
| Count | 569 | 352 |
| Mean (kA) | 32.8 | -14.3 |
| Standard Deviation (kA) | 20.4 | 7.51 |
| Minimum (kA) | 166.7 | -62.9 |
| Maximum(kA) | 7.31 | -3.7 |

Table 5.5: Summary of CG lightning statistics for all four case studies.

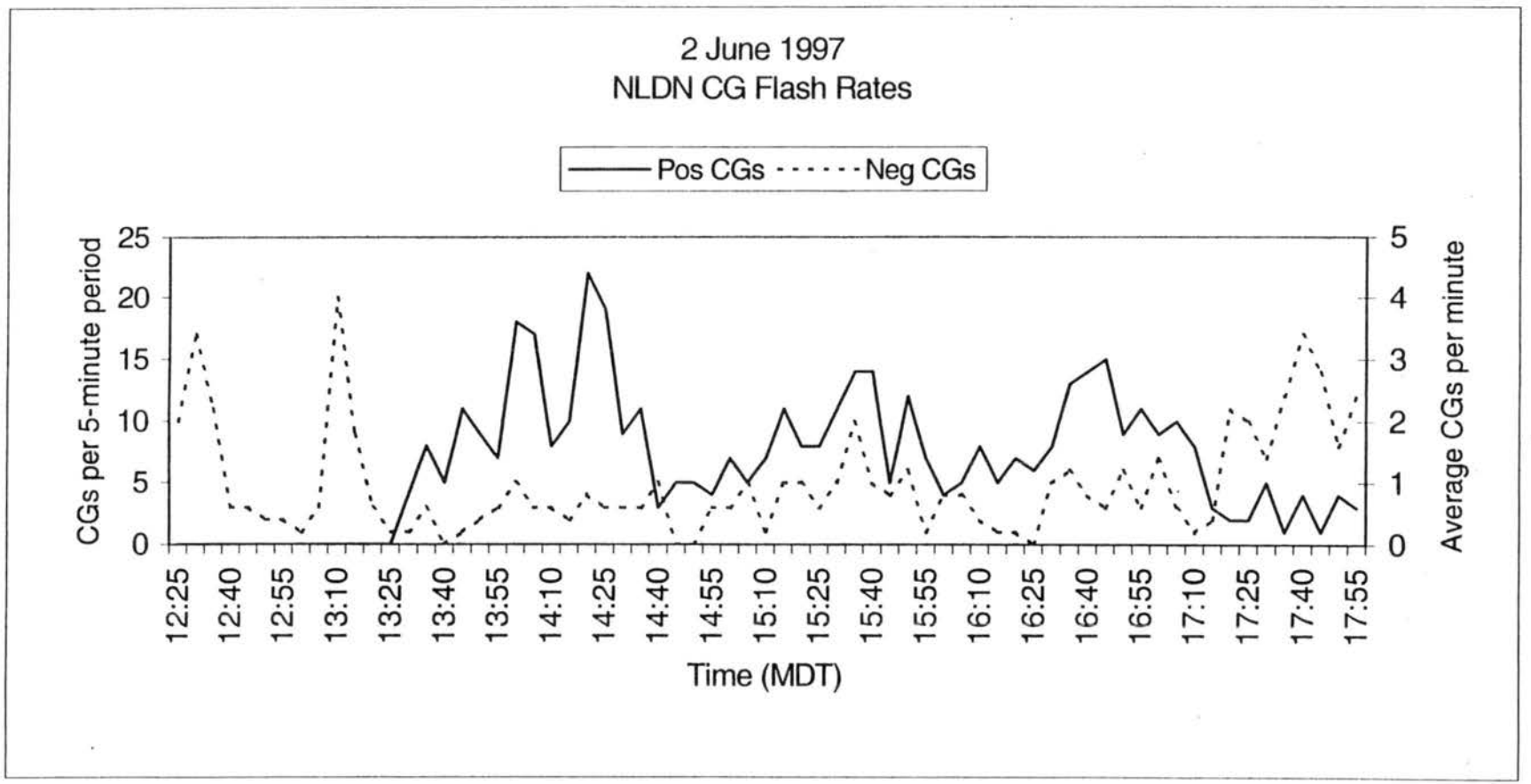


Figure 5.1: 2 June 1997 time-series plot of 5-minute NLDN CG flash rates (left y-axis) and averaged 1-minute flash rates (right y-axis) for each polarity. Positive CG flash rates are plotted with a solid line, with negative CG flash rates plotted with a dashed line.

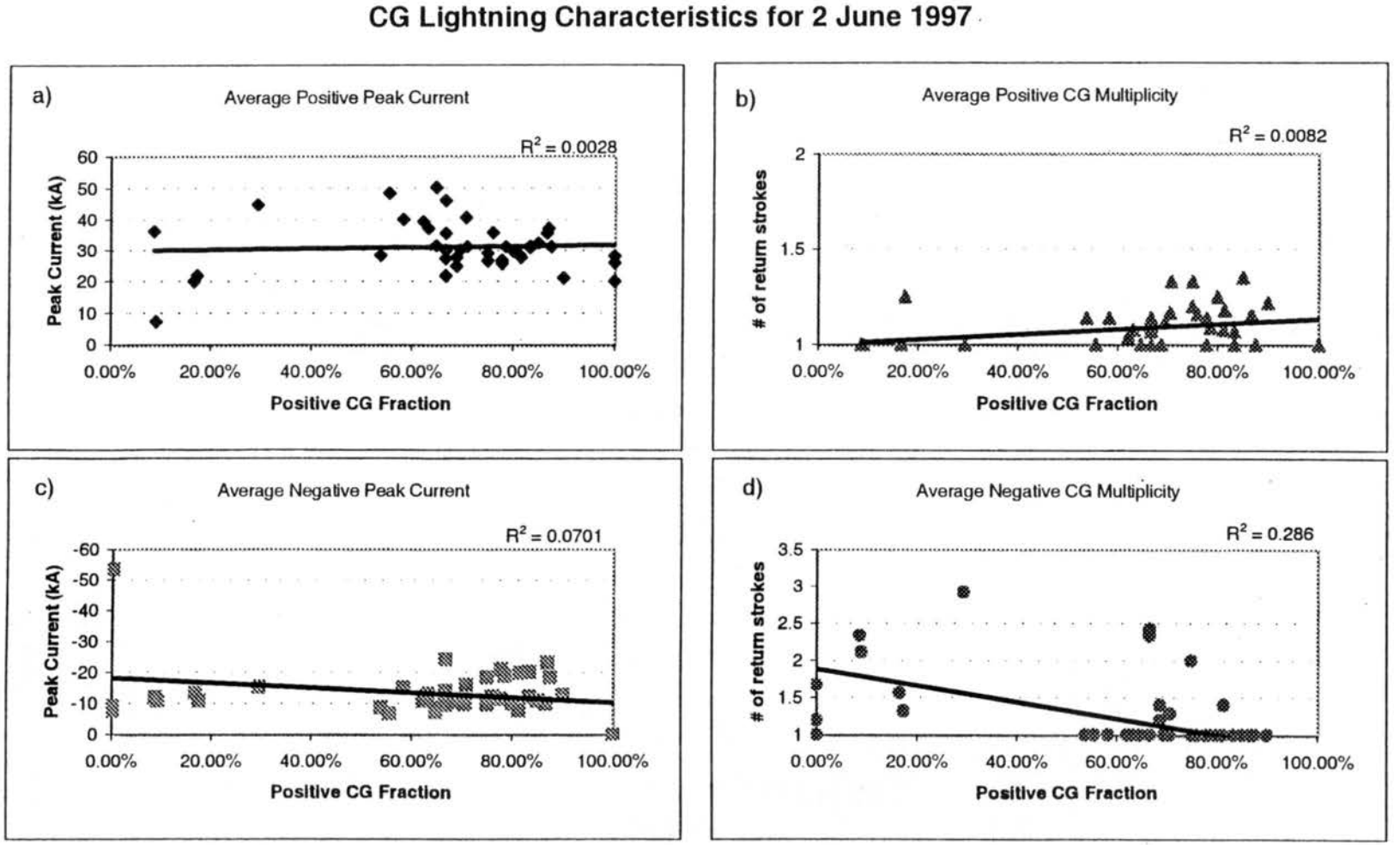


Figure 5.2: Results from calculations determing how CG lightning characteristics, for the 2 June 1997 storm, change with positive CG fraction for (a) average positive peak current, (b) average positive CG multiplicity, (c) average negative peak current, and (d) average negative CG multiplicity. The percentage of positive CG lightning, and resulting statistics were determined by using the CGs occurring during the time frame of each radar volume (typically 5 - 7 minutes).

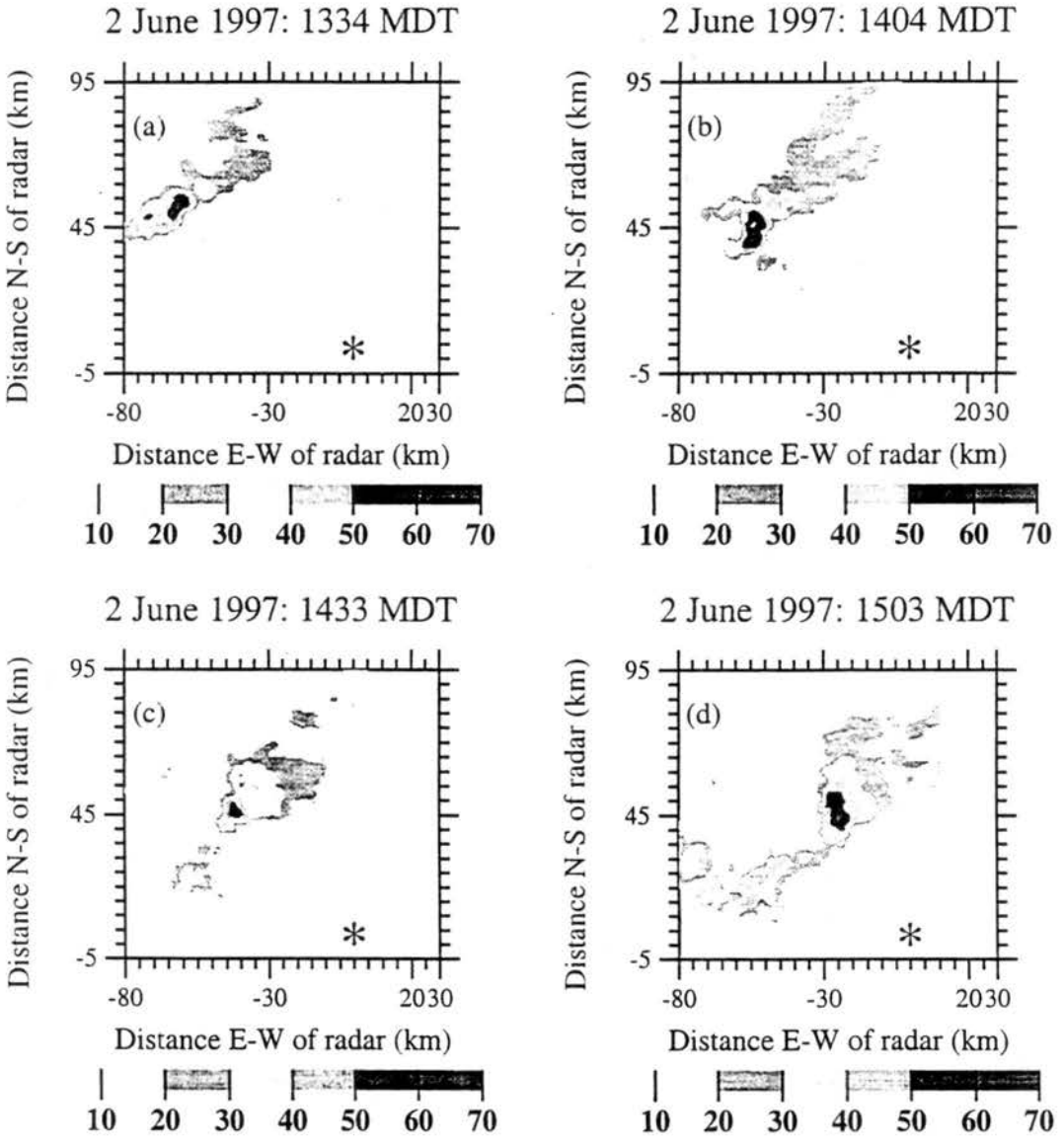


Figure 5.3: Horizontal cross-section of reflectivity (dBZ) obtained from the CSU-CHILL radar at 0.5 km AGL on 2 June 1997. (a) 1334 MDT, (b) 1404 MDT, (c) 1433 MDT, (d) 1503 MDT. The asterisk denotes the location of the radar.

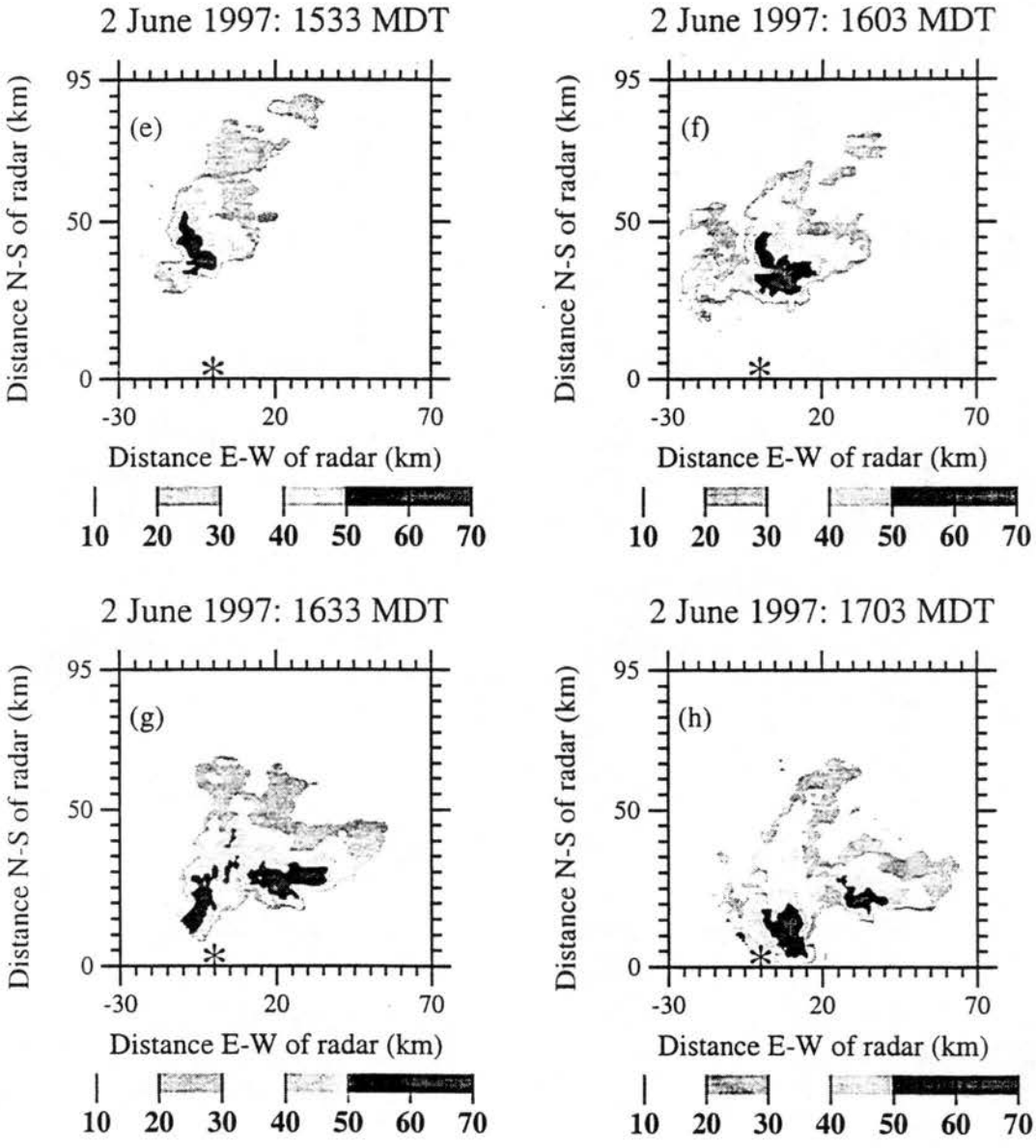


Figure 5.3: (e) 1533 MDT, (f) 1603, (g) 1633 MDT, (h) 1703 MDT.

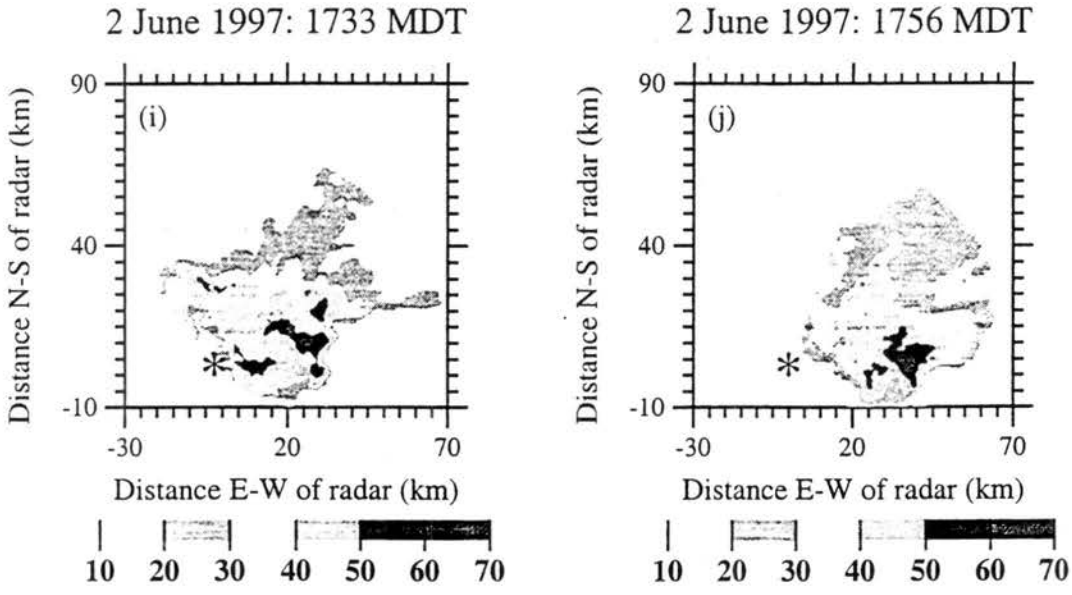


Figure 5.3: (i) 1733 MDT, (j) 1756 MDT.

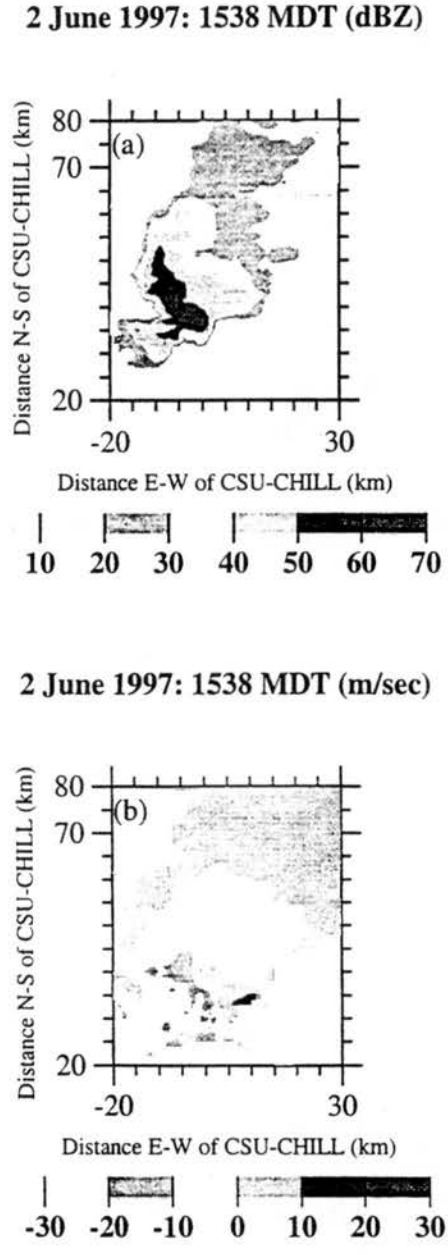


Figure 5.4: Horizontal cross-sections of (a) reflectivity (dBZ) and (b) velocity (m sec $^{-1}$) from the CSU-CHILL radar at 0.5 km AGL at 1538 MDT on 2 June 1997. Note the development of a "hook" echo in the reflectivity data, along with the associated tornado vortex signature (TVS) in the velocity data at x = 0 km, y = 48 km.

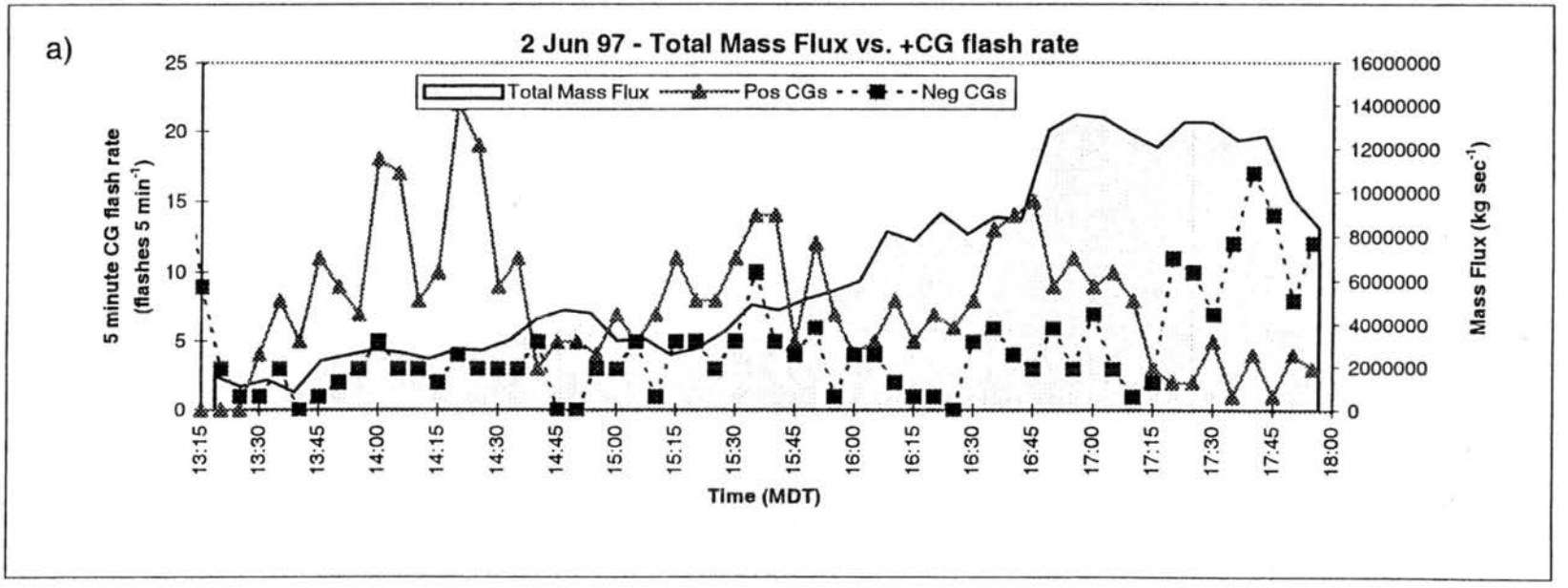


Figure 5.5: 2 June 1997 mass flux time-series (kg $sec^{-1}$) compared with positive and negative flash-rate time-series plots for (a) total mass flux. CG flash rates are plotted as in Fig. 5.1.

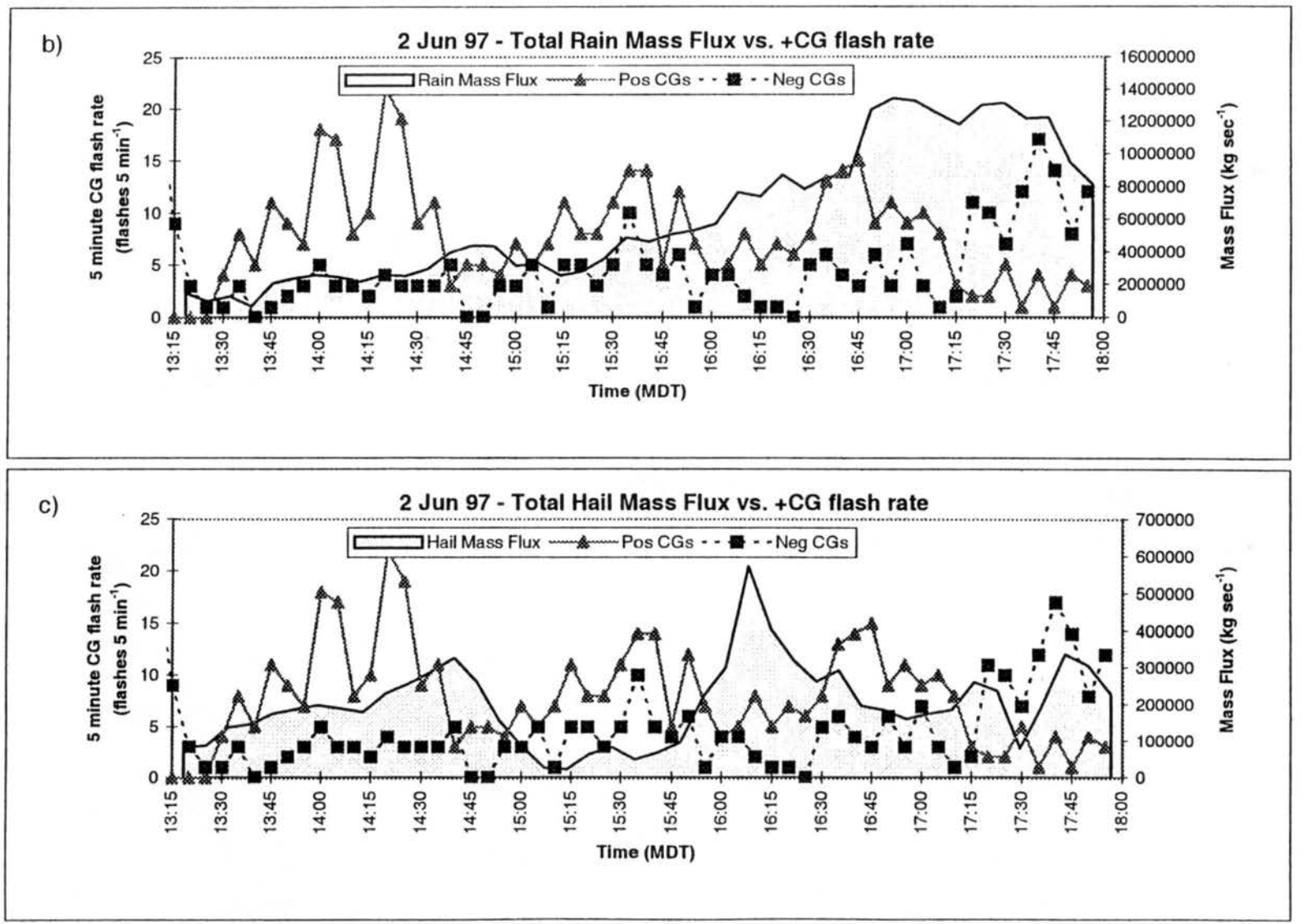


Figure 5.5: (b) rain mass flux, and (c) hail mass flux. Mass fluxes were calculated at an altitude of 0.5 km AGL.

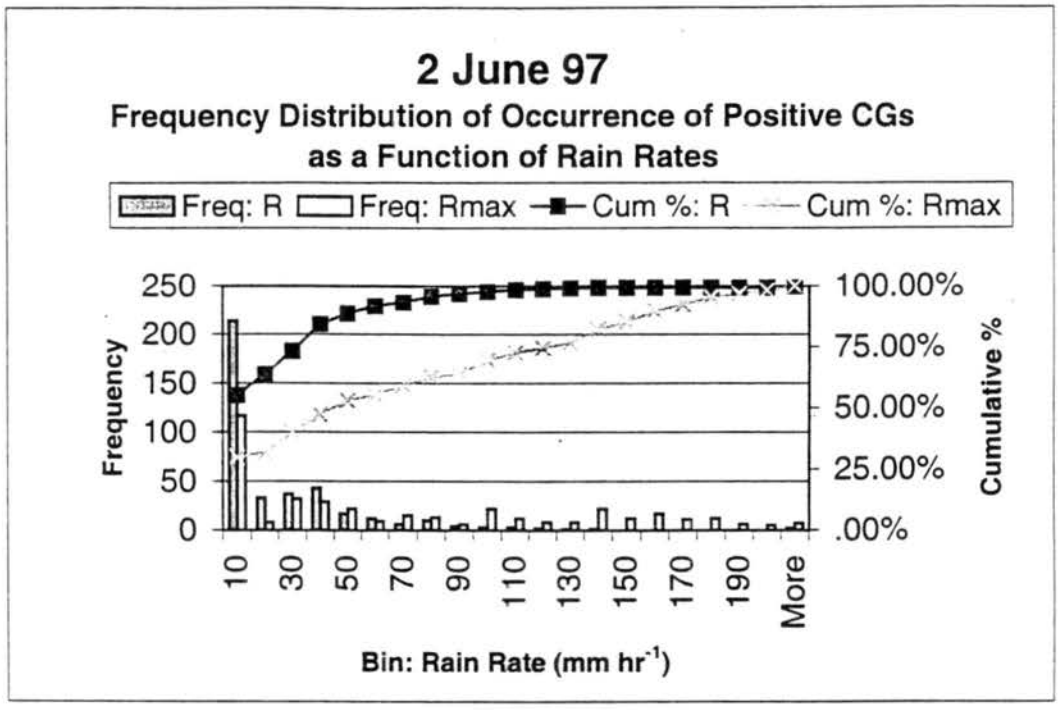


Figure 5.6: Frequency and cumulative percentage histograms of positive CGs as a function of rain rate at ground strike location and maximum rain rate within 10 km of ground strike location.

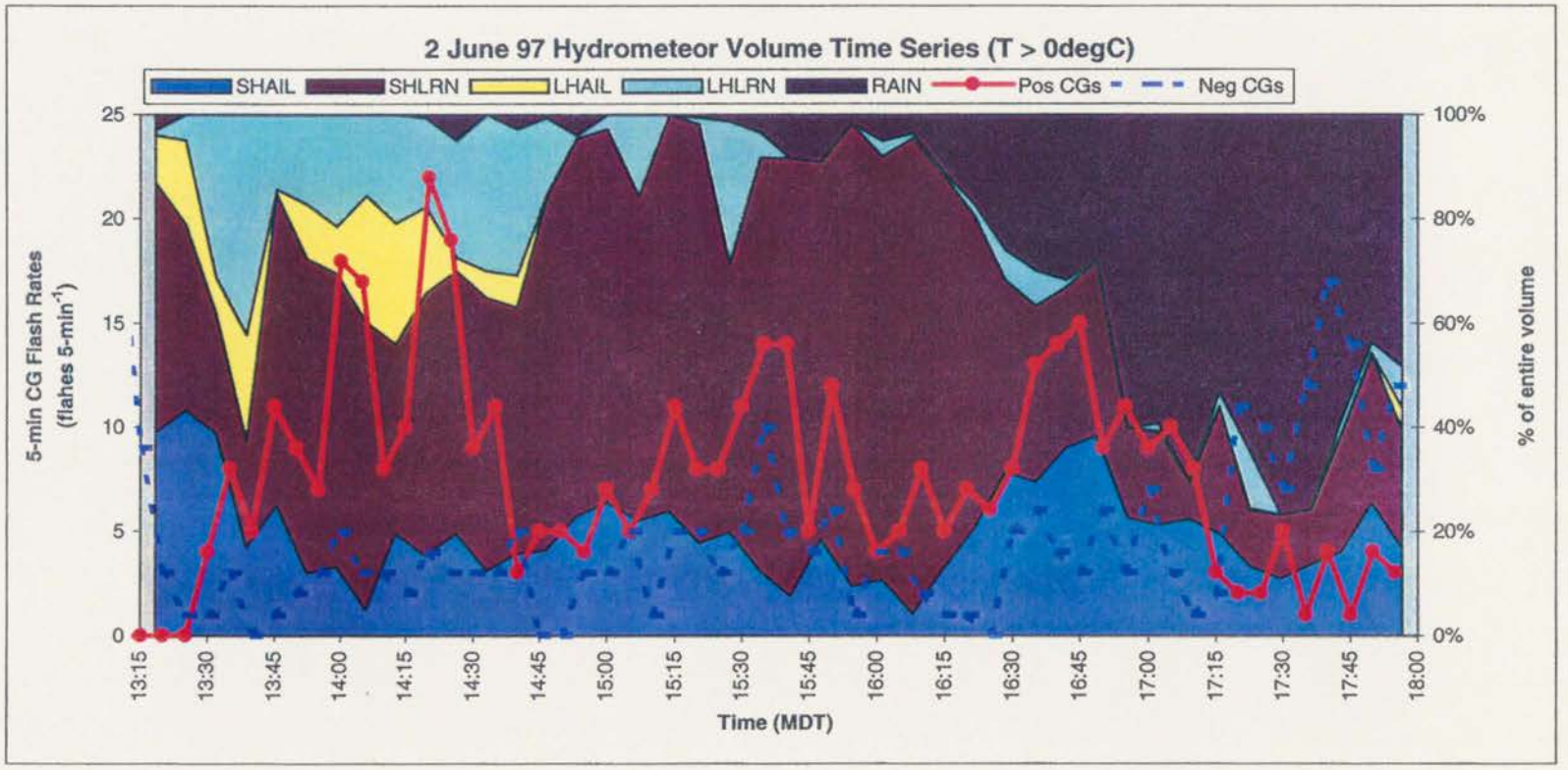


Figure 5.7: 2 June 1997 time-series plot of the percentage of storm volume beneath the melting level (T > 0 °C) comprised of small hail (SHAIL), small hail mixed with rain (SHLRN), large hail (LHAIL), large hail mixed with rain (LHLRN), and pure rain (RAIN) compared to 5-minute flash rates for each polarity as in Fig. 5.2. This plot enables us to determine the relative amounts of storm volume present at each time interval.

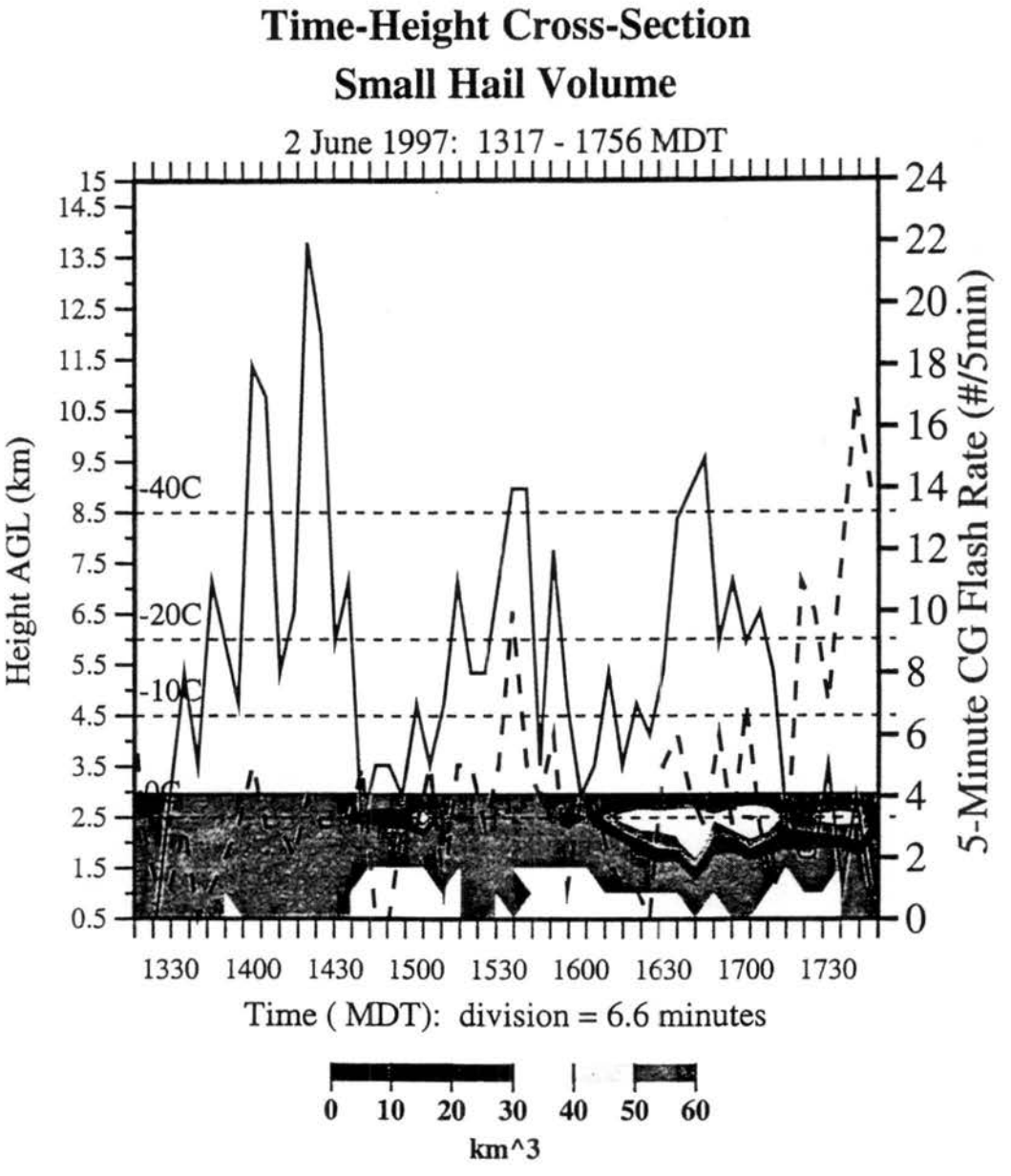


Figure 5.8: 2 June 1997 time height cross-section of small hail volume beneath the melting level compared to 5-minute flash rates for each polarity. Positive flashes rates are denoted by the solid red line, with negative flash rates denoted by the dashed line.

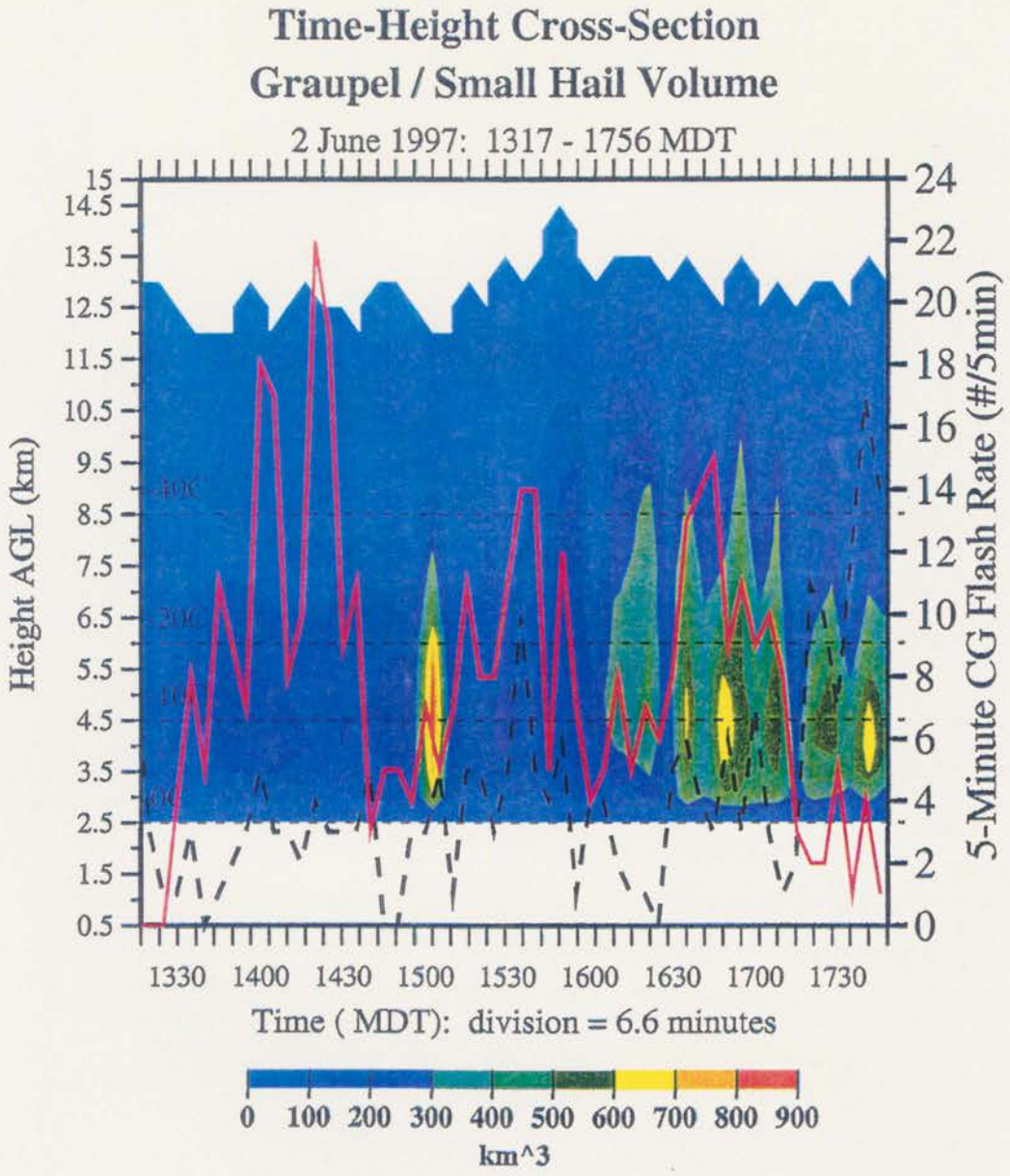


Figure 5.9: As in Fig. 5.8 for graupel and small hail volumes above the melting level.

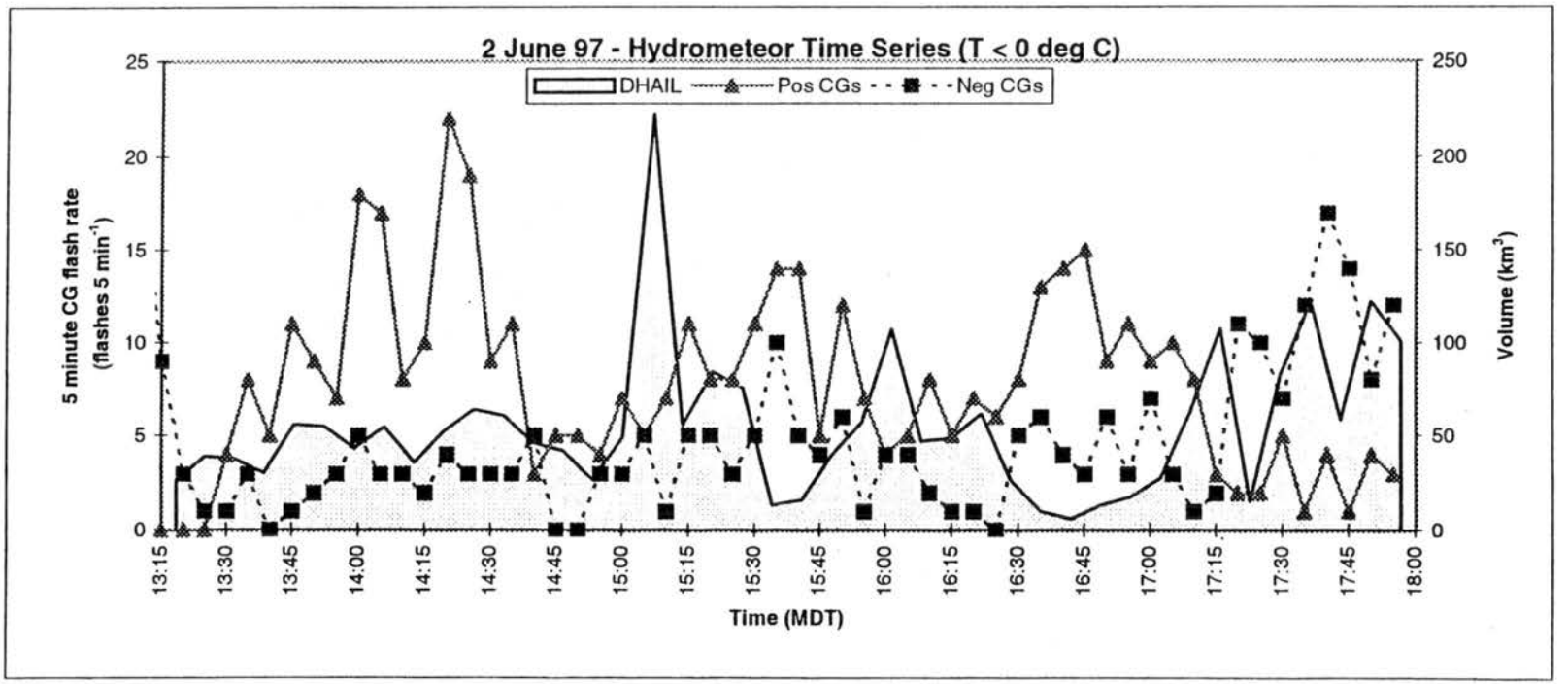


Figure 5.10: 2 June 1997 time-series of large hail (> 1 cm; DHAIL) above the melting level compared to 5-minute flash rates for each polarity.

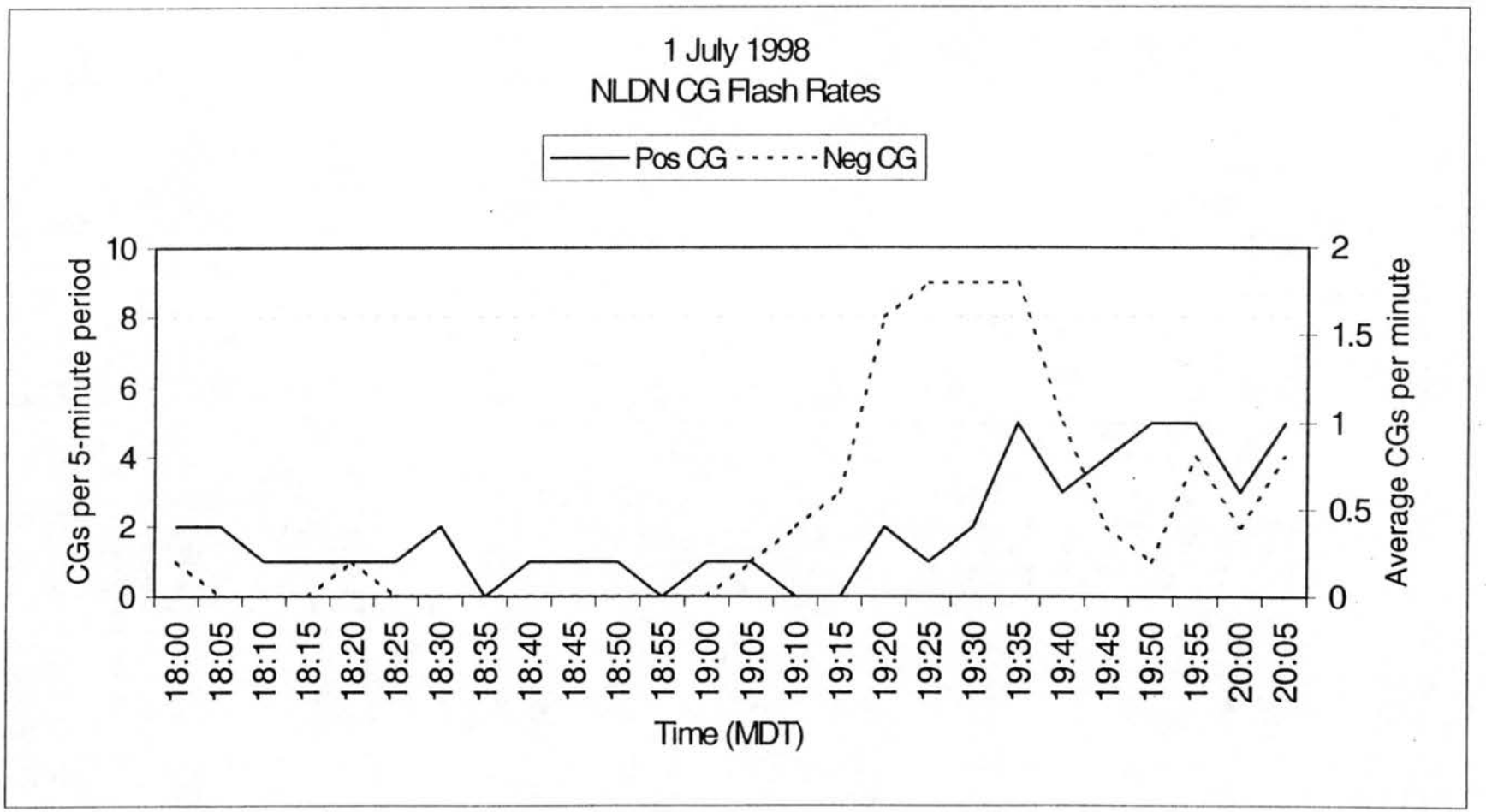


Figure 5.11: As in Fig. 5.1 for 1 July 1998.

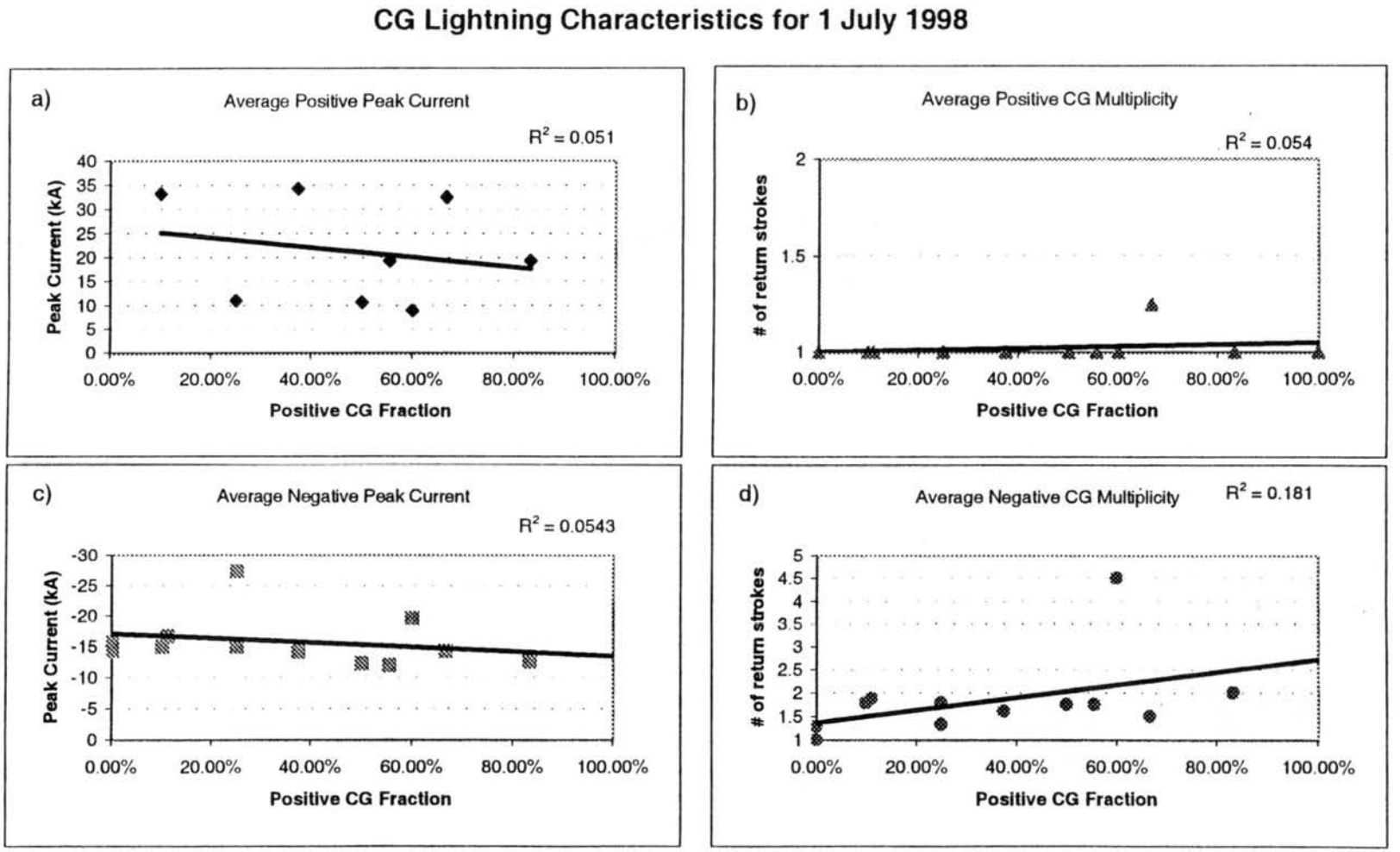


Figure 5.12: As in Fig. 5.2 for 1 July 1998. (a) average positive peak current, (b) average positive CG multiplicity, (c) average negative peak current, and (d) average negative CG multiplicity.

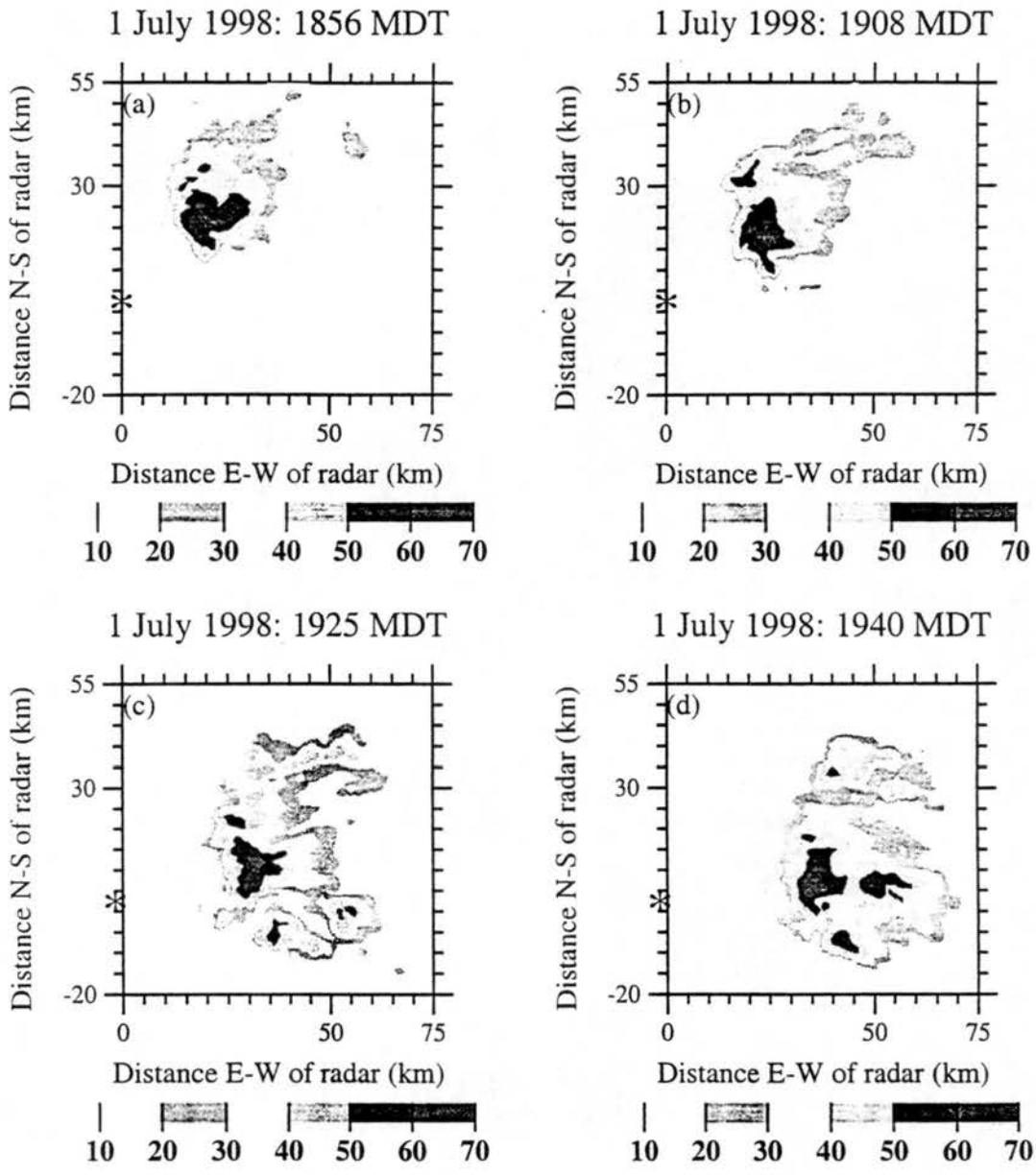


Figure 5.13: As in Fig. 5.3 for 1 July 1998. (a) 1856 MDT, (b) 1908 MDT, (c) 1925 MDT, (d) 1940 MDT.

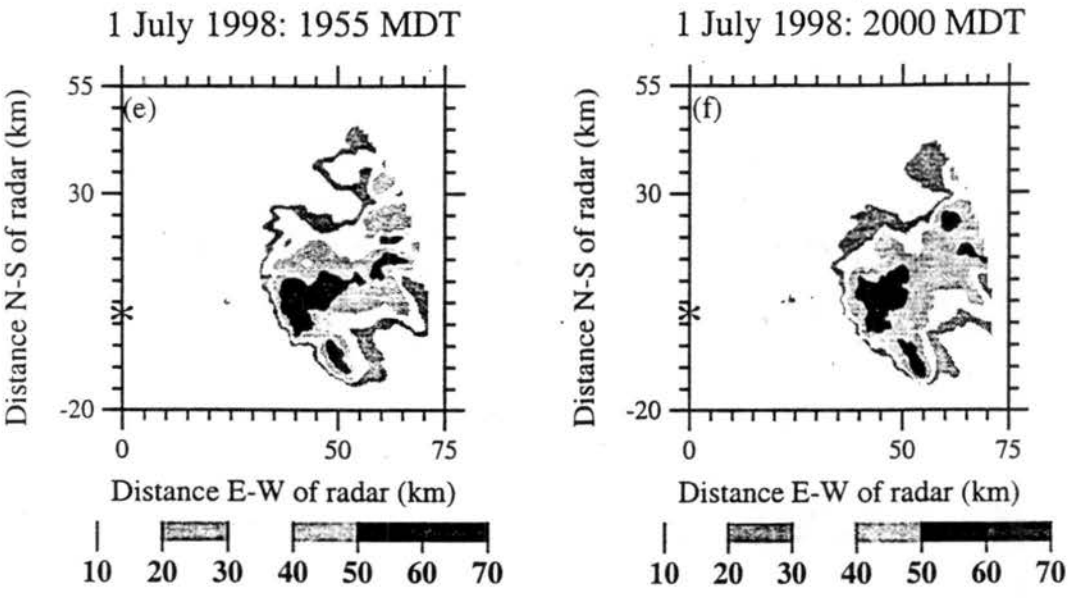


Figure 5.13: (e) 1955 MDT, (f) 2000 MDT.

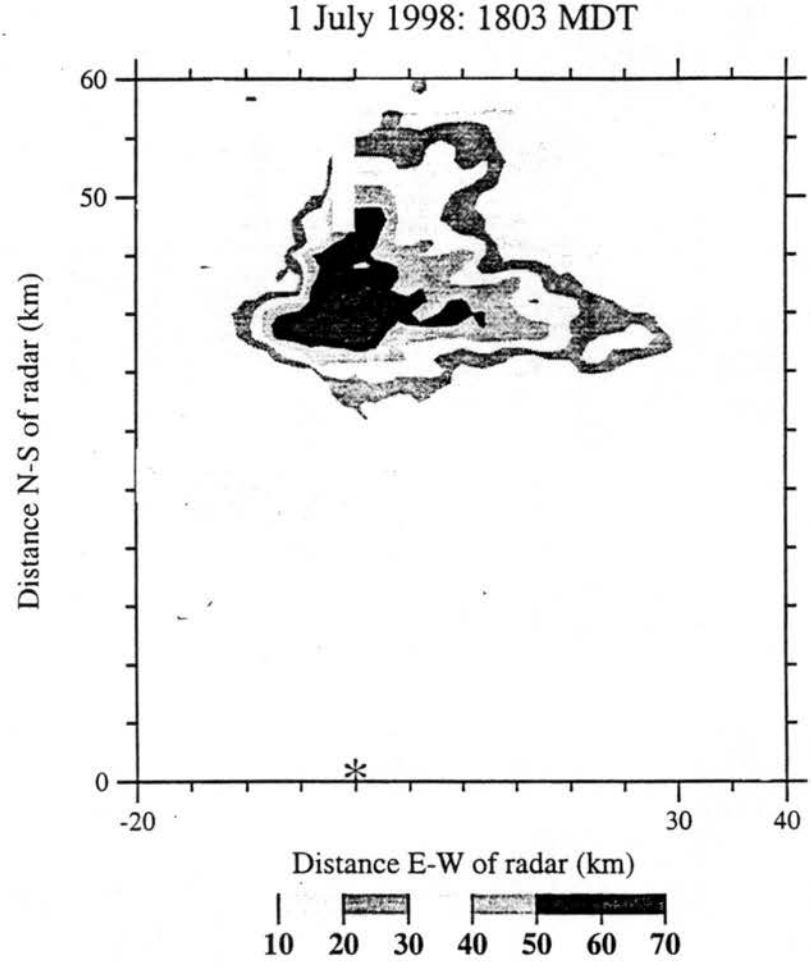


Figure 5.14: As in Fig. 5.13 for 1803 MDT.

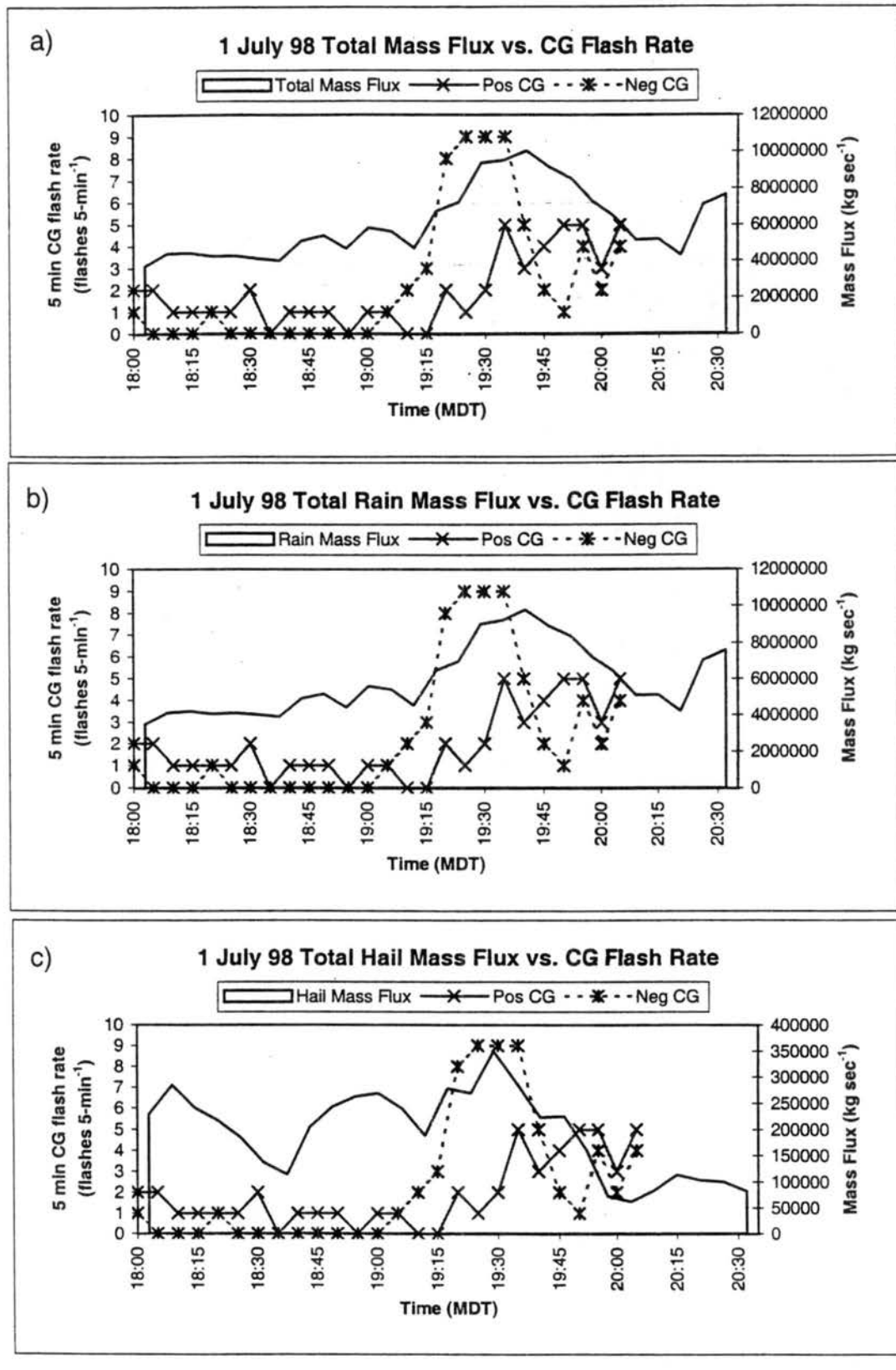


Figure 5.15: As in Fig. 5.5 for 1 July 1998. (a) Total mass flux, (b) rain mass flux, (c) hail mass flux.

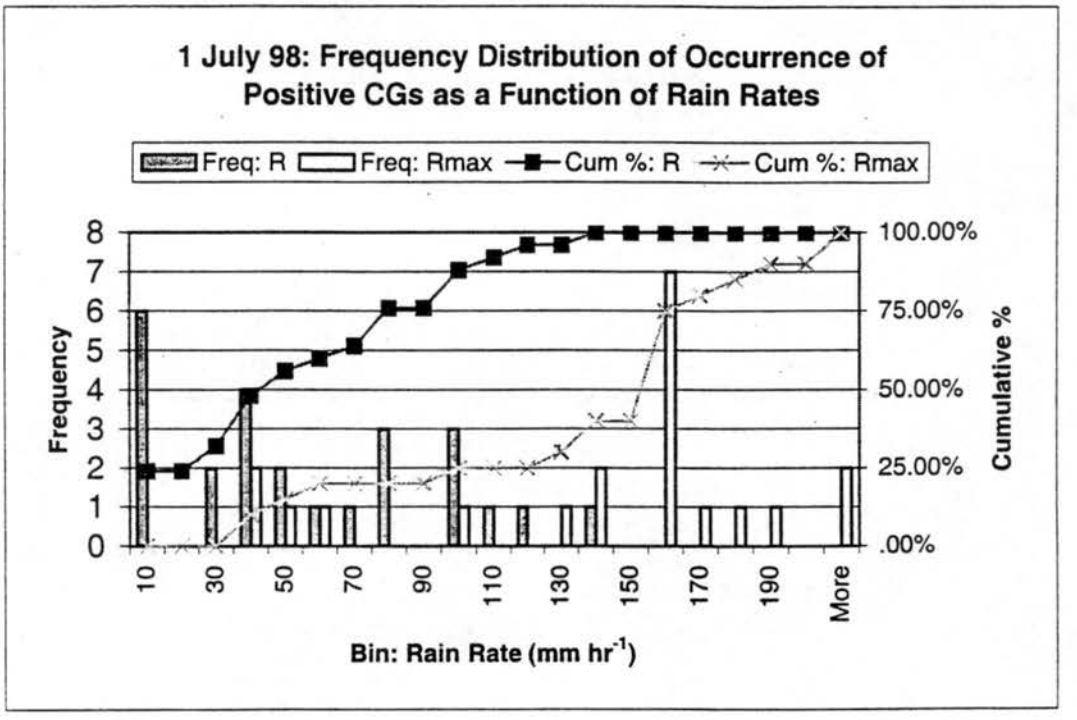


Figure 5.16: As in Fig. 5.6 for 1 July 1998.

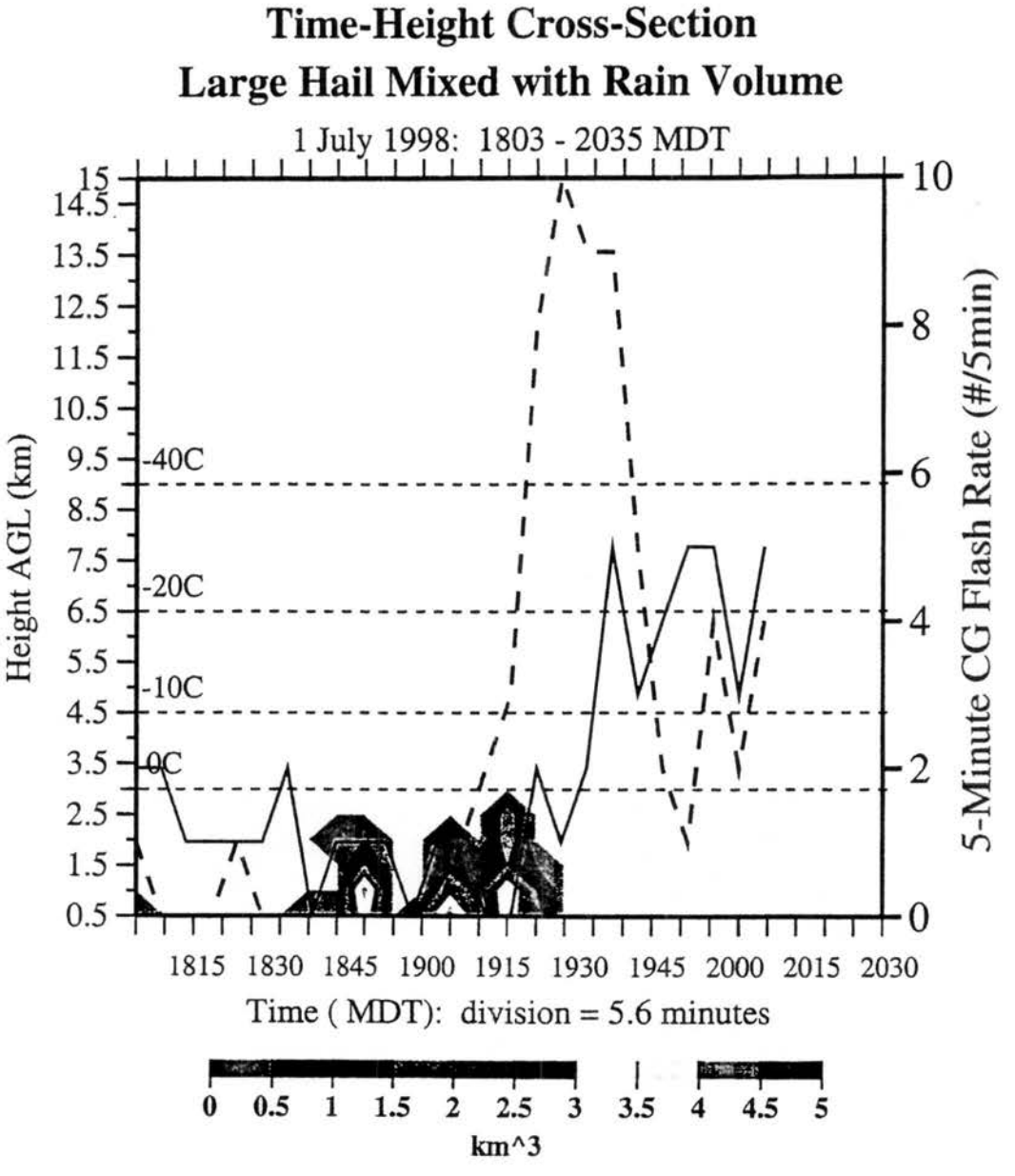


Figure 5.17: As in Fig. 5.8 for volumes of large hail mixed with rain below the melting level for 1 July 1998.

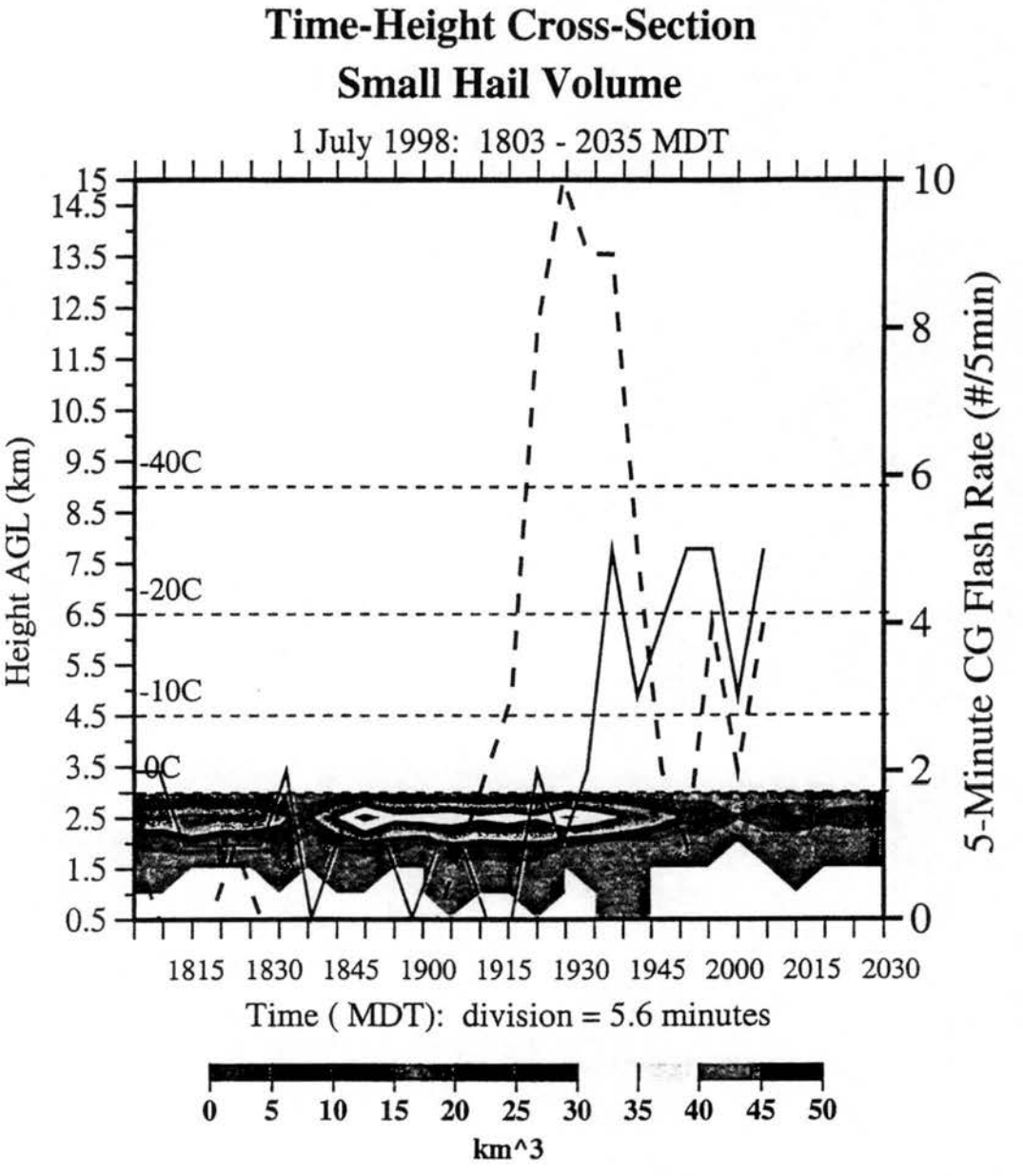


Figure 5.18: As in Fig. 5.17 for small hail volumes below the melting level.

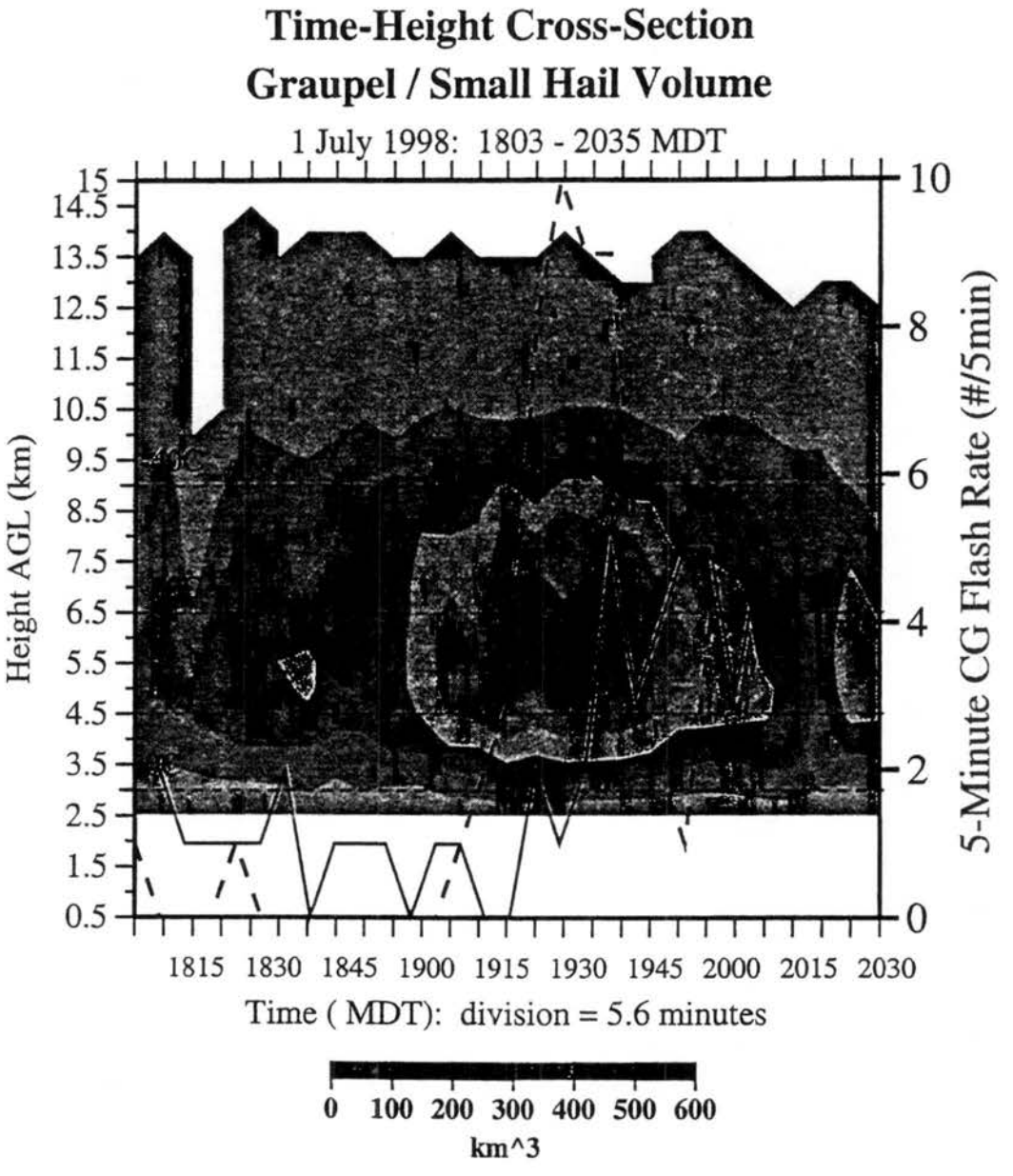


Figure 5.19: As in Fig. 5.17 for volumes of graupel and small hail above the melting level.

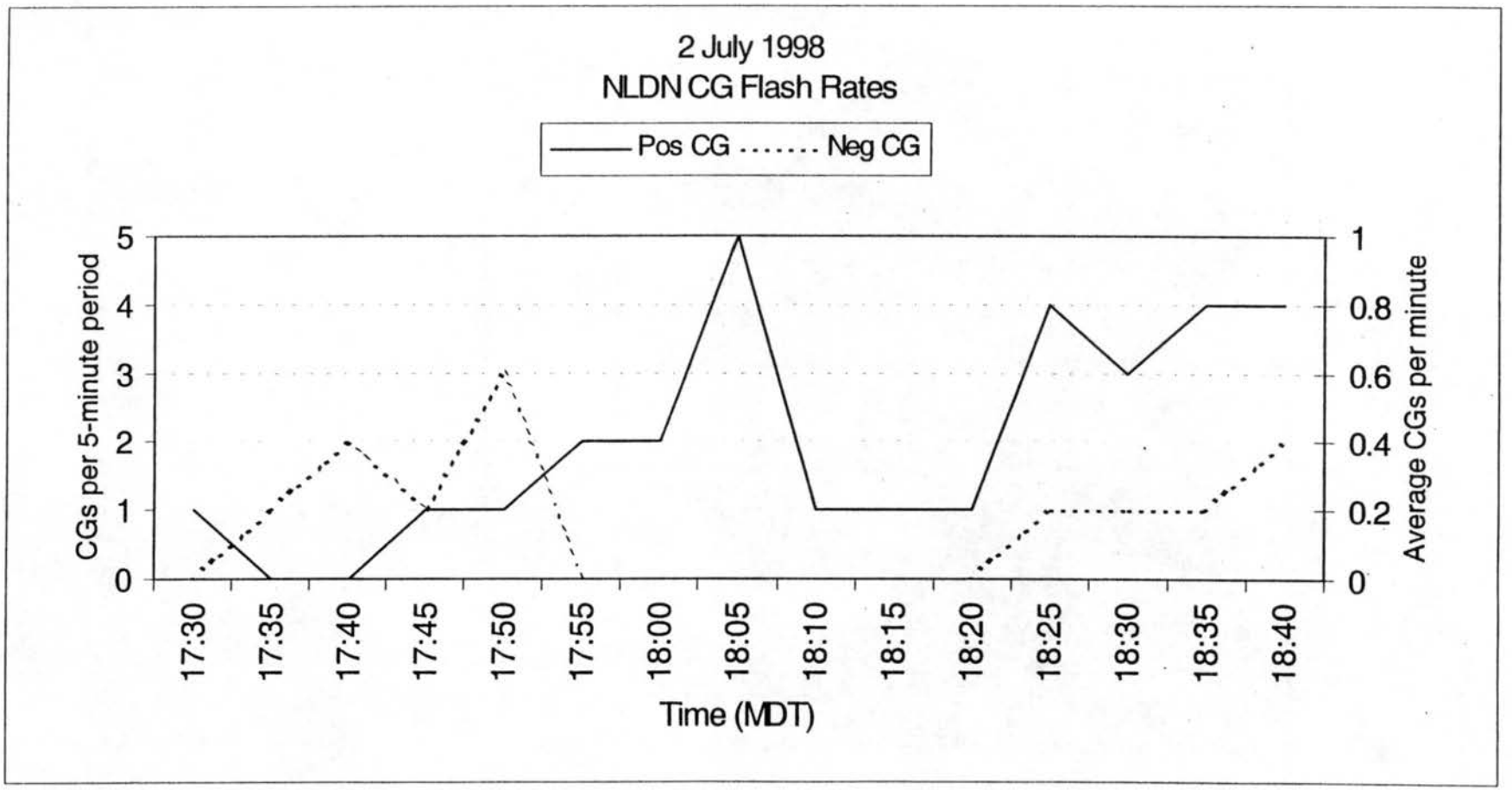


Figure 5.20: As in Fig. 5.1 for 2 July 1998.

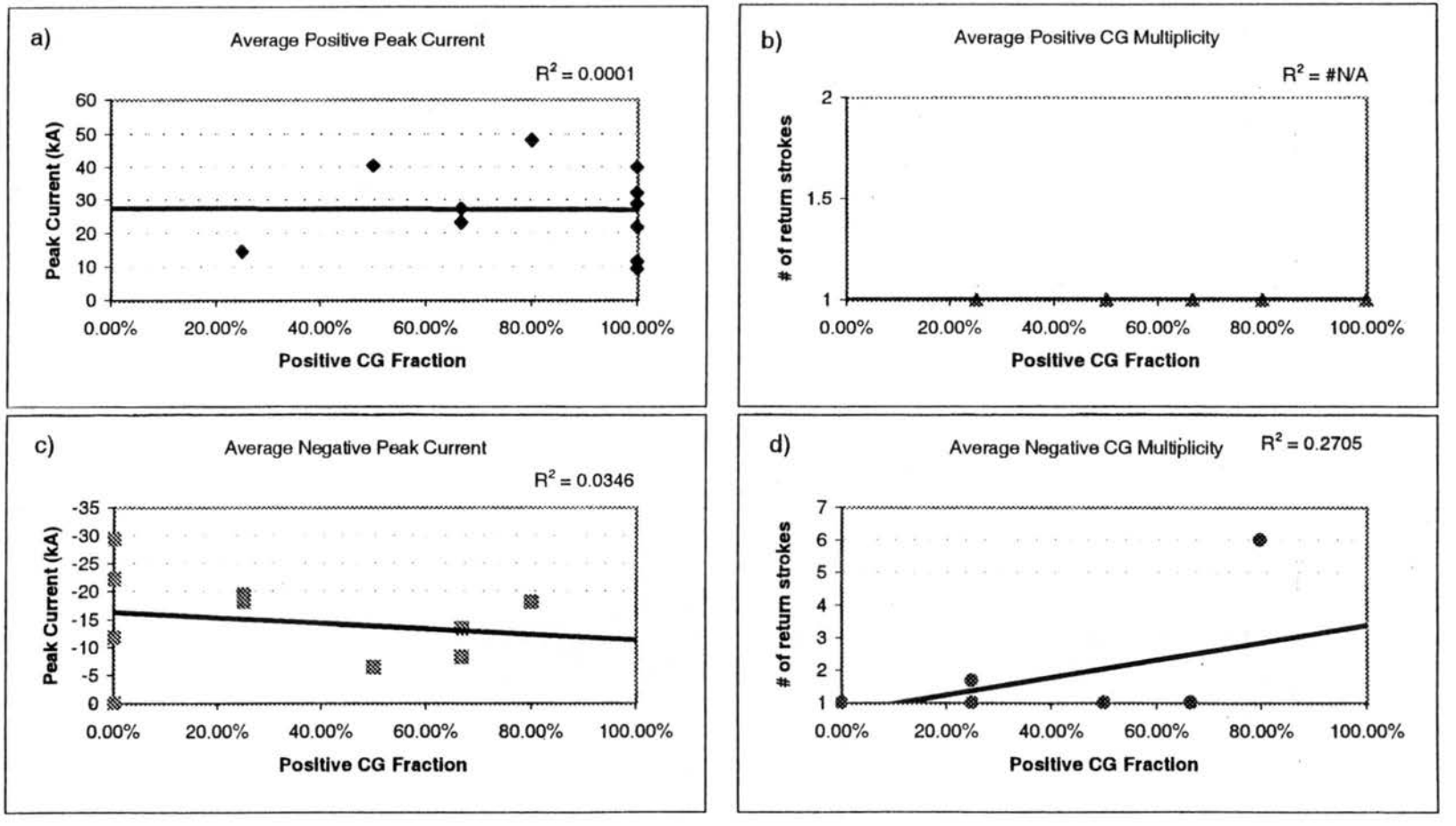


Figure 5.21: As in Fig. 5.2 for 2 July 1998. (a) average positive peak current, (b) average positive CG multiplicity, (c) average negative peak current, and (d) average negative CG multiplicity.

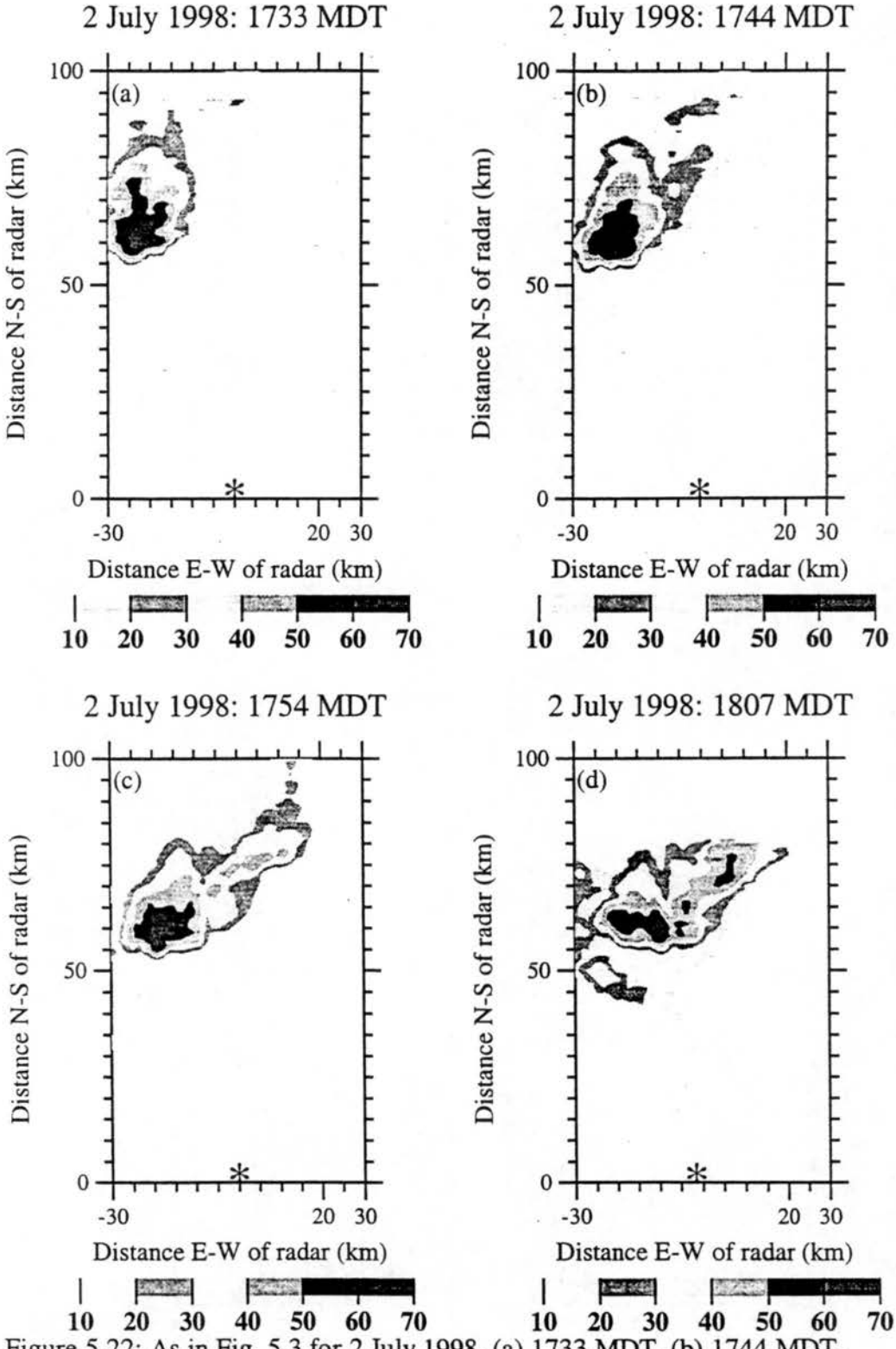


Figure 5.22: As in Fig. 5.3 for 2 July 1998. (a) 1733 MDT, (b) 1744 MDT, (c) 1754 MDT, (d) 1807 MDT.

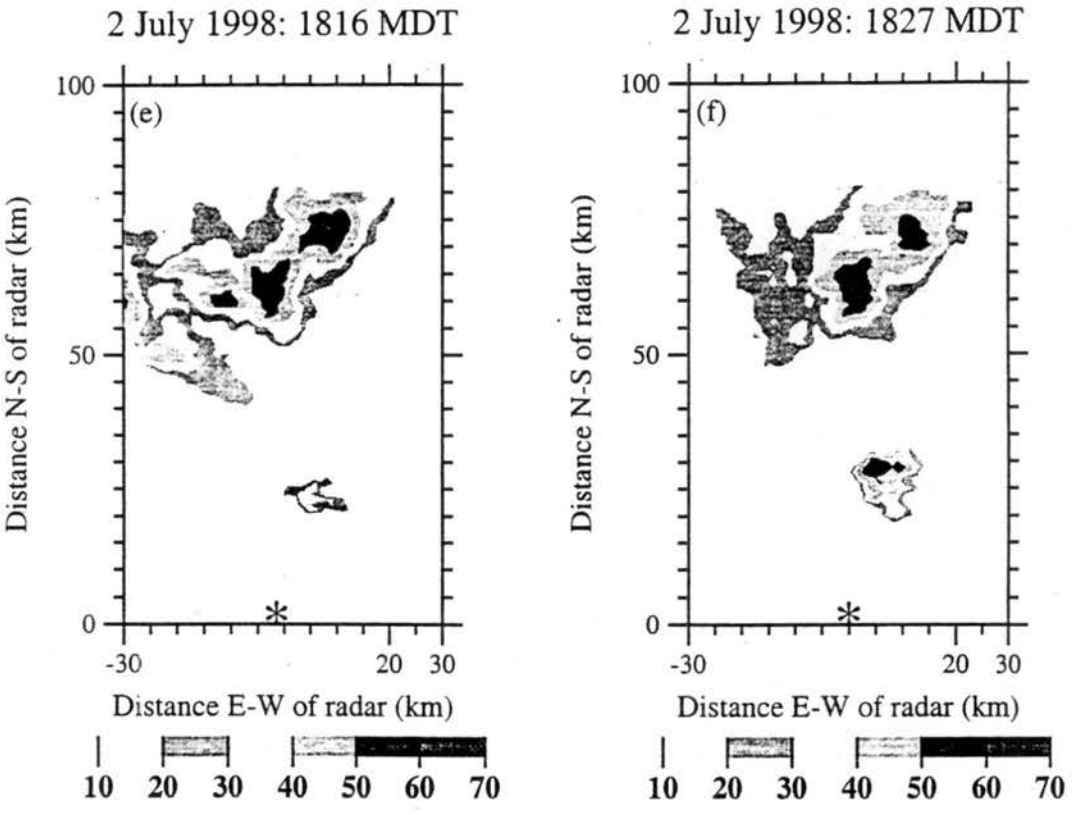


Figure 5.22: (e) 1816 MDT, 1827 MDT.

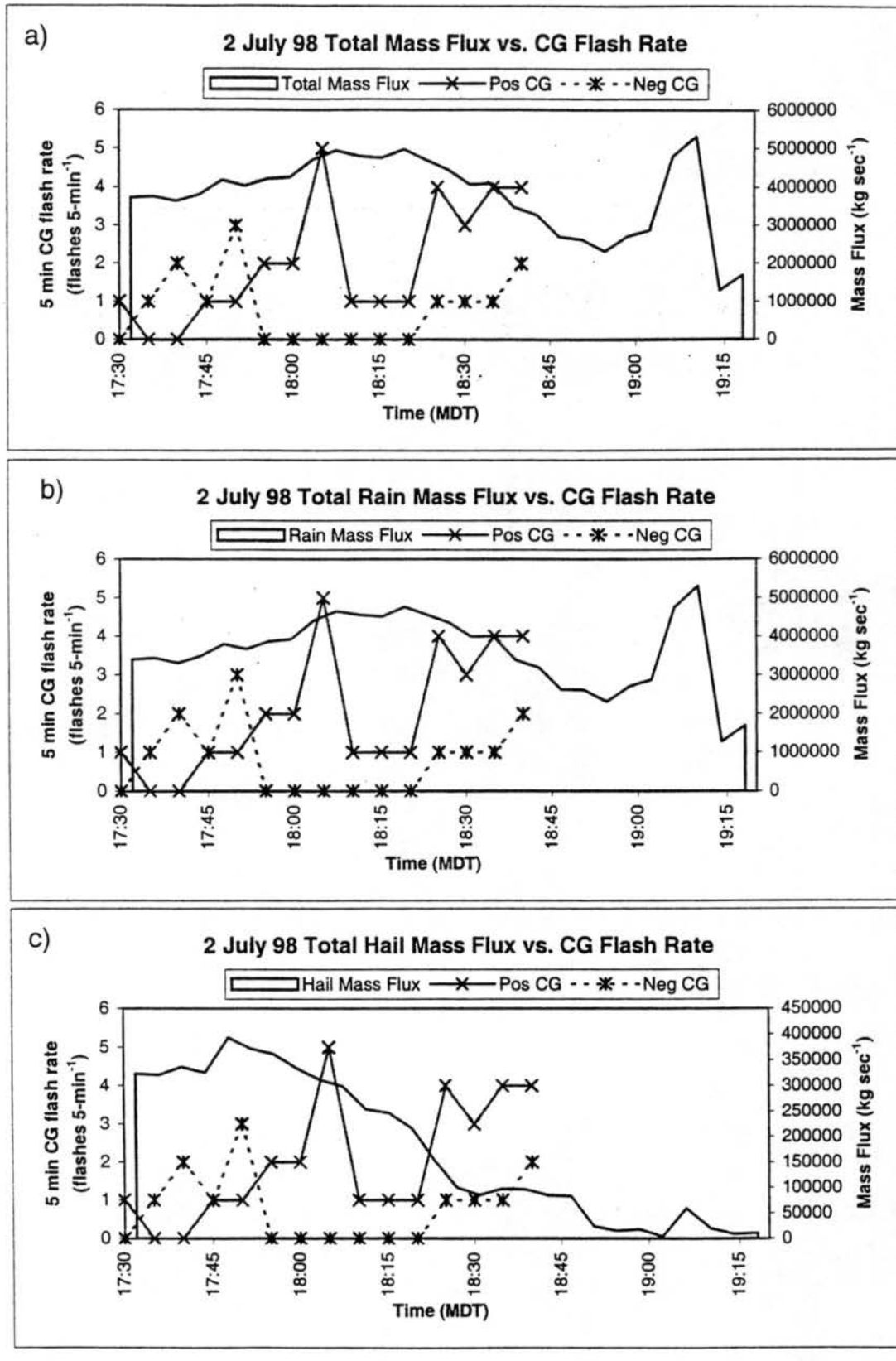


Figure 5.23: As in Fig. 5.5 for 2 July 1998. (a) Total mass flux, (b) rain mass flux, (c) hail mass flux.

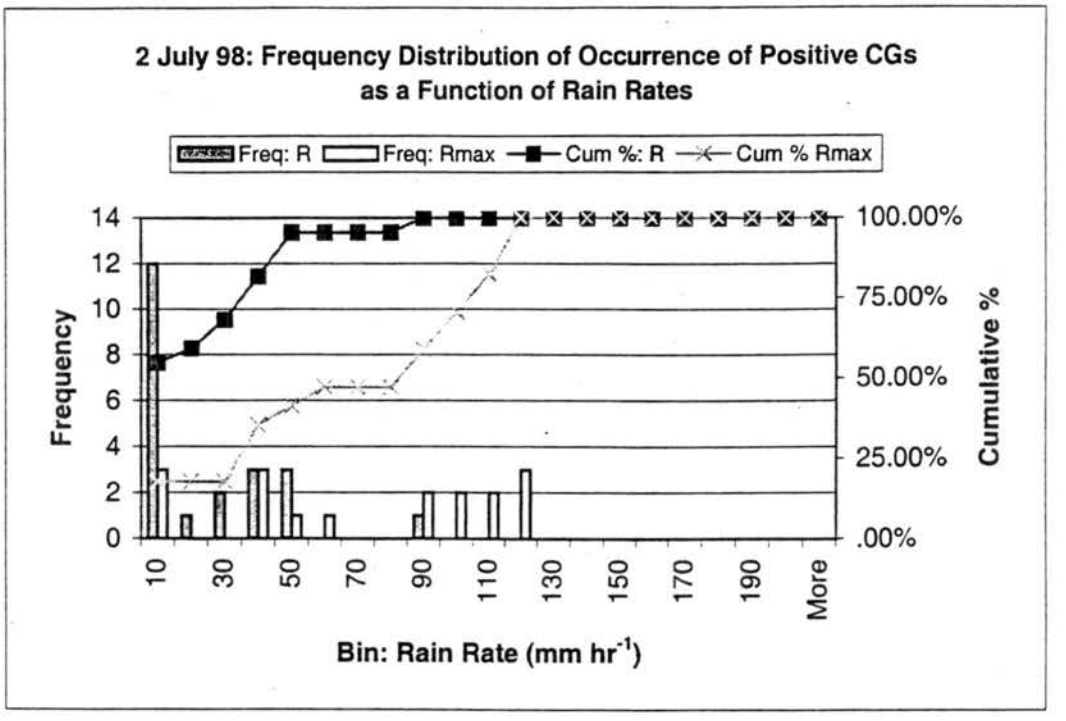


Figure 5.24: As in Fig. 5.6 for 2 July 1998.

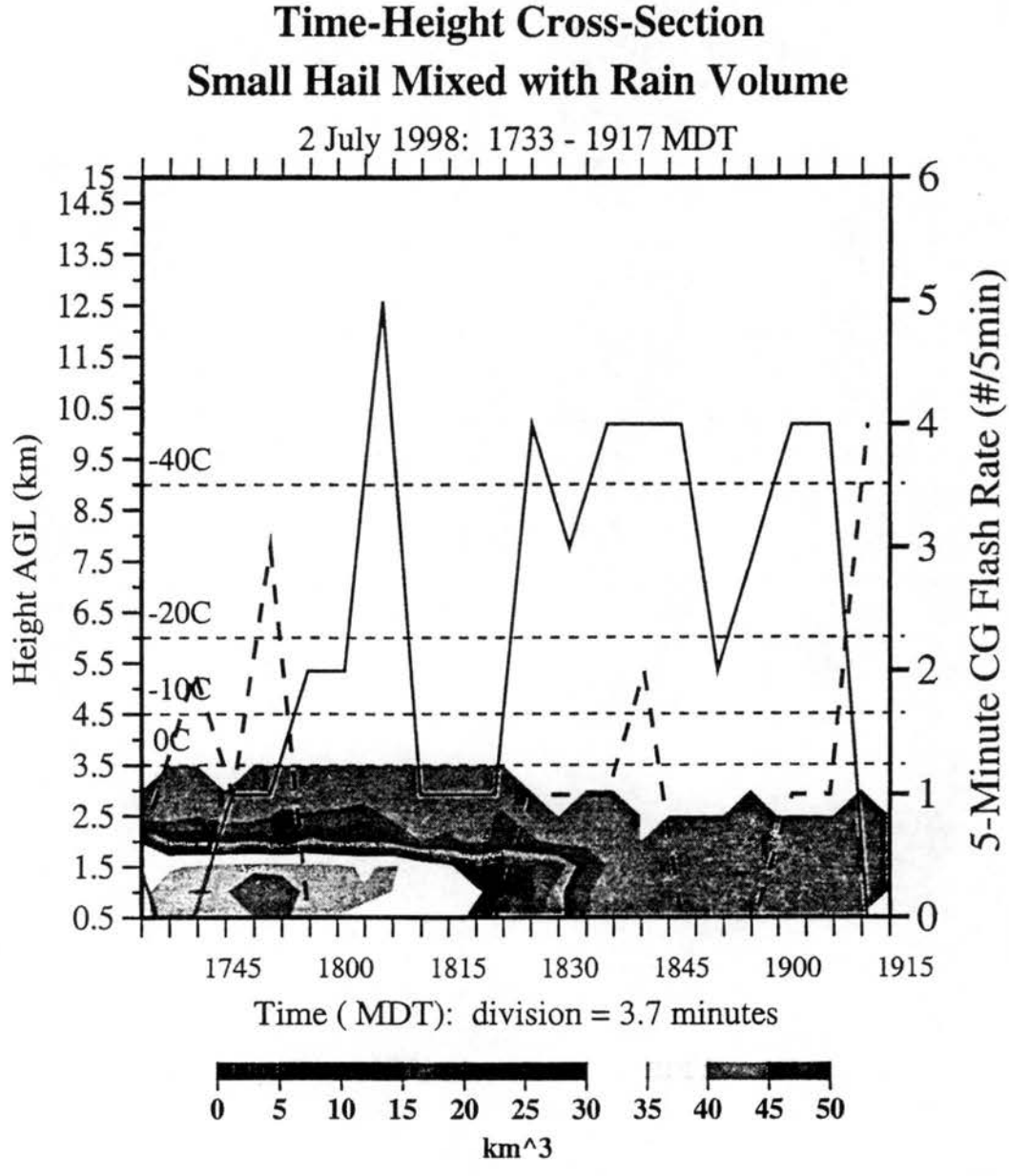


Figure 5.25: As in Fig. 5.8 for (a) volumes of small hail mixed with rain below the melting level for 2 July 1998.

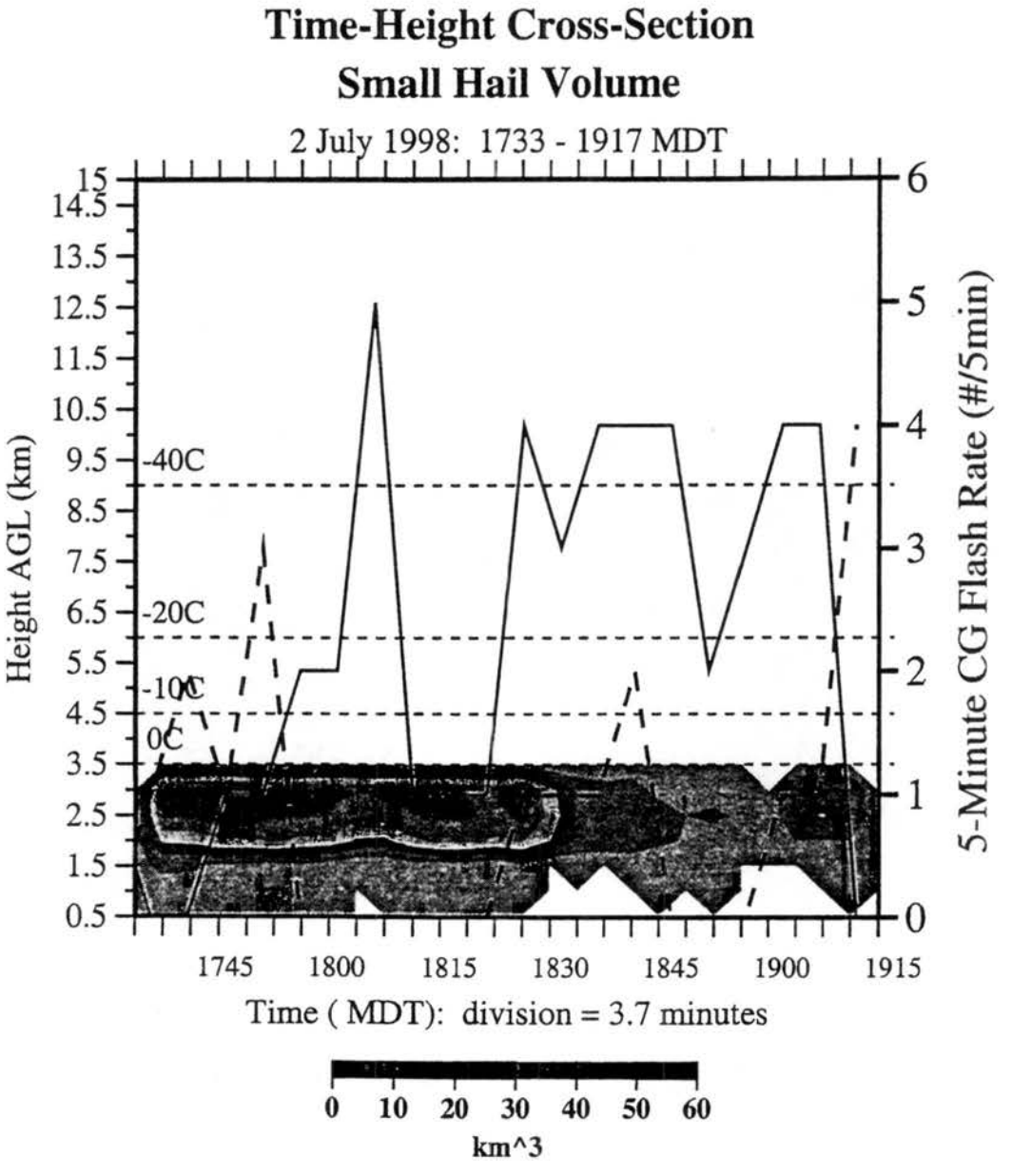


Figure 5.25: (b) Small hail beneath the melting level.

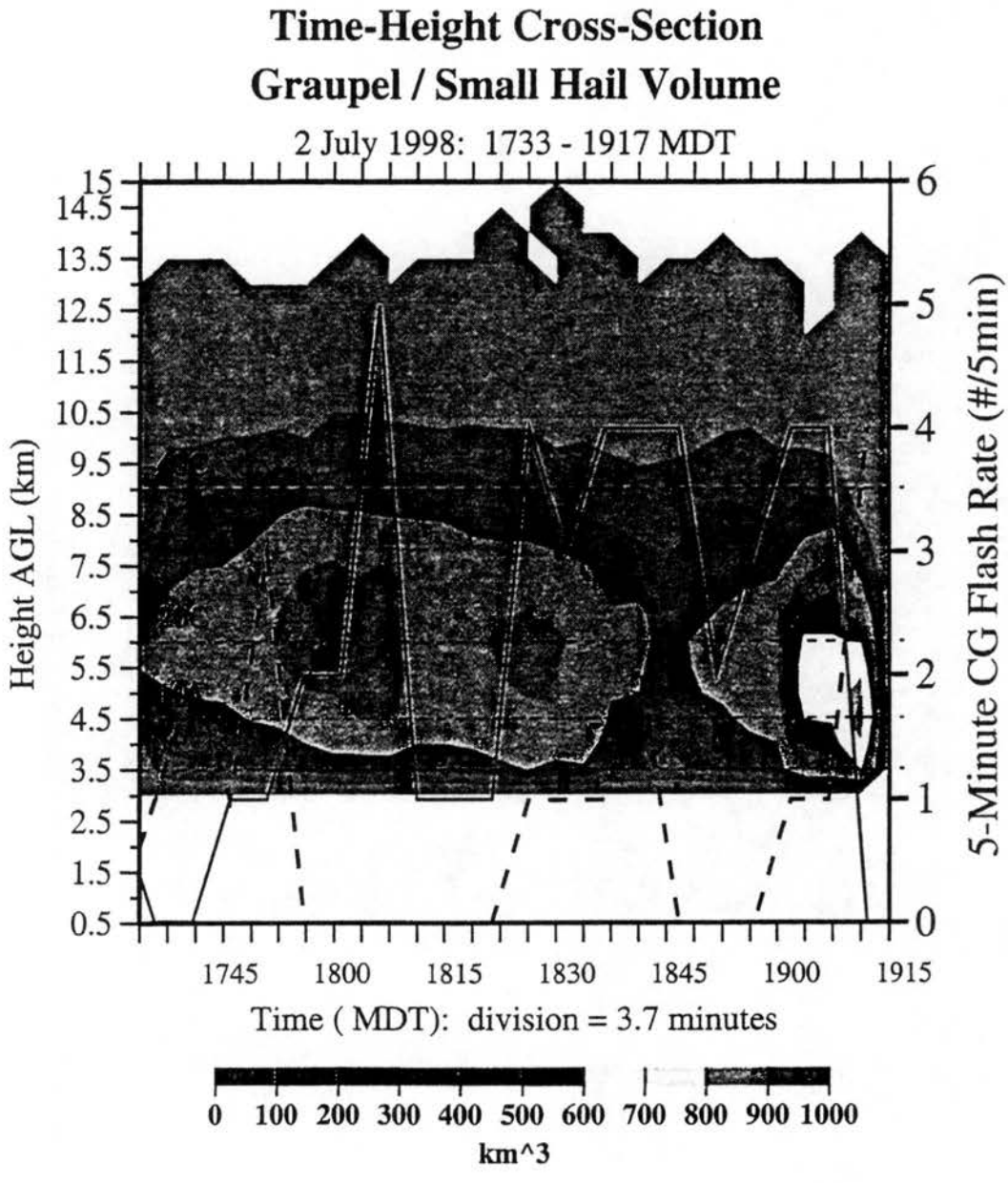


Figure 5.25: (c) Graupel and small hail above the melting level.

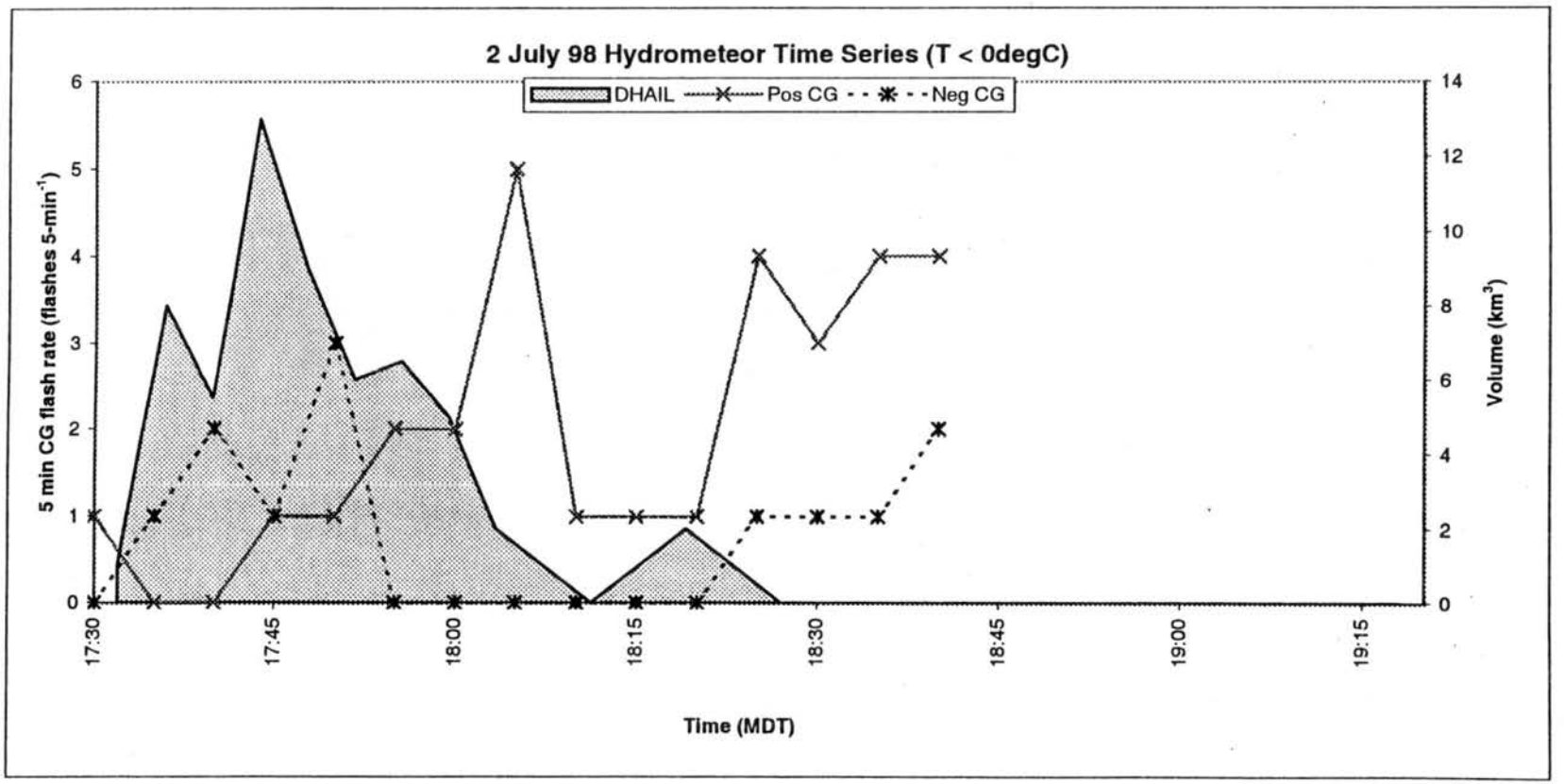


Figure 5.26: As in Fig. 5.10 for 2 July 1998.

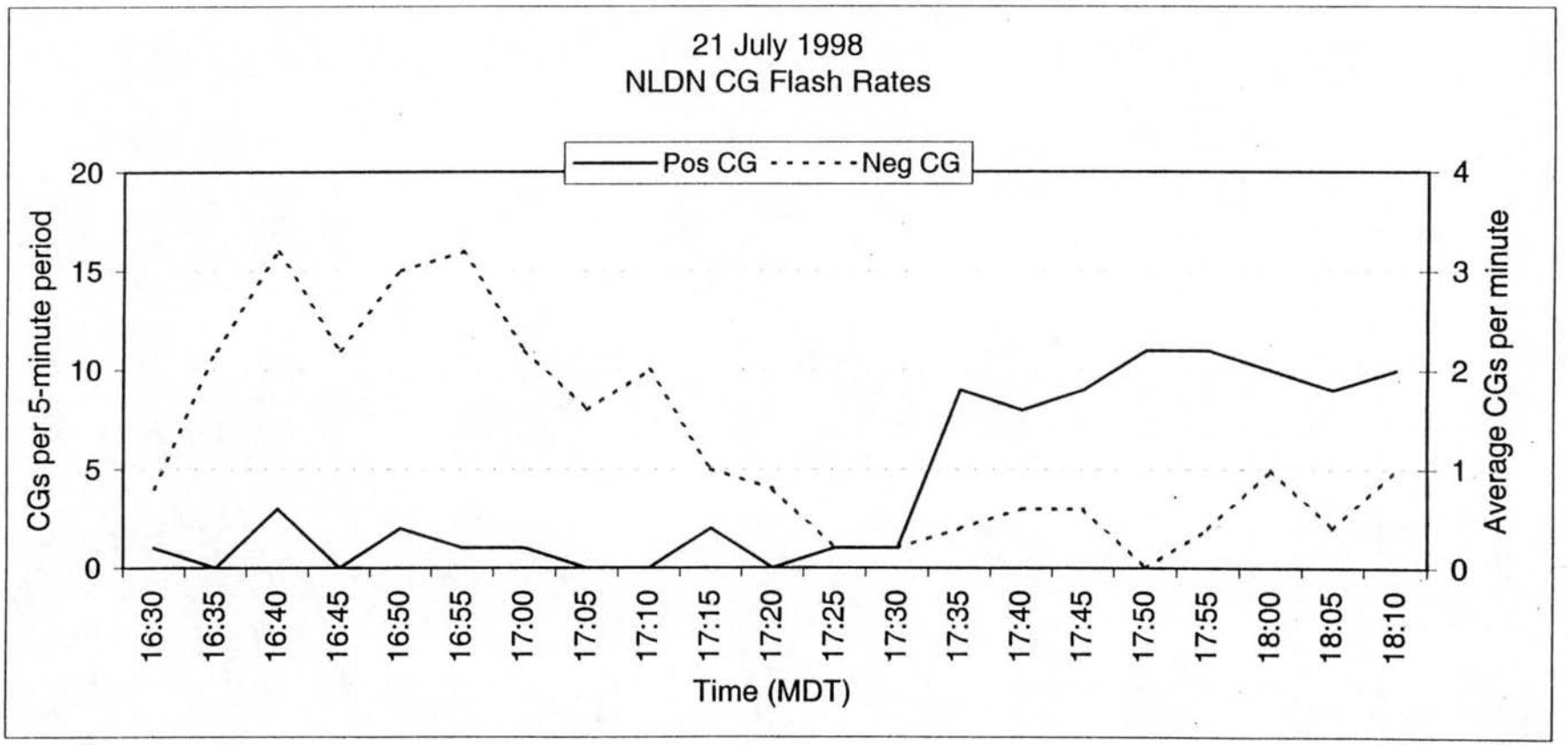


Figure 5.27: As in Fig. 5.1 for 21 July 1998.

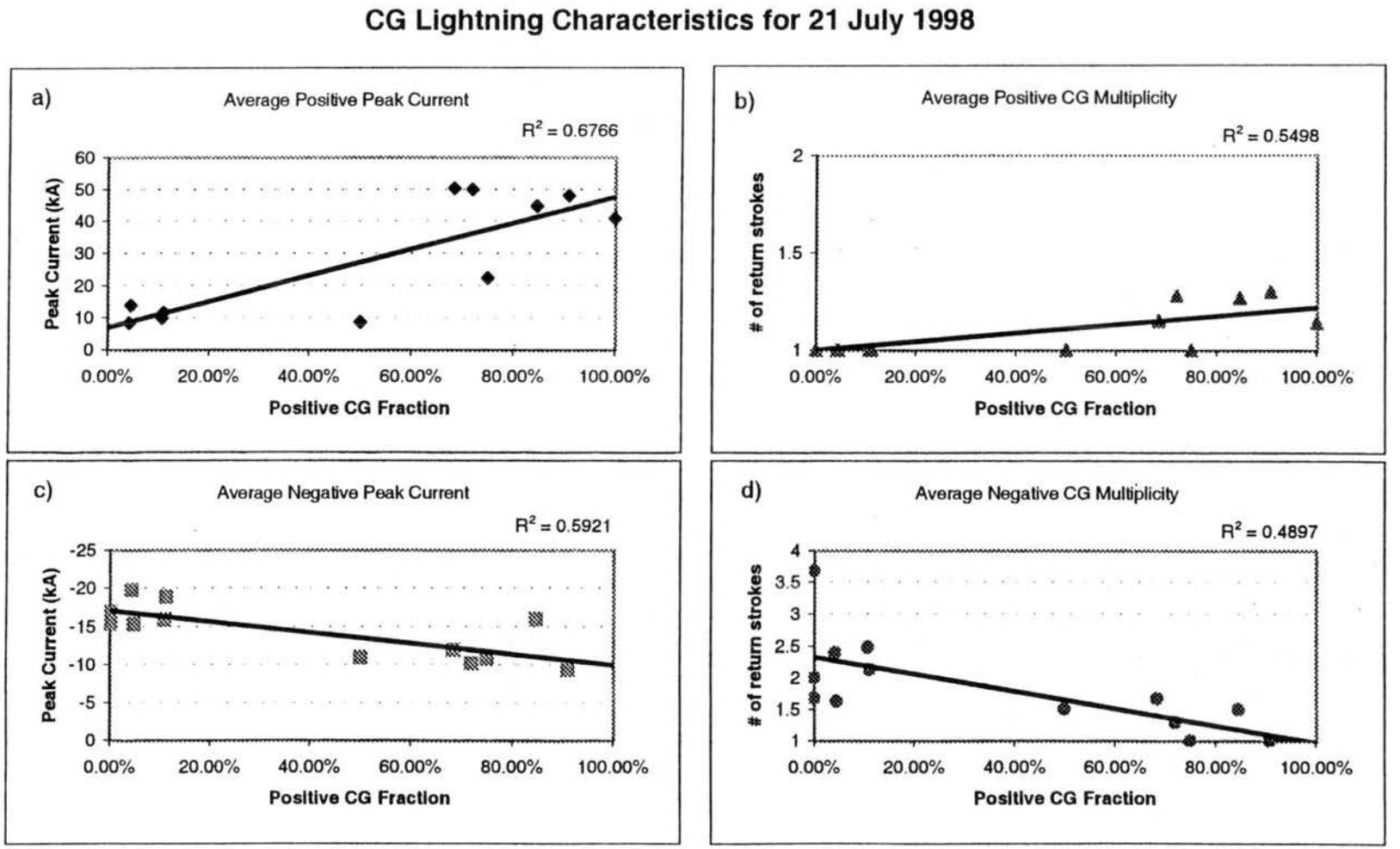


Figure 5.28: As in Fig. 5.2 for 21 July 1998. (a) average positive peak current, (b) average positive CG multiplicity, (c) average negative peak current, and (d) average negative CG multiplicity.

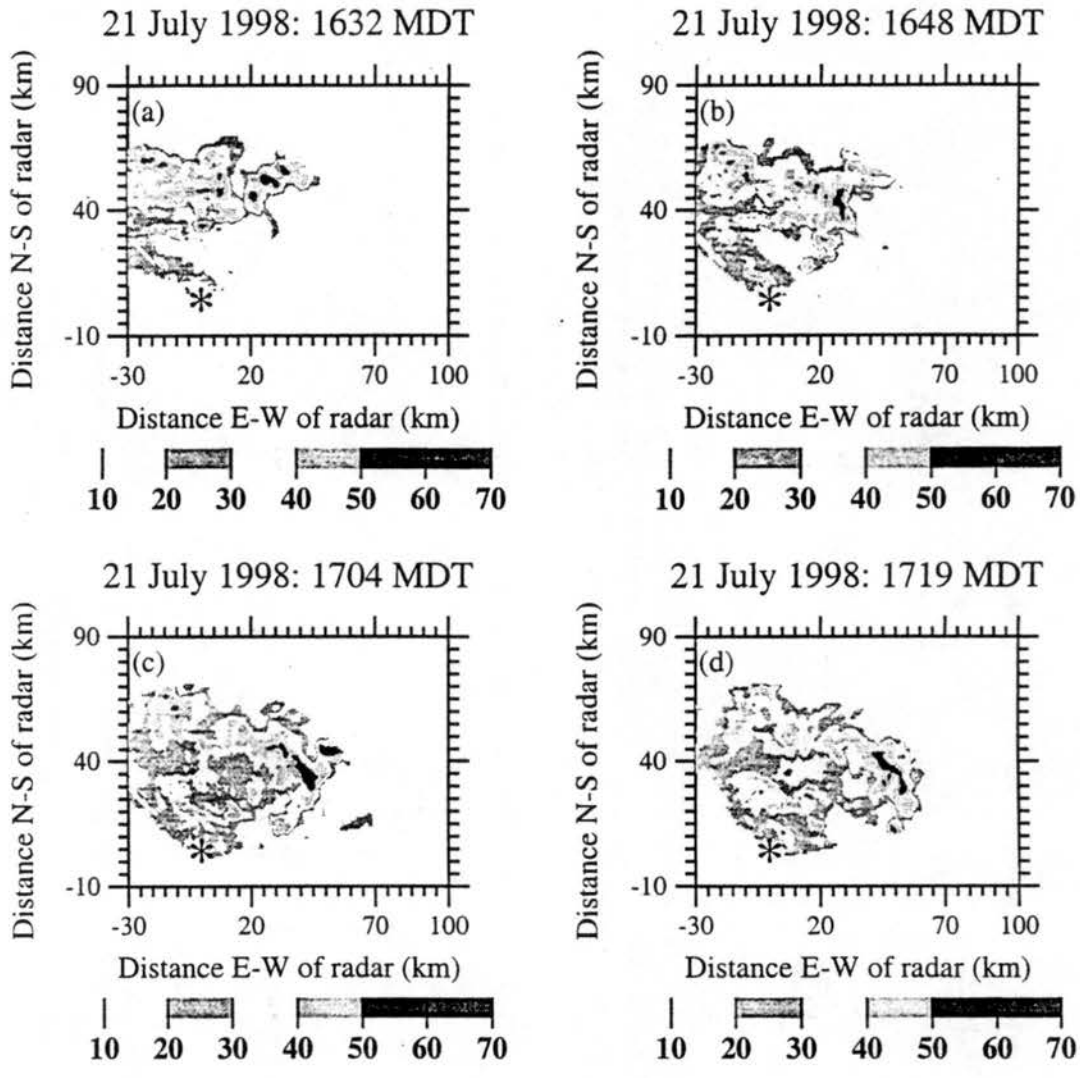


Figure 5.29: As in Fig. 5.3 for 21 July 1998. (a) 1632 MDT, (b) 1648 MDT, (c) 1704 MDT, (d) 1719 MDT.

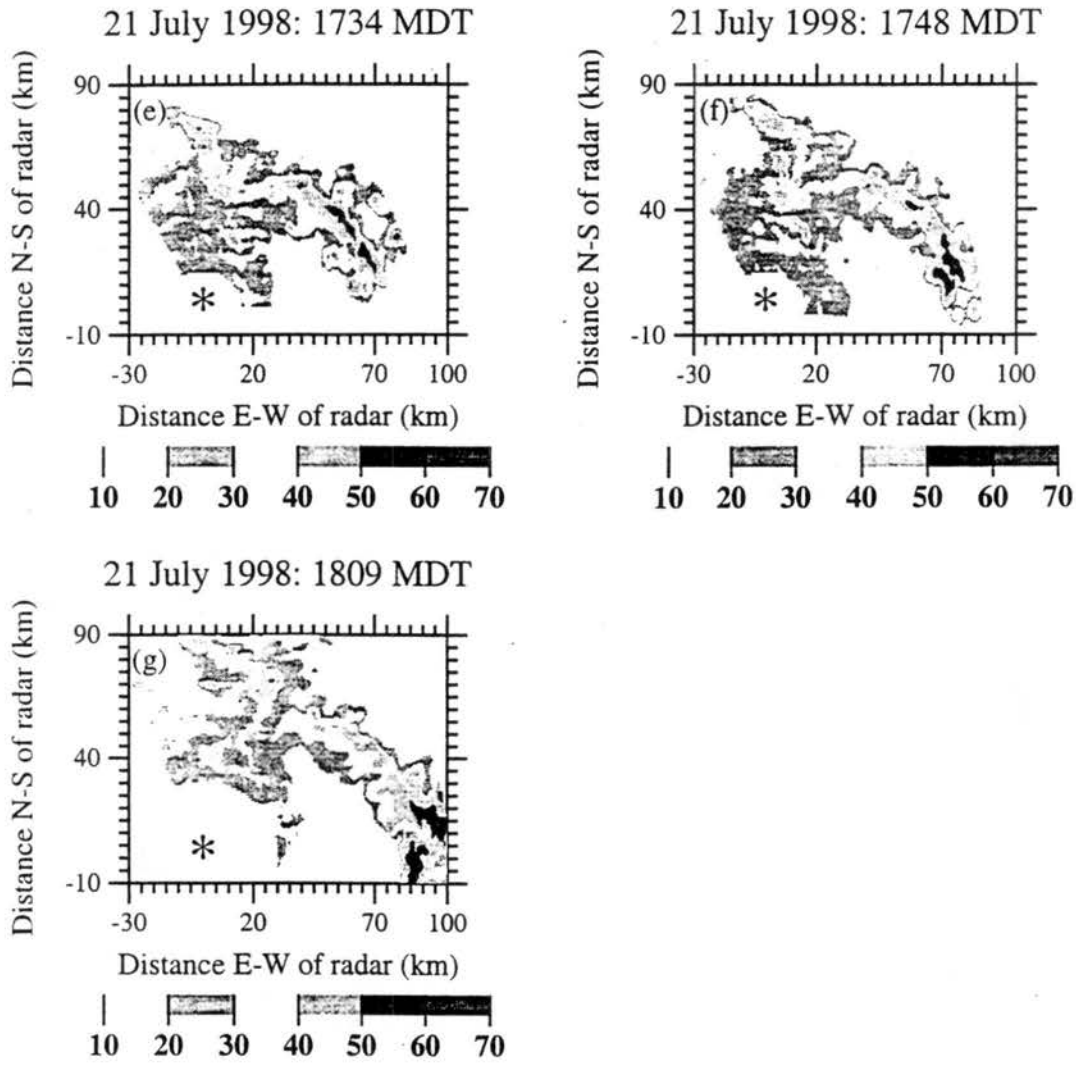


Figure 5.29: (e) 1734 MDT, (f) 1748 MDT, (g) 1809 MDT.

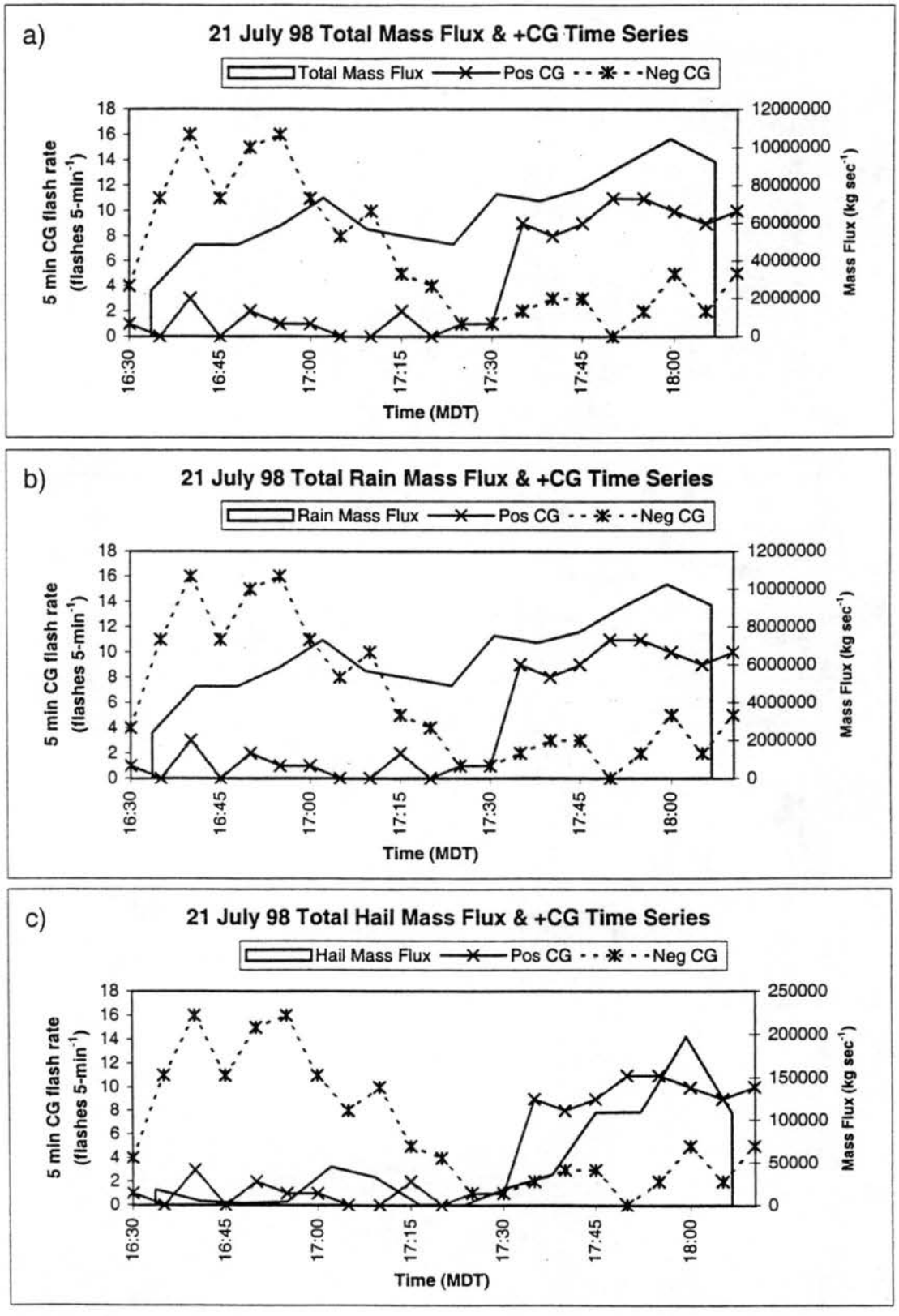


Figure 5.30: As in Fig. 5.5 for 21 July 1998. (a) Total mass flux, (b) rain mass flux, (c) hail mass flux.

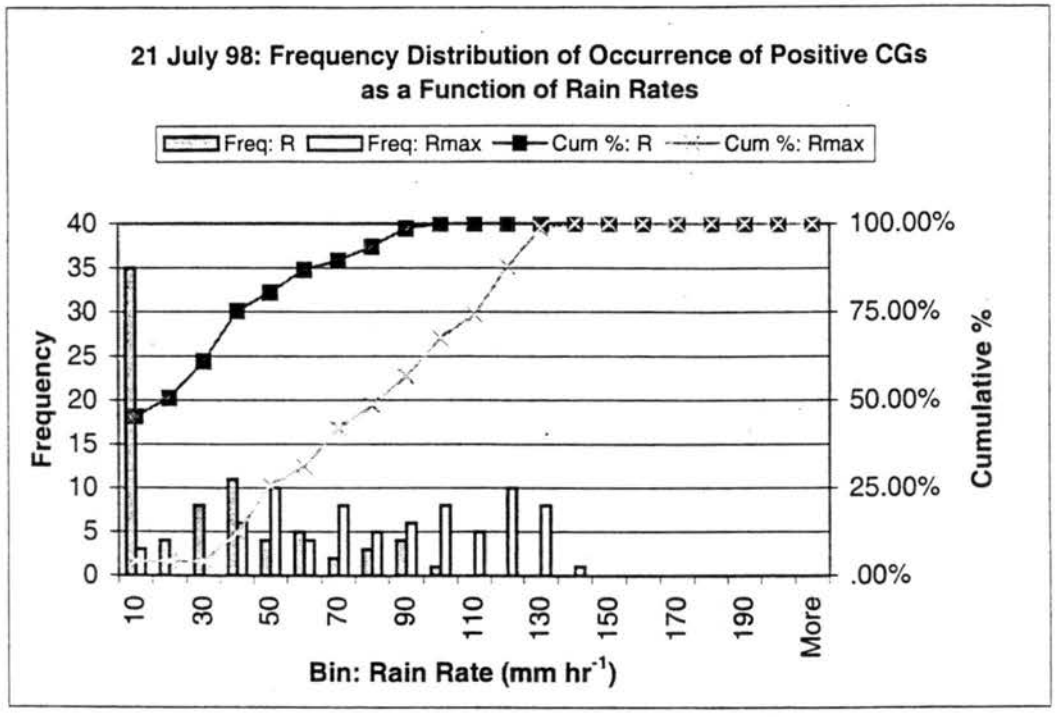


Figure 5.31: As in Fig. 5.6 for 21 July 1998.

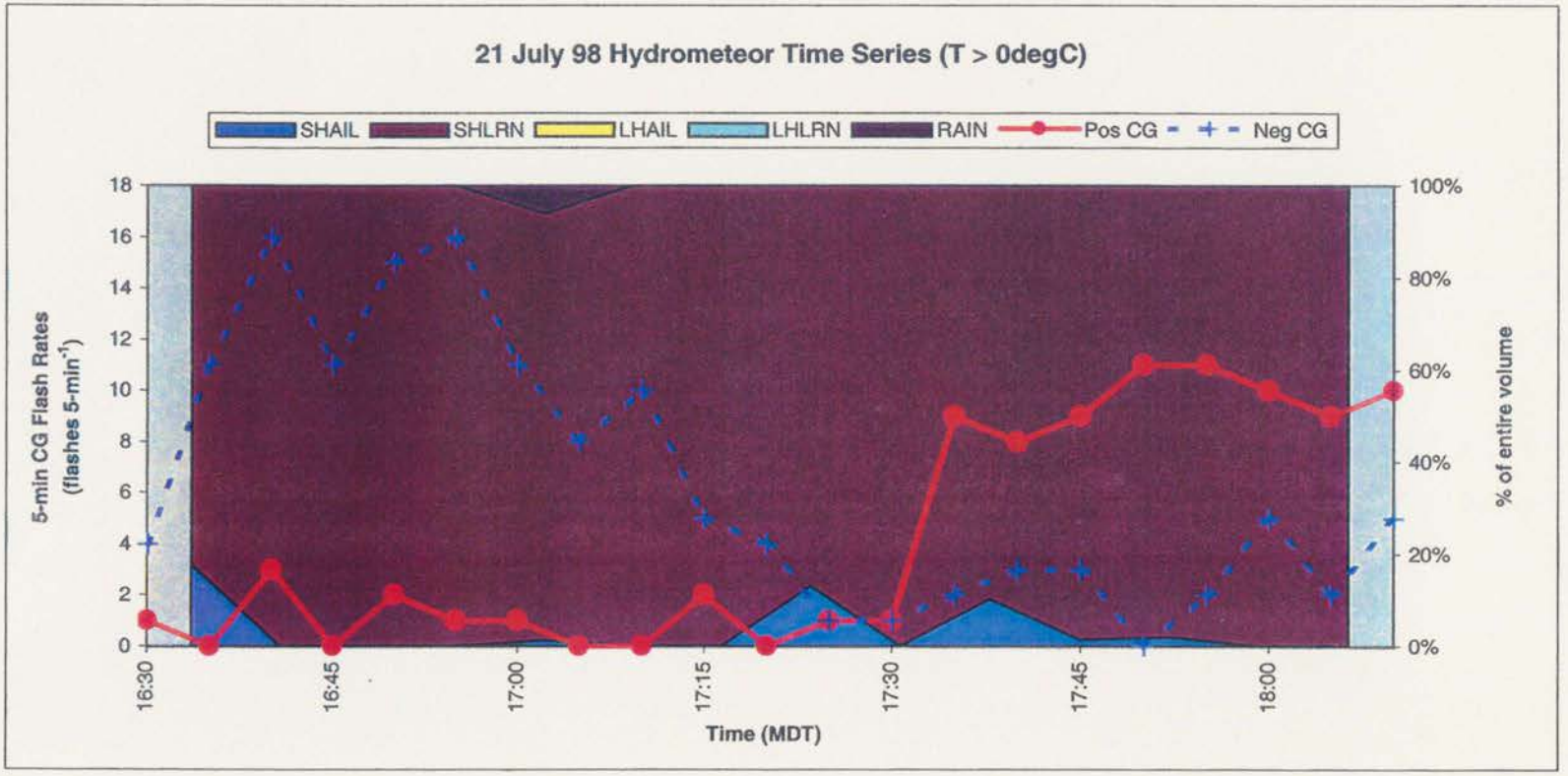


Figure 5.32: As in Fig. 5.7 for 21 July 1998.

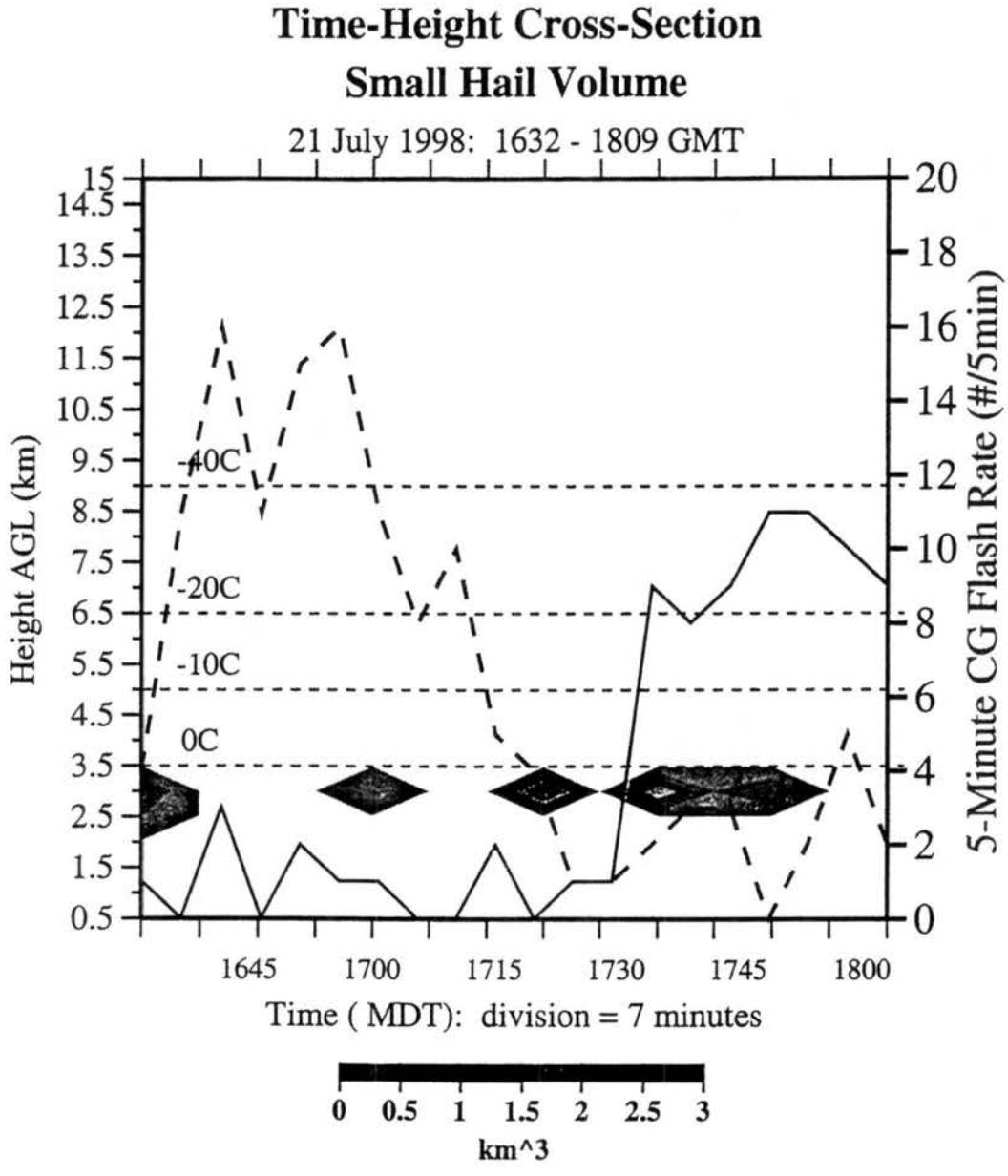


Figure 5.33: As in Fig. 5.8 for volumes of small hail below the melting level for 21 July 1998.

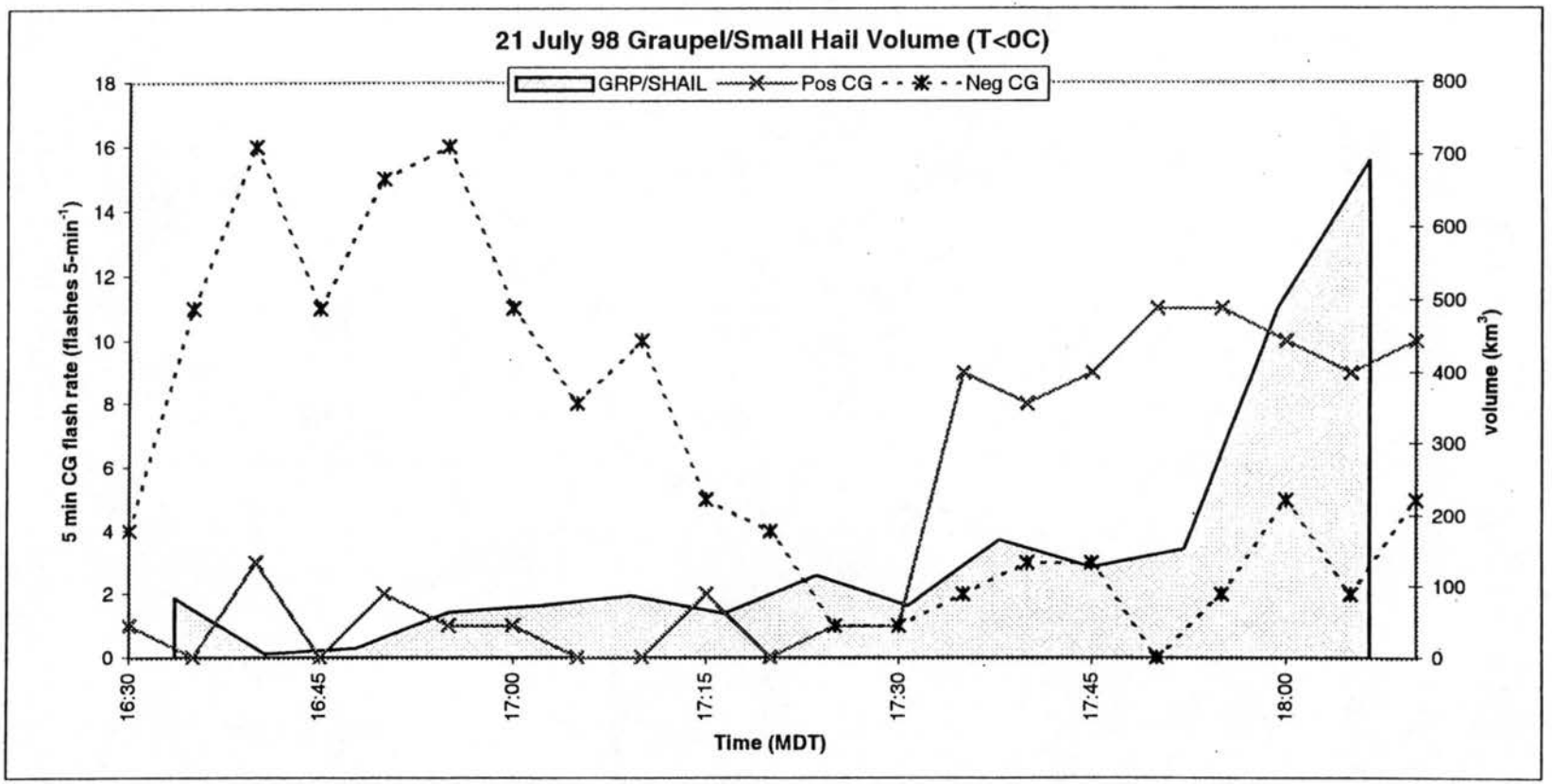


Figure 5.34: As in Fig. 5.10 for volumes of graupel and small hail above the melting level for 21 July 1998.

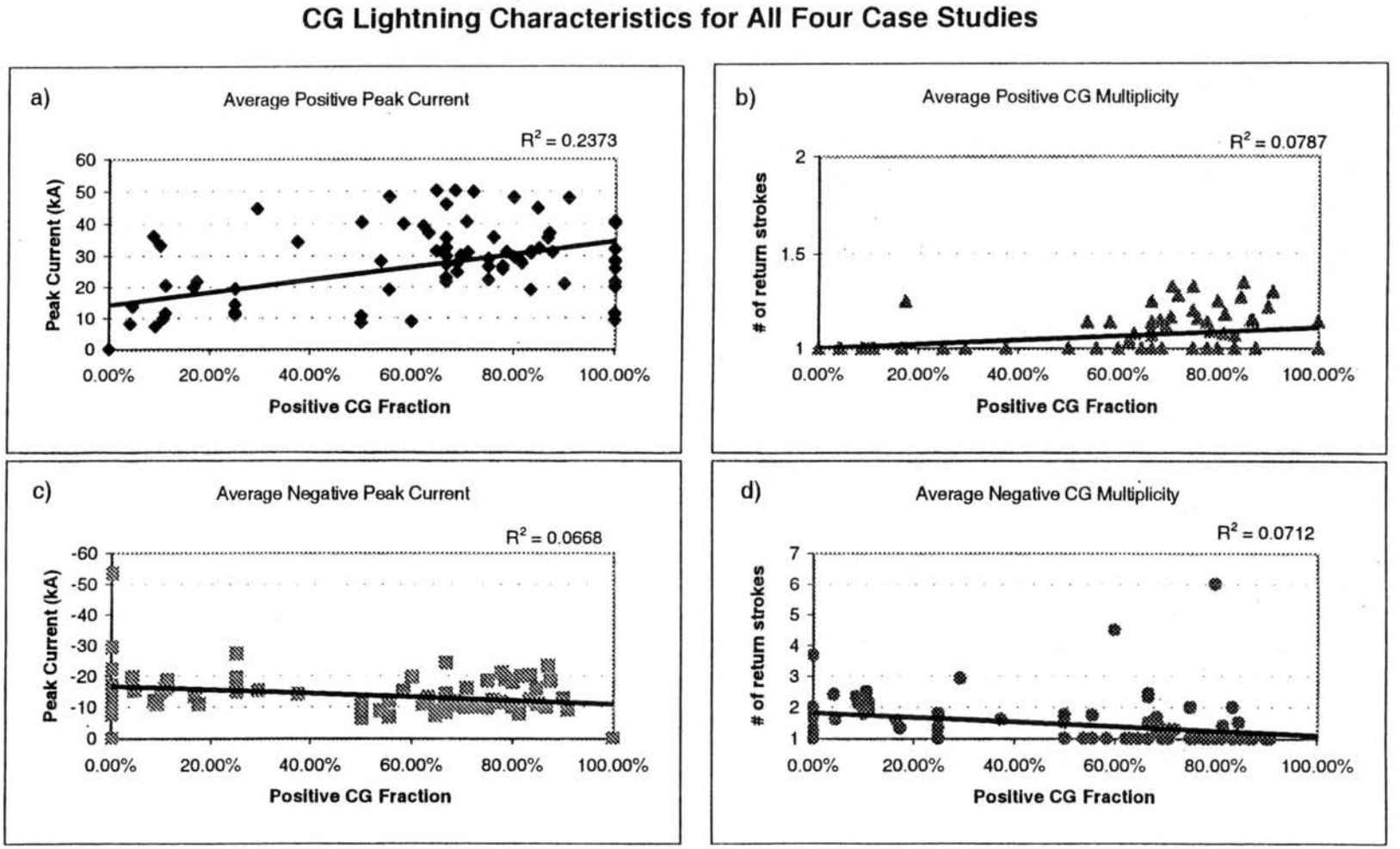


Figure 5.35: As in Fig. 5.2 for all four case studies.

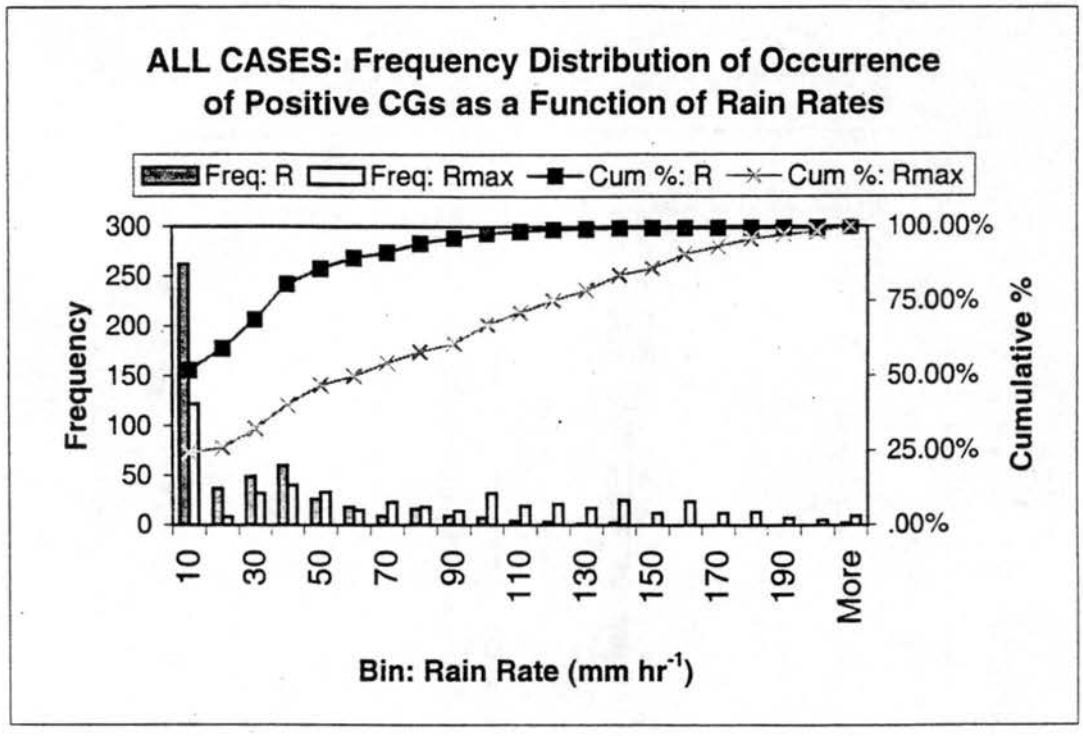


Figure 5.36: As in Fig. 5.6 for all four case studies.

# CHAPTER 6

# CONCLUDING REMARKS AND SUGGESTIONS FOR FUTURE RESEARCH

## 6.1 Concluding Remarks

In this thesis we have documented the spatial and temporal variations of summer season CG lightning activity immediately east of the central Rocky mountains over the period 1996 - 1998. This examination has helped to better describe how CG lightning characteristics (in particular multiplicity and peak current) for each polarity (positive and negative) change as the percentage of positive CG lightning changes. Specifically, we found that as the positive CG fraction within a storm increases, the average positive (negative) peak current increases (decreases). Similarly, our findings revealed that increases in positive CG fraction are associated with small increases in positive CG multiplicity and significant decreases in negative CG multiplicity.

Using the results of our regional climatology as a baseline, we examined the co-evolving microphysical and electrical characteristics of four significant lightning producing storms in northeast Colorado using the CSU-CHILL multiparameter radar and cloud-to-ground (CG) lightning data. Using the multiparameter variables $Z_h$, $Z_{dr}$, $\rho_{hv}(0)$, LDR and $K_{dp}$, emphasis was placed on determining the thee-dimensional distribution of various hydrometeor types in these storms (especially during periods of electrical transition from one CG polarity to another), as well as estimates of rain and hail rates.

The storms chosen for detailed study in this thesis each, at some point in their lifetime, had been dominated by a high density of positive CG lightning. Our goal in examining these cases was to try and determine the mechanism by which positive ground flashes in mature thunderstorms dominate over negative ground flashes. Specifically, we investigated the following hypotheses: (1) the tilted dipole hypothesis, (2) the enhanced lower positive charge hypothesis, and (3) the precipitation "unshielding" hypothesis.

Overall, the majority of our findings tend to support the third hypothesis, precipitation "unshielding", where intense precipitation leads to a large precipitation current which removes charge from the negative charge center, thereby "unshielding" the upper level positive charge center. Once this "unshielding" occurs, conditions are favorable for positive CG lightning. Typically, peaks in positive CG flash rates were observed within 25 minutes of observed peaks in surface mass fluxes, resulting from the descending ice mass aloft.

## 6.2 Suggestions for Future Research

The primary limitations of the present study include the small number of case studies, the lack of knowledge of the source regions of the CG lightning discharges, and the lack of measurements of net charge on hydrometeors within these storms.

Clearly, more detailed case studies of positive CG producing severe storms are required before any definitive statement can be made as to the cause. Future studies of these storms should utilize 3-D interferometric techniques to locate the VHF sources generated by a lightning channel (MacGorman and Rust, 1997). Bulk-hydrometeor identification could then be applied to polarimetric radar volumes to determine regions of

graupel and hail aloft to compare with the source regions of lightning channels located by the interferometer. Further, knowledge of the charge structures within these types of storms would better enable us to definitively relate the various hypotheses discussed above to the occurrence of positive CG lightning.

Furthermore, the hydrometeor partitioning algorithm used in this research was developed from a collection of prior investigations and modeling studies. Since in-situ verification of the presence of graupel and hail aloft in severe storms is not realistic, we must continue to depend on results from dynamical and microphysical models coupled with modeling of back-scattered radiation from various hydrometeor types to provide further evidence linking polarimetric radar signatures to specific hydrometeor types.

## REFERENCES


Avila, E., G. Caranti, and N. Castellano, 1998: Laboratory studies of the influence of cloud droplet size on charge transfer during crystal-graupel collisions. *J. Geophys. Res.*, **103**, 8985-8996.

Balakrishnan, N., and D.S. Zrnic, 1990a: Use of polarization to characterize and discriminate large hail. *J. Atmos. Sci.*, **47**, 1525-1540.

——, and ——, 1990b: Estimation of rain and hail rates in mixed-phase precipitation. *J. Atmos. Sci.*, **47**, 565-583.

Beard, D. V., and D. Chuang, 1987: A new model for the equilibrium shape of raindrops *J. Atmos. Sci.*, **44**, 1509-1524.

Branick, M. L., and C. A. Doswell III, 1992: An observation of the relationship between supercell structure and lightning ground strike polarity. *Weather Forecasting*, **7**, 143-149.

Brook, M., M. Nakano, P. Krehbiel and T. Takeuti, 1982: The electrical structure of the Hokuriku winter thunderstorms. *J. Geophys. Res.*, **87**, 1207-1215.

Butler, C. M., 1998: Microphysical characteristics of ice crystals and snowflakes as revealed by polarimetric radar measurements. MS Thesis, Dep. Atmos. Sci., Colorado State Univ., 100pp.

Carey, L. D., 1995: Multiparameter radar case studies of the microphysical and kinematic evolution of lightning producing storms. MS Thesis, Dep. Atmos. Sci., Colorado State Univ., 228pp.

——, S. A. Rutledge, and B. A. Zajac, 1997: An investigation of the relationship between severe storm reports and positive cloud-to-ground lightning. *Eos, Trans., AGU*, **78**, Fall Meeting Suppl., No. 46.

——, and ——, 1998: Electrical and multiparameter radar observations of a severe hailstorm. *J. Geophys. Res.*, **103**, 13979-14000.

Chandrasekar, V., V. N. Bringi, N. Balakrishnan, and D. S. Zrnic, 1990: Error structure of multiparameter radar and surface measurements of rainfall. Part III: Specific differential phase. *J. Atmos. Oceanic Technol.*, **7**, 621-629.

Cheng, L., and M. English, 1983: A relationship between hailstone concentration and size. *J. Atmos. Sci.*, **40**, 204-213.

Chiu, C. S., and J. D. Klett, 1976: Convective electrification of clouds. *J. Geophys. Res.*, **81**, 1111-1124.

Clodman, S., and W. Chisholm, 1996: Lightning flash climatology in the southern Great Lakes region. *Atmosphere-Ocean*, **32**, 345-377.

Cressman, G. P., 1959: An operational objective analysis system. *Mon. Wea. Rev.*, **87**, 367-374.

Cummins, K. L., E. A. Bardo, W. L. Hiscox, R. B. Pyle, and A. E. Pifer, 1995a: A combined TOA/MDF technology upgrade of the U.S. national lightning detection network. *J. Geophys. Res.*, **103**, 9035-9044.

—, —, —, —, and —, 1995b: A combined technology upgrade of the U.S. national network. Presented at the International Aerospace and Ground Conference on Lightning and Static Electricity, Williamsburg, VA.

—, —, —, —, and —, 1995c: A combined TOA/MDF technology upgrade of the U.S. national network. Proceedings, 10th International Conference on Atmospheric Electricity, Osaka, Japan, 288–292.

—, J. Cramer, and W. L. Hiscox, 1996: NLDN peak current estimates – 1996 update, *Tech. Note 40700*, Global Atmospherics, Inc., Tuscon, Arizona.

—, M. J. Murphy, E. A. Bardo, W. L. Hiscox, R. B. Pyle, and A. E. Pifer, 1998: A combined TOA/MDF Technology Upgrade of the U. S. National Lightning Detection *Network. J. Geophys. Res.*, **103**, 9035-9044.

Curran, E. B., and W. D. Rust, 1992: Positive ground flashes produced by low-precipitation thunderstorms in Oklahoma on 26 April 1984, *Mon. Weather Rev.*, **120**, 544-553.

Doviak, R. J., and D.S. Zrnic, 1993: *Doppler Radar and Weather Observations*, 2nd Ed., San Diego, CA, Academic Press, 562 pp.

Engholm, C. D., E. R. Williams, and R. M. Dole, 1990: Meteorological and electrical conditions associated with positive cloud-to-ground lightning. *Mon. Wea. Rev.*, **118**, 470–487.

Fuquay, D. M., 1982: Positive cloud-to-ground lightning in summer thunderstorms. *J. Geophys. Res.*, **87**, 7131–7140.

Global Atmospherics Inc., 1998: http://www.glatmos.com/nldn/nldn.html

Graham, B. L., R. L. Holle, and R. E. Lopez, 1997: Lightning detection and data use in the United States. *Fire Management Notes*, **57**(2), 4-9.

Holle, R. L., A. I. Watson, R. E. Lopez, D. R. MacGorman, R. Ortiz, and W. D. Otto, 1994: The life cycle of lightning and severe weather in a 3–4 June 1985 PRE-STORM mesoscale convective system. *Mon. Wea. Rev.*, **122**, 1798–1808.

Hubbert, J., and V. N. Bringi, 1995: An iterative filtering technique for the analysis of copolar differential phase and dual-frequency radar measurements. *J. Atmos. Oceanic Technol.*, **12**, 643-648.

Hubbert, J., V. Chandrasekar, V. N. Bringi, and P. Meischner, 1993: Processing and interpretation of coherent dual-polarized radar measurements. *J. Atmos. Oceanic Technol.*, **10**, 155-164.

Idone, V. P., D. A. Davis, P. K. Moore, Y. Wang, R. W. Henderson, M. Ries, and P. F. Jameson, 1998a: Performance evaluation of the U. S. national lightning detection network in eastern New York. 1. Detection eficiency. *J. Geophys. Res.*, **103**, 9045-9055.

—, —, —, —, —, —, and —, 1998b: Performance evaluation of the U. S. national lightning detection network in eastern New York. 2. Location accuracy. *J. Geophys. Res.*, **103**, 9057-9069.

Illingworth, A. J., and J. Latham, 1987: Polarization radar studies of precipitation development in convective storms. *Quart. J. Roy. Meteor. Soc.*, **113**, 469-489.

Jayaratne, E. R., C. P. R. Saunders, and J. Hallet, 1983: Laboratory studies of the charging of soft hail during ice crystal interactions. *Quart. J. Roy. Meteor. Soc.*, **109**, 609-630.

Jones, D. M. A., 1955: 3 cm and 10 cm wavelength radiation backscatter from rain. *Proc. 5th Wea. Radar Confr.*, Boston, Massachusetts, Amer. Meteorol. Soc., 281-285.

Lang, T. J., 1997: Relationship between storm structure and lightning activity in Colorado covection observed during STERAO-A. MS Thesis, Dep. Atmos. Sci., Colorado State Univ., 167pp.

Lang, T. J., S. A. Rutledge, J. E. Dye, M. Venticinque, P. Laroche, and E. Defer, 1999: Anomalously low negative cloud-to-ground lightning flash rates in intense convective storms observed during STERAO-A. Accepted in *Mon. Wea. Rev.*

Lopez, R. E., and R. L. Holle, 1986: Diurnal and spatial variability of lightning activity in northeastern Colorado and central Florida during the summer. *Mon. Wea. Rev.*, **114**, 1288–1312.

—, —, and T. A. Heitkamp, 1995: Lightning casualties and property damage in Colorado from 1950 to 1991 based on Storm Data. Weather and Forecasting, 10, 114-126.

—, M. W. Maier, and R. L. Holle, 1991: Comparison of the signal strength of positive and negative cloud-to-ground lightning flashes in northeastern Colorado. *J. Geophys. Res.*, **96**, 22,307–22,318.

Lushine, J. B., 1996: Underreporting of lightning deaths in Florida. Preprints, International Lightning Detection Conference, Tucson, Arizona, Global Atmospherics, Inc., Tucson, 13pp.

MacGorman, D. R., and D. W. Burgess, 1994: Positive cloud-to-ground lightning in tornadic storms and hailstorms. *Mon. Wea. Rev.*, **122**, 1671–1697

MacGorman, D. R., and W. D. Rust, 1997: *The Electrical Nature of Storms*. In print.

Maier, L. M., E. P. Krider, and M. W. Maier, 1984: Average diurnal variation of summer lightning over the Florida peninsula. *Mon. Wea. Rev.*, **112**, 1134–1140.

Mogil, H. M., M. Rush, and M. Kutka, 1977: Lightning---An update. Preprints, 10th Conference on Severe Local Storms, Omaha, Nebraska, American Meteorological Society, Boston, 226-230.

National Lightning Safety Institute, Nov 1998: http://www.lightningsafety.com/nlsi-lls/nlsi_annual_usa_losses.htm

Orville, R. E., 1991: Lightning ground flash density in the contiguous United States-1989. *Mon. Wea. Rev.*, **119**, 573–577.

—, 1994: Cloud-to-ground lightning flash characteristics in the contiguous United States: 1989-1991. *J. Geophys. Res.*, **99**, 10833-10841.

—, and A. C. Silver, 1997: Lightning Ground Flash Density in the contiguous United States: 1992-95. *Mon. Wea. Rev.*, **125**, 631–638.

—, R. A. Weisman, R. B. Pyle, R. W. Henderson, and R. E. Orville, Jr., 1987: Cloud-to-ground lightning flash characteristics from June 1984 through May 1985. *J. Geophys. Res.*, **92**, 5640–5644.

Oye, R., and R. E. Carbone, 1981: Ineractive Doppler editing software. *Preprints, 20th Conf. Radar Meteor.*, Boston, Massachusetts, Amer. Meteorol. Soc., 683-689.

Pierce, E. T., 1955: The development of lightning discharges. *Quart. J. Roy. Meteor. Soc.*, **81**, 229–240.

Pruppacher, H. R., and K. V. Beard, 1970: A wind tunnel investigation of the initial circulation and shape of water drops falling at terminal velocity in air. *Quart. J. Roy. Meteor. Soc.*, **96**, 247-256.

Reap, R. M., 1986: Evaluation of cloud-to-ground lightning data from the western United States for the 1983-84 summer seasons. *J. Climate Appl. Meteor.*, **25**, 785–799.

——, and D. R. MacGorman, 1989: Cloud-to-ground lightning: climatological characteristics and relationships to model fields, radar observations, and severe local storms. *Mon. Wea. Rev.*, **117**, 518–535.

Reynolds, S. E., M. Brook, and M. F. Gourley, 1957: Thunderstorm charge separation. *J. Meteorol.*, **14**, 426-436.

Rust, W. D., W. L. Taylor, D. R. MacGorman, and R. T. Arnold, 1981a: Research on electrical properties of severe thunderstorms. *Bull. Amer. Meteor. Soc.*, **62**, 1286–1293.

——, ——, ——, and ——, 1981b: Positive cloud-to-ground lightning flashes in severe convective storms. *Geophys. Res. Lett.*, **8**, 791-794.

——, D. R. MacGorman, and S. J. Goodman, 1985: Unusual positive cloud-to-ground lightning in Oklahoma storms on 14 May 1983, in *Preprints, 14th Conf. On Severe Local Storms, Indianapolis, IN, Amer. Meteor. Soc.*, 372–375.

Rutledge, S. A., and D. R. MacGorman, 1988: Cloud-to-ground lightning activity in the 10–11 June 1985 mesoscale convective system observed during the Oklahoma–Kansas PRE-STORM Project. *Mon. Wea. Rev.*, **116**, 1393–1408.

——, C. Lu, and D. R. MacGorman, 1990: Positive cloud-to-ground lightning in mesoscale convective systems. *J. Atmos. Sci.*, **47**, 2085–2100.

Sachidananda, M., and D. S. Zrnic, 1987: Rain rate estimates from differential polarization measurements. *J. Atmos. Oceanic Technol.*, **4**, 588-598.

Saunders, C. P. R., W. D. Keith, and R. P. Mitzeva, 1991: The effect of liquid water on thunderstorm charging. *J. Geophys. Res.*, **96**, 11007-11017.

Seimon, A., 1993: Anomalous cloud-to-ground lightning in an F5 tornado-producing supercell thunderstorm on 28 August 1990. *Bull. Amer. Meteor. Soc.*, **74**, 189–203.

Stolzenburg, M., 1990: Characteristics of the bipolar pattern of lightning locations observed in 1988 thunderstorms. *Bull. Amer. Meteor. Soc.*, **71**, 1331–1338.

——, 1994: Observations of high ground flash densities of positive lightning in summertime thunderstorms. *Mon. Wea. Rev.*, **122**, 1740–1750.

Straka, J. M., and D. S. Zrnic, 1993: An algorithm to deduce hydrometeor types and contents from multiparameter radar data. Preprints, 26th Conf. Radar Meteor. Norman, Oklahoma, Amer. Meteor. Soc., 513-515.

Takahashi, T., 1978: Riming electrification as a charge generation mechanism in thunderstorms., *J. Atmos. Sci.*, **35**, 1536-1548.

Takeuti, T., M. Brook, D. J. Raymond, and P. Krehbiel, 1978: The anomalous winter thunderstorms of the Hokuriku coast. *J. Geophys. Res.*, **83**, 2385-2394.

Vonnegut, B., 1963: Some facts and speculations concerning the origin and role of thunderstorm electricity, *Meteorol. Monogr.*, **5**, 224-241.

Wagner, P. B., and J. W. Telford, 1981: Cloud dynamics and an electric charge separation mechanism in convective clouds. *J. Res. Atmos.*, **15**, 97-120.

Williams, E. R., 1989: The tripole structure of thunderstorms., *J. Geophys. Res.*, **94**, 13151-13167.

Zajac, B. A., 1998: Climatological characteristics of cloud-to-ground lightning activity in the contiguous United States, MS Thesis, Dep. Atmos. Sci., Colorado State Univ., 119pp.

Zrnic, D. S., Bringi, V. N., Balakrishnan, N., Aydin, K., Chandrasekar, V., and J. Hubbert, 1993: Polarmietric measurements in a severe hailstorm. *Mon. Wea. Rev.*, **121**, 2223-2238.